

A Novel Approach to Topological Graph Theory: with R-K Diagrams & Gravitational Wave Analysis*

Animikh Roy[†] and Andor Kesselman[‡]

School of Mathematical & Physical Sciences, University of Sussex, United Kingdom.

Pathr.ai, Mountain View, California, United States of America.

(Dated: July 3, 2023)

Graph Theory and Topological Data Analytics (TDA), while powerful, have many drawbacks related to their sensitivity and consistency with TDA & **Graph Network Analytics**. In this paper, we aim to propose a novel "**Event-Driven**" approach for encoding vectorized associations between data points for the purpose of enabling smooth transitions between Graph and Topological Data Analytics.[1] [2] [3] We conclusively reveal effective ways of converting such vectorized associations to simplicial complexes representing micro-states [4] in a Phase-Space, resulting in filter specific, Homotopic self-expressive, event-driven unique topological signatures which we have referred as "**Roy-Kesselman (R-K) Diagrams**" with Persistent Homology. These diagrams emerge from filter-based encodings of "**R-K Models**". We finally aim to provide an efficient computational framework via the "**R-K Pipeline**" which can be used via the "**R-K Toolkit**" to obtain filter based ML driven models for unique topological signature identification and classification problems. This pipeline would be responsible for shape invariant encoding in strong correspondence with topological network divergence as global-macro-state properties of high-dimensional datasets.[5] The validity and impact of this approach were tested specifically on high-dimensional (parameter specific) raw and derived measures from the latest **LIGO** datasets published by the **Gravitational Wave (LIGO) Open Science Centre** [6] [7] along with testing a generalized approach for a non-scientific use-case, which has been demonstrated using the **Tableau Superstore Sales** dataset.[8] The results obtained verify the basis of this novel approach in the following ways: (1) Distinct event-driven topological structures were generated from the data, both in case of the LIGO data and the Super-Store Sales data. (2) These topological structures have emergent properties that when evaluated and compared to, have the capacity to provide meaningful insights into the data that standard data analysis techniques would not identify. For example, topological differences were exposed in the analysis that could not be exposed over metric based analysis such as 'Euclidean Distance', 'Mahalanobis Distance', and other standard metric based distance measures. (3) The resulting structures provide an extensible representation, which can be applied to different methods of analysis, such as: classification, identification, segmentation, etc. In both case studies, the final results were trained with a unique non-gradient, combinatorial approach. With respect to store sales data, unique topological structures were derived between distinct purchase events with a loss (measured in similarity between a set of R-K Diagrams) in the range of [0.78, 0.88]. In the case of the classification case study with LIGO data analysis, we recorded a high accuracy of compact binary classifications, and an average similarity measure of BH-BH Mergers falling between the range of [0.91, 0.96] and NS-NS Mergers between a range of [0.85, 0.91]. Inter-class similarity measures between black holes, neutron stars (NS-NS), (NS-BH)& candidate PBH were found to be between 0.78 & 0.83 with distinctly different R-K Diagrams (which could improve significantly with additional injection studies and support data beyond the 92 confirmed CBC-events studied in this paper). Therefore, we believe the findings of our work will lay the foundation for many future scientific and engineering applications of stable, high-dimensional data analysis with the combined effectiveness of **Topological Graph Theory** transformations.[9][10]

I. INTRODUCTION

A. Overview

In this paper, we aim to provide a novel computational framework for efficient and simplified Topological Graph

Analysis [5] [11] [10] [12] [13] on high-dimensional structured datasets with hierarchical embeddings that are consistent with the mathematical foundations and advancements in boths Graph Theory [14] and Topology.[1] Our objectives and motivation are driven towards the creation of a fundamental "**Event-Driven Topological-Graphs Analysis**" tool that could automatically generate distinct and unique signatures for the efficient identification and classification of "**Events**" and "**Entities**" based on the choice of "**Lens**"(As explained in 4.5.5) with similar or dissimilar attributes derived from scientific or enterprise data with specific ontological properties. The central idea of "**Event-Driven Topological-Graph Analysis**" is based on the topological cluster-

* "R-K" stands for "Roy-Kesselman" based on the last names of the original authors of this novel approach; Animikh Roy & Andor Kesselman

[†] Department of Astronomy, University of Sussex,UK.
www.royspaceboy.com; ar505@sussex.ac.uk

[‡] Principal Software Engineer, Pathr.ai, California, USA.; andor@henosisknot.com

ing [15] [16] of all attributes around a central "***Event-Node***" which serves as a static (unchanging) context for all dependent attribute clusters. Such attribute-clusters have their own "*Directed-Acyclic-Graphs*" [17] [18] that ensure their uniqueness and inter-dependencies based on a particular domain Ontology. Thus unique topological signatures are obtained using domain-specific filters or threshold constrains on underlying fundamental structural graphs called "**Roy-Kesselman (R-K) Models**" represented by tensors in n-dimensional space, which are reduced to consistent "*Topohedrons*" (Polyhedrons that preserve topological invariance under geometric transformations or perturbations of state) with persistent Homology called "**Roy-Kesselman (R-K) Diagrams**". Similar "*Topological Events*" would produce unique **R-K diagrams** which remain static and unchanging under perturbations caused due to changes in data values at the row level or the influx of data in terms of new/additional rows. On the other hand, different "*Topological Events*" would produce distinctly different **R-K diagrams** based on perturbations caused by the influx of data in terms of new/added rows or additional independent attributes in terms of columns driven by Hierarchical-Feature-Extractions with respect to a particular domain Ontology.

We also aim to present a scalable domain-agnostic pipeline called the "**R-K Pipeline**" with a customisable Toolkit called the "**R-K Toolkit**" for different domain ontologies and for parameter optimizations, which would be responsible for following: (1) Shape invariant encoding (2) Topological Event Identification (3) Topological Classification & (4) Isometric Compression of high-dimensional graphs without the loss of essential information or generality. Each step of our novel approach and methodology have been thoroughly tested on scientific (LIGO Open Science) [6] [7] and commercial (Tableau Superstore Sales) datasets, producing efficient and consistent results that could be applied towards future studies on parametrised classification of Event-Signatures and Data-Entities in the field of Topological Graph Theory.[10] This would also allow for the combination and analysis of multiple datasets and data-streams in real-time, such as in the case of Multi-messenger Astronomy.

B. Motivation

Graph Theory (**GT**) [11] [19] [14] and Topological Data Analysis (**TDA**) [5] [3] have recently emerged as independent novel frameworks for extracting hidden meaning and underlying insights from the study of geometric structure, shape and connections of such vast and complex datasets. [20] [21] However modern computational tools lack the technology, efficiency and flexibility to consistently carry out Graph Theory Network Analysis with hierarchical connections with localised clustering due to the inherent variability that could encode directed

relationships in the affine connexions [22] [23] of the data-points in phase space, in order to build homotopic manifolds and simplicial complexes[24].[2] [25][3] They also lack a consistent framework to mathematically define and classify the global properties of the same network through an effective means to smoothly transit between Graph and Topological structures as established theoretically in Topological Graph Theory (TGT)[12] [13]. This would prevent the additional burden of having to regenerate the entire data geometry from scratch due to lack of persistent homology between the two models.[26] [27] [3].

C. Objectives

Being able to showcase TDA and GT capabilities via smooth mathematical transformations on the same data network (consisting of one or more datasets and data streams) without the necessity to recreate its underlying geometric structure encompasses an enormous field of untapped potential taking inspiration from Topological Graph Theory [9] [10] in modern scientific Big-data Analytics.[24][28] [29] This academic paper explores the possibility of consistently improving existing GT and TDA technologies with enhanced geometric compatibility while preserving their respective mathematical properties through simple Vectorized Associations in Phase Space.[30] This research also aims to facilitate a smooth transition between these two advanced analytical methodologies by using machine learning to fine tune effective and unique "*Event-Driven*" topological signatures that manifest as self-expressive homotopic[31] [25] "*Roy-Kesselman Diagrams*" (R-K Diagrams).

These are shown as a special category of Polyhedrons that maintain Topological Invariance[32] [33] and Persistent Homology when projected onto a Phase Space. These "*Topohedrons*" or filtered R-K Diagrams can be generated via filter-based ML driven optimizations on the underlying n-dimensional data set, which are preserved within the underlying Topological Space. This work allows for future research into the preservation of Homotopy of such "*Topohedrons*" under continuous deformations brought about by any changes in Topological Network Entropy due to data perturbations. It also formulates such implications through mathematical and computational models as shown in this paper.[34]

The findings of this work have seminal implications on high-dimensional, complex scientific data sets especially in the context of Dark Matter and Gravitational Wave Analysis[7] [35] with LIGO-Virgo datasets without the necessity of conventional clustering and binning techniques. [36] We also justify it's scope and validity on a generalized non-scientific use case on commercial Tableau Super Store Data . It also replaces the existing Mapper algorithms [2] with a holistic analytical framework that goes well beyond partial clustering and addresses **Persistent Homology** [1] [37] for Topological shape rendering with built-in **Isometric Data Com-**

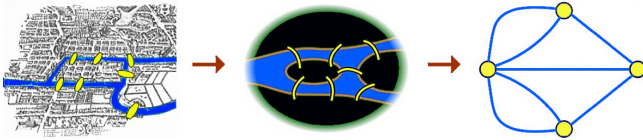


Figure 1. The above diagram shows the Königsberg bridge problem and its corresponding resolution by Leonhard Euler that lead to the introduction of graph theory and the subsequent birth of the branch of mathematical topology

pression capabilities.[33] [38] [39]

II. MATHEMATICAL BACKGROUND

In this section we shall elaborate on the mathematical formulations and conceptual foundations upon which we aim to build this novel approach towards Topological Graph Theory with some unique data modelling characteristics. This section will also contain all corresponding references to the latest and most relevant research in the respective fields of Topology & Graph Theory & Topological Data Analysis.

A. Eulerian Graph Theory & the Birth of Topology

Graph theory is a well-established and versatile branch of mathematics that is primarily concerned with networks of points connected by lines. The subject of graph theory had its beginnings in recreational mathematical problems in the early 17th century, especially those related to the historical drawing of graphs stemming from cartographic representation of geographic regions. [40] However, it has currently grown into a significant area of mathematical research, with applications in Chemistry, Biology, Operations Research, Social Sciences, Computer Science, Natural language processing [41] and Big-Data Analytics.[42] [43] The history of graph theory may be specifically traced to 1735, when its founding father, Swiss Mathematician Leonhard Euler solved the Königsberg bridge problem. [44] The Königsberg bridge problem was an old puzzle concerning the possibility of finding a path over every one of seven bridges that span a forked river flowing past an island—but without crossing any bridge twice. Euler argued that no such path exists. His proof involved only references to the physical arrangement of the bridges, but essentially he proved the first theorem in graph theory.[45]

It is important to note, that in the field of Graph Theory, the term "*graph*" does not refer to data charts, such as the likes of line graphs or bar graphs pertaining to the graphical visualization of data. Instead, it refers to a set of Vertices (V) (i.e., points or nodes) and Edges (E) (or lines) that connect the vertices. When any two vertices are joined by more than one edge, then such a

graph is called a "*Multi-graph*". [46][44] A graph without any loops and with a maximum of one edge between any two vertices is called a *simple graph*. When each and every vertex of a graph is connected by an edge to every other vertex, then such a graph is called a *complete graph*. Moreover, it is important to note in the context of this paper, a direction is assigned to each edge of a graph to produce what is known as a *Directed Graph* or *Digraph*.[17] We shall be dealing with such Directed Graphs for the remaining part of this paper.

Another useful concept in Graph Theory that of the *path*. In this field, a path is defined as any route along the edges of a graph.[44] A path may follow a single edge directly between two vertices, or it may follow multiple edges through multiple vertices.[11] If there is a path linking any two vertices in a graph, then such a graph is called a *connected graph*. A path that begins and ends at the same vertex without traversing any edge more than once is called a circuit, or a closed path. A circuit that follows each edge exactly once while visiting every vertex is known as an Eulerian circuit, and the graph is called an Eulerian graph. An Eulerian graph is connected and, in addition, all its vertices have even degree.[47] [48] Such Eulerian Graphs shall be taken into consideration in the computational framework of our novel approach.

It is also important to know that the histories of graph theory and topology are closely related, and the two areas share many common problems and techniques even today, [49] [40] especially in the domains of mathematics and computer science. Such similarities can be traced back to Euler, who referred to his work on the Königsberg bridge problem as an example of *geometria situs* or the “geometry of position”; while on the other hand, the development of topological ideas during the 19th century became famously known as *analysis situs*, or the “analysis of position” thereby interlinking these two fundamental pillars of mathematics.[44][46] As a further extension to the foundation of GT in 1750, Euler discovered the polyhedral formula $V - E + F = 2$ relating the number of vertices (V), edges (E), and faces (F) of a polyhedron (a solid object in 3D geometry with each enclosed surface or face represented by polygons). [49][47]

The vertices and edges of all such polyhedrons form graphs on its surface, and this notion led to consideration of graphs on other surfaces such as a torus (the surface of a solid doughnut) and how they divide the surface into disk-like faces. Euler’s formula was soon generalized to surfaces as $V - E + F = 2 - 2g$, where g denotes the genus, or number of “doughnut holes,” which help determine their Euler Characteristic. [50] Having considered a surface divided into polygons by an embedded graph, mathematicians began to study ways of constructing surfaces, and later more general spaces, by pasting polygons together. This was the beginning of the field of Combinatorial Topology, which later, through the work of the French mathematician Henri Poincaré and others, grew into what is known as Algebraic Topology. [1] [45] [49] Such concepts related to polyhedrons and Euler

Characteristics that link the concepts of Graph Theory and Algebraic Topology through Combinatorics, serve as the theoretical basis for the mathematical formulations of our approach.

B. Topological Data Analytics

Topological Data Analytics or TDA [20] [3] is a mathematical methodology that is often represented as a useful computational framework or tool for high-dimensional data (i.e. data with multiple independent columns, variables or features across different datasets) analysis developed initially by Herbert Edelsbrunner, Afra Zomorodian, Gunnar Carlsson, and his graduate student Gurjeet Singh.[2] [51] [3] The core idea of TDA is based on the founding principle of Gunnar Carlson et.al[21] which states that, high-dimensional & complex data sets (with multiple features and parameters) have intrinsic topological shape that can be represented in n-dimensions using generalized coordinate systems.[3] However, such shapes can then be assigned extrinsic characteristics and context-based meaning, thus enabling a robust and scalable framework of data labelling, classification and analysis. Such computational frameworks of topological analysis can be further enhanced and automated using Machine Learning and Neural Networks as elaborated in the later sections of this paper. the first data analysis framework using TDA was popularized by Carlsson's paper in 2009 called "**Topology & Data**" [26] that later turned TDA into a hot field in applied mathematics, and also found many applications in Data-Science and Big-data Analytics.[24][29] [10] However, the mathematical foundations that drive TDA had been laid years before by others in the fields of Topology, Group Theory, Linear Algebra and Graph Theory as discussed earlier and referenced in this paper.

As evident today, an important feature of modern science and engineering is that data of various kinds is being produced at an unprecedented rate. [24] [29] This partly because of new experimental methods, and in partly because of the increase in the availability of high powered computing technologies.[28] [52] It is also clear that the nature of the data that we obtain today is significantly different. For example, it is now often the case that we are given data in the form of very long vectors, where all but a few of the coordinates turn out to be irrelevant to the questions of interest, and further that we don't necessarily know which coordinates are the most relevant ones for the ideal solution. A related fact is that the data is often very high-dimensional, which severely restricts our ability to visualize it. The data obtained is also often much noisier than in the past and has more missing information (missing data).[26]

This is particularly so in the case of scientific data related to high throughput data [53] from micro-arrays in biology or other sources such as particle accelerators in high-energy physics, or in the case of multi-messenger

data-streams in modern-day Astronomy. thus our ability to analyse such data, both in terms of quantity and the nature of the data, is clearly not keeping pace with the data being produced.[29] In this paper, we will discuss how geometry and topology can be applied to make useful contributions to the analysis of various kinds of data. Our aim is to establish that geometry and topology are very natural tools to apply in this direction, since geometry can be regarded as the study of distance functions, and in any statistical data-analysis model, we often end up applying such distance functions on large finite sets of data. The mathematical formalism which has been developed thus far for incorporating geometric and topological techniques deals with point clouds, i.e. finite sets of points equipped with a distance function. It then adapts tools from the various branches of geometry to the study of point clouds. The point clouds are intended to be thought of as finite samples taken from a geometric object, perhaps with noise.[3] [2] [5]

However, our novel approach is different from traditional methods of topological analysis using point cloud data, in that it is primarily "*Event-Driven*" in its technique, which appeals to a limited but widely applicable sub-set of Topological Graph Analysis where in hierarchical relationships can be determined between various dependent and independent column attributes of a dataset and can be then connected to a contextual "*Event*" or "*Entity*" based on the choice of a "*Lens*", which will be further explored in our work. In all cases under consideration related to our approach, the characteristics features of a dataset are associated to a central static context known as an "*Event-Node*" with independent features and variables associated with such events mapped to it in separate attribute clusters. This gives rise to well-defined hierarchical feature based multi-graphs with nodes and directed edges which represent the "*micro-states*" of an Event, while its "*macro-state*" is determined by the overall topology of the R-K diagrams with distinctive macro features such as holes, voids, loops etc. which can be characterised with the help of Betti-Numbers which are unique to different classifications determined by domain specific filters and ontological parameters.

Now we shall note some of the key problems that occur when applying traditional statistical & geometric methods to data analysis that we aim to address using our analytical framework and pipeline:

- ***High-dependence on Qualitative Information:***

One important goal of Data Analysis at its core, is to allow the user to obtain knowledge about the data, i.e. to understand how it is organized on a large scale. For example, if we imagine that we are looking at a data set constructed somehow from diabetes patients, it would be important to develop the understanding that there are two types of the disease, namely the juvenile and adult onset forms.[3][51] Once that is established, one of course wants to develop quantitative methods for distinguishing them, but the first insight about the distinct forms of the disease is key which needs to be qualified in non-

topological analytical frameworks, where as differences in topological signatures of data pertaining to such patients can enable automated segregation for easier understanding and classification.

- **Metrics are not Theoretically Justified:** In physics and Astronomy, the phenomena studied often support clean explanatory theories which tell one exactly what metric to use. In biological problems, on the other hand, this is much less clear. But in certain cases it is far from clear how much significance to attach to the actual data points and distances, particularly at large scales and in developing fields of research such as in the case of Gravitational Wave Astronomy (LIGO, Virgo , etc.). Thus Topological frameworks such as ours would allow for smooth and effective measures of noise reduction in a phase-space independent of any metric dependencies while retaining the vital information isometrically, even in the case of transformations such as projection or compression.

- **Coordinates are not Natural:** Although we often receive data in the form of vectors of real numbers. However, it is frequently the case (in physics, astronomy and various branches of modern science) that the coordinates, like the metrics mentioned above, are not natural in any sense. Therefore it is incorrect to restrict ourselves to studying properties of the data which depend on any particular choice of coordinates. Note that the variation of choices of coordinates does not require that the coordinate changes be rigid motions of Euclidean space. It is often a tacit assumption in the study of data that the coordinates carry intrinsic meaning, but this assumption is often unjustified [3] [51] [26] and can be effectively addressed in frameworks involving Topological Graph Analysis.

- **Summaries are more valuable than individual parameter choices:** In traditional approaches so far, a popular method of clustering a point cloud is the so-called single linkage clustering, in which a graph is constructed whose vertex set is the set of points in the cloud, and where two such points are connected by an edge if their distance is $\geq \epsilon$, where ϵ is a parameter. [26] [24] Some work in clustering theory has been done in trying to determine the optimal choice of ϵ , but it is now well understood that it is much more informative to maintain the entire "*Dendrogram*" [18][17] of the set, which provides a summary of the behaviour of clustering under all possible values of the parameter at once. It is therefore productive to develop other mechanisms in which the behaviour of invariants or construction under a change of parameters can be effectively summarized such as in the case of our novel framework.

We shall now discuss how Topological Graph Analysis could serve as an important and relevant way for addressing all the above mentioned problems especially to understand how they may be relevant in the case of formulating and justifying this novel approach for specific Analysis on Scientific and Ontology driven datasets that can be used to build useful Knowledge-Graphs and subsequent R-K Diagrams :

quent R-K Diagrams :

(1) Topology and Graph theory are the best candidates in the branch of Analytics to deal with qualitative geometric information. This includes the study of what the connected components of a space are, but more generally it is the study of connectivity information, which includes the classification of micro-geometric properties such as nodes, edges and directions of DAGs [17] to signify micro-state differences. While, macro-geometric properties are distinguished based on holes, voids, loops and higher dimensional surfaces within the space which are represented by distinct Euler Characteristics and Betti Numbers [47] [48] of the specific unique topology. This suggests that extensions of topological & graph methodologies, such as DAGs, Euler Characteristics, Betti Numbers, Homotopy & Homology, should be helpful in studying them qualitatively.[25] [54]

(2) Topology & Graph Theory study geometric properties in a way which is much less sensitive to the actual choice of metrics than straightforward geometric methods, which involve sensitive geometric properties such as curvature. [1] In fact, topology ignores the quantitative values of the distance functions and replaces them with the notion of infinite nearness of a point to a subset in the underlying space. This insensitivity to the metric is useful in studying situations where one only believes one understands the metric in a coarse way.[20]

(3) Topology studies only properties of geometric objects which do not depend on the chosen coordinates, but rather on intrinsic geometric properties of the objects. Therefore it allows for a coordinate-free analytical approach. [3] [26]

(4) The idea of constructing summaries over whole domains of parameter values involves understanding the relationship between geometric objects constructed from data using various parameter values. The relationships which are useful involve continuous maps between the different geometric objects, and therefore become a manifestation of the notion of Functoriality, i.e, the notion that invariants should be related not just to objects being studied, but also to the maps between these objects.[55] Functoriality is central in algebraic topology in that the functoriality of homological invariants [16] is what permits one to compute them from local information, and that functoriality is at the heart of most of the interesting applications within mathematics. Moreover, it is understood that most of the information about topological spaces can be obtained through diagrams of discrete sets, via a process of simplicial approximation.[25] [56]

C. Topological Graph Theory

The connection between graph theory and topology led to a sub-field called Topological Graph Theory.[9] [10] An important problem in this area concerns planar graphs. These are graphs that can be drawn as dot-and-line diagrams on a plane (or, equivalently, on a sphere) without

any edges crossing except at the vertices where they meet. Complete graphs with four or fewer vertices are planar, but complete graphs with five vertices or more are not. The use of diagrams of dots and lines to represent graphs actually grew out of 19th-century chemistry, where lettered vertices denoted individual atoms and connecting lines denoted chemical bonds (with degree corresponding to valence), in which planarity had important chemical consequences. The first use, in this context, of the word graph is attributed to the 19th-century Englishman James Sylvester, one of several mathematicians interested in counting special types of diagrams representing molecules.[57]

Topological graph theory deals with ways to represent the geometric realization of graphs. Typically, this involves starting with a graph and depicting it on various types of drawing boards: 3-space, the plane, surfaces, books, etc. This field mainly uses topological methods to study graphs. For example, planar graphs have many special properties. The field also uses graphs to study topology. For example, the graph theoretic proofs of the Jordan Curve Theorem, or the theory of voltage graphs depicting branched coverings of surfaces, provide an intuitively appealing and easily checked combinatorial interpretation of subtle topological concepts [12] [10] that serve as the fundamental basis of this novel approach and are established as a part of our computational framework.

1. Directed Acyclic Graphs

In our paper, we enable a topological graph theory framework through DAG's at the micro level which can be defined as follows:

A directed acyclic graph is a graph $(N, E) \in G$ where G is a graph N are nodes and E are edges. It is a restricted general graph, in that there are no edge cycles, such that an edge can be described as E_{N_i, N_j} where $i \neq j$ and the path of edges never roll back onto itself. The benefit of a DAG is the compositability of it, and the ability to make complicated and general pipelines from it.

D. Phase Space & Projections

In the last century, the development of modern physics has been partially driven by the incorporation of a few key concepts. A phase space is the spatial representation of all possible states of a dynamical system, where each point uniquely identifies a state. A Topological Phase Space can be defined as the n-dimensional spatial representation of the same using a generalized Curvilinear Coordinate system allowing for all possible coordinate transformations and perfect isometric compressions while preserving geometric invariance. The concept of Phase Space in itself is a simple but powerful idea that emerged in the second half of the 19th century, during the golden era of differential geometry, and it is at the core

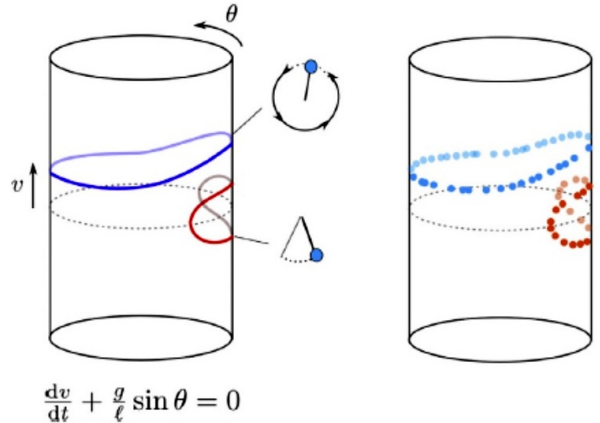


Figure 2. the above diagram shows that the phase space of a simple pendulum is a two-dimensional cylinder, where the periodic coordinate corresponds to the angle of the pendulum with respect to the vertical, and the longitudinal coordinate to its angular velocity

of modern classical, quantum, and statistical mechanics. The trajectory that a dynamical system describes in the phase space as it evolves with time contains rich information about the system. For instance, by looking at the shape of the trajectories that a pendulum describes in its phase space, we can infer the existence of different dynamical regimes, or the ratio between the length of the pendulum and the acceleration of gravity.

Each point in this space specifies a unique combination of the position and velocity and uniquely determines the subsequent evolution. For small angular velocities, the pendulum oscillates back and forth around the equilibrium point. For large velocities, the pendulum describes a circular motion.

E. Homotopy & Homology

Homotopy [25] [58] is defined as a continuous deformation of one continuous function $f(x)$ to another continuous function $g(x)$ without break in topology from shearing and tearing resulting in discontinuities or the formation of holes or gluing resulting from merger of holes that would also result in discontinuous functions. This gives rise to the notion of “essential-sameness” whereby one geometric shape can be continuously deformed into any other without tearing or shearing just like a doughnut can be converted to a mug with one hole via a smooth transformation with continuous deformations. Conversely, the doughnut cannot be converted into a sphere without gluing in terms of merging the space in between and hence such geometric shapes can be considered “essentially-different” as they cannot be inter-converted into smooth functions via continuous deformations as shown in the figure below.[31]

We can describe the formalism in more standard math-



Figure 3. the above figure shows how the geometric shape of a cup $f(x)$ can be smoothly transformed into that of a doughnut $g(x)$ using continuous deformations without any discontinuities or break in topology resulting from tearing, shearing or gluing as both geometric figures begin and end with 1 hole and thus abide by the notion of “essential-sameness” in Topology.

ematical terms as follows: From the above definition and description, we can say that two continuous maps $f, g : X \rightarrow Y$ are said to be "**Homotopic**" if there is a continuous map $H : X \times [0, 1] \rightarrow Y$ such that $H(x, 0) = f(x)$ and $H(x, 1) = g(x)$. We also say that a map $f : X \rightarrow Y$ is a homotopy equivalence if there is a map $G : Y \rightarrow X$ so that $f \circ g$ is homotopic to the identity map on Y and $g \circ f$ is homotopic to f . Two spaces X and Y for which there exists a homotopy equivalence $f : X \rightarrow Y$ are said to be homotopy equivalent. A space that is homotopy equivalent to the one point space is said to be *contractible*. [59] [31]

Definition: Thus we can conclude that for any topological space X , in Abelian group A , with integer $j \geq 0$, there is assigned a group $H_j(X, A)$ which defines the Homotopy.

Functionality: For any A and j as above, and any continuous map $f : X \rightarrow Y$, there is an induced homomorphism $H_j(f, A) : H_j(X, A) \rightarrow H_j(Y, A)$. Therefore, one has $H_j(f \circ g, A) = H_j(f, A) \circ H_j(g, A)$ and $H_j(Id_X; A) = Id(H_k(X, A))$. These conditions are called collectively *functionality*.[55]

Homotopy invariance: If f and g are homotopic, then $H_j(f, A) = H_j(g, A)$. It follows that if X and Y are homotopy equivalent, then $H_j(X, A)$ is isomorphic to $H_j(Y, A)$.[33] [60]

Normalization: $H_0(\star, A) \approx A$, where \star denotes the one point space.

Betti numbers: For any field F , $H_j(X, F)$ will be a vector space over F . Its dimension, if finite, will be written as $\beta_j(X, F)$, and will be referred to as the j -th Betti number with coefficients in F . The j -th Betti number corresponds to an informal notion of the number of independent j -dimensional surfaces. If two spaces are homotopy equivalent, then all their Betti numbers are equal with the following properties:

Property 1: For any topological space X with a finite number of path components, $\beta_0(X)$ is the number of path components.

Property 2: If the first Betti number β_1 of the letter "B" above is two, and for the letter "A" it is one, for any

field F , then in this case, it provides a formalization of the count of the number of loops present in the space. [61] [26]

Homology is defined as a concept in algebraic topology that provides a powerful tool to formalize and handle the notion of topological features of a topological space or of a simplicial complex in an algebraic way. For any dimension j , the j -dimensional “holes” are represented by a vector space H_j whose dimension is intuitively the number of such independent features. For example the 0-dimensional homology group H_0 represents the connected components of the complex, the 1-dimensional homology group H_1 represents the 1-dimensional loops, the 2-dimensional homology group H_2 represents the 2-dimensional cavities and so on.[62] [27] [63]

F. Euler Characteristics & Betti Numbers

The Euler Characteristic is a useful tool in mathematics that is used to classify topological characteristics of various classes of polyhedrons, based only on a relationship between the numbers of vertices (V), edges (E), and faces (F) of any geometric figure.[61]

Mathematically, it can be defined as a number X , such that: $X = V - E + F$ where $V, E \& F$ represents the number of Vertices, Edges & Faces of the polyhedron respectively. The Euler Characteristic can also be represented as: $X = 2(1 - g)$ where $g = X/2 - 1$ is known as the genus of the polyhedron [57] which can be understood intuitively as the “number of holes” in the polyhedron or geometric figure. The genus theorem states for a polyhedron embedded on an orientable closed surface - or the corresponding combinatorial orientated map -, the Euler characteristic $X = V - E + F$ is always an even integer, possibly negative, and that, c being the number of connected components of the polyhedron, its genus $g = c - \chi/2$ is a natural number. In fact, g corresponds to the number of holes in the surface of the polyhedron. When $g = 0$, the surface is without holes, and the polyhedron is said to be planar. When it is also connected ($c = 0$), it satisfies the Euler formula which is a special case of the Euler Characteristic, given by: $V - E + F = 2$; for instance, in the case of a cube that has 8 vertices, 12 edges and 6 faces: $V - E + F = 8 - 12 + 6 = 2$.[54] [50]

However, our special concern for understanding the genus of a polyhedron is its relation to Betti Numbers and Euler Characteristics in Topology. Betti numbers are topological objects which were proved to be invariants by Poincaré, and used by him to extend the polyhedral formula to higher dimensional spaces. Informally, the Betti number is the maximum number of cuts that can be made without dividing a surface into two separate pieces. Formally, the n^{th} Betti number is the rank of the n^{th} homology group of a topological space. Betti numbers can be related to Euler Characteristics of Polyhedrons and their genus via the following mathematical relation.[64] [65] [61]

$$X = \sum_{n \geq 0} (-1)^n \beta_n (\sum) = 2(c - g) \quad (1)$$

where the n^{th} dimensional Betti number β_n is the dimension of the n^{th} homology group $H_n(\sum)$ of the $SC\sum$. These are important metrics that would characterize the topology of the data and would be significant in various steps of our computational pipeline in the following sections.[47] [50] [57] [62] [58]

G. Simplicial Complexes

The concept of Simplicial Complexes [25] [66] are quite essential to Homology that applies to all topological spaces (singular homology) relies on the linear algebra of infinitely generated modules over the ring Z in defining homology groups, and for this reason it is not useful from a computational point of view. Computations can be carried out by hand using a variety of techniques (long exact sequence of a pair, long exact Mayer-Vietoris sequence, excision theorem, spectral sequences), but direct computation from the definition is not feasible for general spaces.[62] However, when one is given a space equipped with particular structures, there are often finite linear algebra problems which produce correct answers, i.e. answers which agree with the singular technique. A particularly nice example of this applies when the space in question is described as a “simplicial complex”. [56] [67]

H. Persistent Homology

Persistent homology [27] [54] [27] can be explained as a method for computing stable topological features of a dataset through evaluating transformations over varying parameters, such as spatial resolutions against point cloud data. It gives a multi-scale view of the topology of a space by capturing the evolution of topology with increasing (or decreasing) resolutions. It is a powerful tool to compute, study and encode efficiently multi-scale topological features of nested families of simplicial complexes and topological spaces. It not only provides efficient algorithms to compute the Betti numbers of each complex in the considered families, as required for homology inference in the previous section, but also encodes the evolution of the homology groups of the nested complexes across the scales.[64] The input data for the computation of persistent homology is often represented as a point cloud. The output is a set of real number pairs (the birth and death times) documenting the spatial resolutions where each topological feature first appears (birth) and when it disappears (death). The pairs are usually plotted either as a set of lines, called bar-codes, as a set of points in a 2D plane, called a persistence diagram, or as a persistent landscape. Most implementations of

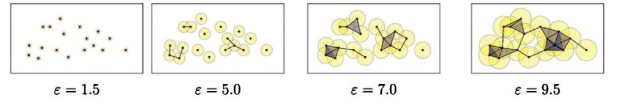


Figure 4. The figure above shows a schematic diagram representing a data cloud, and how the filtration process results in outcomes of various overlapping of balls from different proximity parameters ϵ (shown in the upper column). The bottom column is barcodes scanning through a full-range of proximity parameter ϵ values. β_0 and β_1 denote the 0-dimensional and 1-dimensional Betti numbers, which can be deduced from the subfigures to be roughly $18 \rightarrow 11 \rightarrow 4 \rightarrow 1$, and $0 \rightarrow 0 \rightarrow 1 \rightarrow 2$, respectively.

the persistent homology are done over point cloud data via the Mapper algorithm [2], however the core concept of persistent homology extends past its traditional implementation on point cloud data in ways such as data related to knowledge graphs.[1][62]

Example: We shall now consider a typical example of how Persistent Homology has been implemented thus far in the domain of Topological Data Analytics. So, in order to demonstrate the concept of persistent homology, let us imagine we have collected a bunch of data points that we refer to as a data cloud. For the next step, let us imagine that there is a control parameter called the proximity parameter ϵ , which defines the radius of an imaginary ball centered at each of these data points.[3] [51][68]

Now, when we gradually increase ϵ , the balls will grow outwards and eventually touch other balls. The overlapping of these balls form a unique topological characteristic that is unique to this dataset, and hence we can use this unique topological characteristic to differentiate nuances in the topologies of different point clouds. This filtration process can be demonstrated and visualized in the figure below:[69]

Thus standard practices in TDA use a similar encoding and filtration process, as shown above to convert a point cloud that is made from brain functional signals, or a correlation matrix from examples such as time series data, to filtration diagrams. From these filtration diagrams, we can calculate barcodes, persistence diagrams, and other TDA metrics for further applications of Persistent Homology.[63][27]

Thus, Persistent homology can be explained as a method for computing topological features of a data set (point cloud) at different spatial resolutions. It gives a multi-scale view of the topology of a space by capturing the evolution of topology with increasing (or decreasing) resolutions. It is a powerful tool to compute, study and encode efficiently multi-scale topological features of nested families of simplicial complexes and topological spaces. It not only provides efficient algorithms to compute the Betti numbers of each complex in the considered families, as required for homology inference in the previous section, but also encodes the evolution of

the homology groups of the nested complexes across the scales.[62][27][70] [53]

I. Topological Projection & Isometric Compression of Graphs

The mathematics of projection[32] is defined in terms of a mapping of a set or other mathematical structures such as operations, metrics or topology into a subset (or sub-structure), which is equal to its square for mapping Function Composition which can be mathematically defined as a function $h(x)$ such that $h(x) = g(f(x))$ That is, the functions $f: X \rightarrow Y$ and $g: Y \rightarrow Z$ are composed to yield a function that maps x in X to $g(f(x))$ in Z .[71] Projections can be intuitively explained as casting a shadow of geometric points or objects on a plane or a sheet of paper. For example the shadow projection of a point on a plane or a sheet of paper is the point itself; whereas, the shadow projection of a 3-D sphere is a closed circle which is equal to the square of its mapping function and can be used to obtain the original topology of the 3-D sphere without the loss of essential information.[60]

The mathematical appeal and utility of projection is that it's fundamentally elementary and geometric with a finite number of degrees of freedom; once the acceptance domain and the dimensions of the spaces used in the construction are chosen which allows for easier manipulation of higher dimensional data and applying essential filters and transformation in the domain of TDA. This also helps us to obtain all essential information from high-dimensional data sets while carrying out efficient noise reduction. It also preserves and amplifies the essential nature of such datasets for analysis and obtaining useful insights from its underlying attributes and relationships.[33][20] [21]

In the field of Topology, we mostly work with the special class of point sets obtained by cut and projection from the integer lattice Z^N which is generated by an orthonormal base of R^N . In short we can call a projection method pattern T on $E = R^d$ a pattern of points (or a finite orientation of it) given by the orthogonal projection onto E of points in a strip $(KE) \cap Z^N \subset R^N$, where E is a subspace of R^N and KE is the so-called acceptance strip, a flattening of E in R^N defined by some suitably chosen region K in the orthogonal complement E^\perp of E in R^N . The pattern T thus depends on the dimension N , while also depending on the positioning of E in R^N and the shape of the acceptance domain K . When this construction was first made, the domain K was taken to be the projected image onto E^\perp of the unit cube in R^N and this choice gives rise to the so-called canonical projection method patterns in Topology and TDA that are useful concepts which are essential in establishing a feasible and seamless way to carry out near-lossless topological projections and isometric compression of data-structures represented by DAGs and multi-graphs in this novel approach.[60] [32]

The application of isometric compression of graphs [72] [39] is further useful as the mathematics of Topology allows for unique possibilities that provide methods for creating compressed representations of data sets that retain all features of the original data set via efficient techniques such as Isometric Compression. These represent the various relationships among points in the data set. The representation is in the form of a topological network or combinatorial graph, which is a very simple and intuitive object to work with using graph layout algorithms and allows for the comparative analysis of all essential attributes of the original high-dimensional dataset without loss of essential information. This provides a unique and necessary advantage over standard graphical visualizations and data plots which only address and compare 2 or more limited subset of variables, dimensions or columns of the high-dimensional dataset.[38]

III. PROPOSING A NOVEL APPROACH

In this section we propose a Novel Approach in Topological Graph theory with Roy-Kesselman Diagrams (R-K Diagrams; a terminology derived from the last names of the co-authors of this paper i.e. Animikh Roy & Andor Kesselman) as a useful extension to standardised methods of Topological Data Analysis and Graph Theory Analysis while facilitating smooth transitions between the two techniques as described in the previous sections. The following methodology proposed in this paper, implemented via the computational framework and pipeline are also in consistency with the mathematical formulations and theorems of Topology and Graph Theory which serve as the foundation of this novel approach. The aim of this novel approach is to enable identification, classification, segmentation and simulation of distinct topological data signatures from high-dimensional data-sets consisting of three or more independent variables to enable coordinate-independent, multi-modal analysis of all local (micro) and global (macro) data properties associated to a particular "event"-lens applied to the data-set. This approach also allows for multi-variable machine learning optimization via the measures of distance and similarities between the micro-geometric properties (i.e. nodes, edges, DAGs) using Graph Theory and macro-geometric properties (i.e. simplicial complexes, homology and persistence, betti-numbers, homotopy, isometry and topological invariance) using Topological Data Analysis. Each concept mentioned or introduced in this section will be explored in greater details in the following sections of this paper.

A. Motivation

As mentioned earlier, the motivation for this approach takes root in the appeal of "*Event-Driven Topology*" which is based on the topological clustering of all at-

tributes around a central “Event-Node” that serves as a static (unchanging) context for all dependent attribute clusters. The choice of event nodes are determined by a choice of “Lens”, for example, in the case of the Tableau Super Store Data, a lens could be classified as a purchase event related to an order. Alternatively, a lens could also be changed to represent an entity such as a customer with all associated attribute clusters representing customer data. Such attribute clusters can dynamically evolve in time due to perturbations caused by the influx of data in terms of new/added rows or additional independent attributes in terms of columns driven by ”Hierarchical-Feature-Extractions” with respect to a particular domain Ontology.

B. Objectives

The objectives of our Novel Approach can be summarised as follows:

(1) To build a computational framework based on the mathematical foundations of Topological Graph Theory that allows for the flexibility to switch between graph theory analysis and TDA on all datasets pertaining to physical systems as defined in section 4.2.1 and a subset of non-physical systems with inherent ontology and domain specific knowledge graphs as defined in section 4.2.2.

(2) To provide a novel framework that allows *“Event-Driven” Topological Signatures* based on the choice of lenses as defined in section 4.5.5 along with domain specific node masks and filter functions as defined in section 4.5.2.

(3) To extract hierarchical features from a given dataset as discussed in section 4.4, while linking them to a central ”Event-Node” and to generate a hierarchy that is centred around an event based on the choice of a lens that allow for effective generation of unique *“Event-Driven” Topological Signatures*.

(4) Creating a framework that would allow for the analysis of differences in micro-geometric properties (such as nodes, edges and DAG’s) via graph analysis while allowing for the study in differences of macro-geometric property (such as holes, voids & loops) with the help of *Euler characteristic* and *Betti numbers* as discussed in section 4.5.7.

(5) By generating unique signatures across a set, the R-K Diagrams could be utilized to form a basis for traditional Machine Learning models such as identification, clustering, classification, and segmentation as discussed in section V H 5 in greater detail. The possibilities of applications would only be constrained by the input layer being an R-K diagram (or graph).

IV. COMPUTATIONAL PIPELINE

A. R-K Toolkit

We have built and implemented a generalized software-package called R-K Toolkit [73] to build R-K Diagrams and R-K Models by running R-K Pipelines. The master repository for all the code related to this paper involving the toolkit, pipeline, diagrams and implementation case-studies can be found on https://github.com/animikhroy/rk_toolkit_pipeline_diagrams, which has been made publicly available for building extensions and review purposes. The R-K toolkit package serves as a computational framework to build a component called an R-K Pipeline (described in sub-section: IV C), and can be found open sourced, at https://github.com/andorsk/rk_toolkit. It is a is a generalized code package implemented to aid users in the process of building “R-K Diagrams” and “R-K Models” via the “R-K Pipeline”. It provides a computational framework to build a functional component called the R-K Pipeline, which can be used to transform any NxM Tensor with 3 or more independent physical/ontological variables, into a R-K Model. An “R-K Model” is then processed with domain appropriate “Range-Filters” and “Leaf-Linkers” to render unique topological signatures and graph visualizations that are known as R-K Diagrams.

The R-K Toolkit was built in python, and converts the core mathematical concepts described in this paper into computational representations that can be used on real data. Similar to how other libraries such as Sci-Kit [74] provide base components like the Pipeline object [75], to be extended later by a user or by native extensions, R-K Toolkit operates similarly by providing the base building blocks such as a R-K Pipeline and R-K Diagram, to be extended by the user or by native representations. As an example, if one were to want to classify a Hodgkins vs. Non-Hodgkins disease along with their 4 stages of metastasis as distinct topological signatures that are divergent from healthy patients, one could construct their own R-K Pipeline out of the toolkit, to potentially generate unique topological structures and R-K Diagrams. The R-K Toolkit’s design was done explicitly with the intent to be extended later, with the expectations that new and more robust methods will be included into framework over time. Any computation carried out using the R-K Toolkit leading to a set of actions to build and generate R-K diagrams can be defined as the **R-K Workflow**.

The R-K Toolkit provides many advantages over starting from scratch. We submit that there are 9 main advantages to using the R-K Toolkit for building future models.

1. The R-K Toolkit provides in build validation for components, such as adherence to a DAG and valid transforms
2. A pipeline framework is provided to chain steps to-

gether with accordance to the computational steps to be described below

3. Visualization's are provided to assist with rendering of R-KModels and converting them into R-KDiagrams.
4. Pre-built transforms provide baseline transforms for testing
5. Various Optimizations and Machine Learning implementations will be present in the R-KToolkit for various use cases
6. Built in mechanisms to provide inverse operations
7. Our toolkit allows for plug and play of well defined domain ontologies pertaining to knowledge graph or custom ontologies pertaining to a structured dataset
8. This framework can be extended to include many datasets as long as it conforms to the data requirements
9. The R-K Pipeline is built in such a way that it could in theory support streams for real time classification and identification use cases, however future work would be required to update this feature in further details.

To apply the toolkit to a dataset, one would import the relevant components into their code (similar to how you would Sci-Kit), define a R-KPipeline, and then run the pipeline. It is entirely in the control of the user *how* they desire to build their pipeline as most pipelines will vary across domains and data. The intent with this paper, and with the core concepts of the R-K Pipelines, are that despite the divergence of implementations, the foundational building blocks of an R-K Pipeline will always remain the same.

We acknowledge that this is the first implementation of the R-K toolkit, but it has shown good promise with useful results on the below use cases, but future work is required to make it more robust for it's application across different domains.

1. R-K WorkBench

To help users get started quicker, we provide a docker image called R-KWorkbench [76], which wraps the ML-Workspace [77] with packages relevant to building R-KDiagrams built into the core image. The README file details how to use it for the purpose of independent use by researchers and programmers.

B. Data Qualification Criterion

Let us now address the data qualification criteria and its associated constraints for the R-K pipeline that would allow for the accurate execution of our analytical framework pertaining to "Event-Driven" Topological Graph Analysis. In this approach, we shall not be addressing the study of unstructured point-cloud data as addressed in the traditional TDA frameworks of the past [2] [26] [20] but focus on a subset of data with well-defined hierarchical features that can be extracted automatically as a part of this pipeline and linked to the corresponding inter-dependencies of columns and rows in relation to the chosen context for the purpose of segregation (ref:4.5.5) and classification of meaningful events and entities within such data-sets.

We start by defining $D_i(\forall i \in N)$ as the input dataset to the R-K Toolkit; where $M_j(\forall j \in N)$ is a measure within the dataset. For example, Mass and Spin are measures on the LIGO dataset.[7] Then for any such dataset D_i containing M_j measures to be accepted into the R-K Model Framework, it must adhere to the following constraints:

- It must be able to derive a hierarchy of relationships between measures such that the Dendogram of hierarchy H describes how one measure relates to another.
- It must be able to segregate independent variables and their corresponding dependencies in separate attribute clusters of the "Event-Node".
- It must have at least 3 mutually-independent variables pertaining to the well-defined attributes of "Physical Systems" & "Non-Physical Systems" as detailed below.

1. Physical Systems

The Datasets pertaining to "Physical Systems" must contain at least 3 *mutually independent variables* related to the 7 Fundamental Quantities of Physics [78] to meet the minimum criteria for generating an R-K Diagram in accordance with consistent Topological Properties that can be distinguished using appropriate filtering & divergence criteria.

In physics, a physical system is a portion of the physical universe chosen for analysis. Everything outside the system is known as the environment. The environment is ignored except for its effects on the system. Any system defined in the realm of science and engineering can be referred to as a physical system with independent variables that have the following fundamental dimensions: *mass, length, time, temperature, electricity, luminous intensity & count/amount of substance/matter*. [23] An example of hierarchical clustering using the well defined relationships of dependent and independent variables pertaining

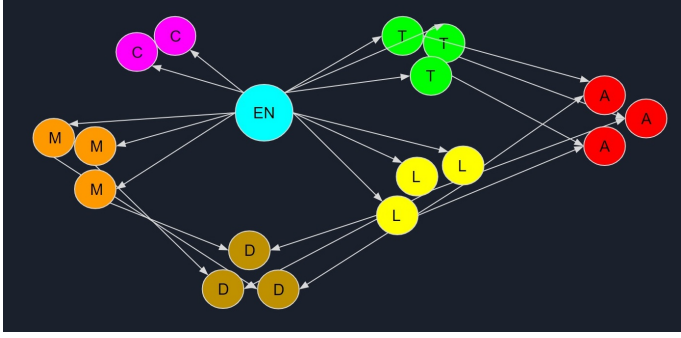


Figure 5. The above structural graph represents an unfiltered R-K model, where EN stands for the central Event Node based on the choice of an arbitrary lens representing a physical phenomenon or entity. T, L, M & C Represent the mutually-independent clusters of Time, Length, Mass and Charge. A & D represent the derived/dependent clusters of Acceleration and Density respectively.

to physical systems is shown below with respect to a fundamental structural graph in the R-K model framework, which can be filtered specifically to obtain unique event-driven R-K Diagrams.

2. Non Physical Systems with Knowledge-Graphs

The Data-sets pertaining to “Non-Physical Systems” must contain a well-define Knowledge Graph related to a specific domain Ontology that contains parent nodes with 3 or more mutually independent attributes to meet the the minimum criteria of generating an R-K Diagram in accordance with consistent Topological Properties that can be distinguished using distinct Divergence criteria.

Such independent attributes should allow for the classification and separation of variables based on direct or derived relationships with fundamental physical dimensions and associated independent variables such as:

E.g. Age of a person can be separated as a time variable while the weight of the person is a derived from the independent mass variable and the height of that person can be separated as a length variable. All other attributes have a secondary/ derived dependence on the fundamental independent variables. However, the R-K Pipeline would allow for the addition/classification of any additional domain specific independent variables based on a specific domain ontology relevant in a non-scientific commercial use-case such as in the case of the Tableau Super Store Data-set.[79]

3. Derived Relationships

Derived relationships are relationships that are determined by the data itself, and are learned during analysis. For example, it may be possible to derive an ontology from physical system consisting existing fundamen-

tal measures such as mass, time, and length in order to obtain derived measures such as force, momentum, and acceleration.

4. Data Assumptions

A directed relationship exists between metrics M such the formula $\text{Edge}_{M_i \rightarrow M_j}$ would describe a directed relationship between M_1 and M_2 . For the approach to be effective, there exists some combinations of filter and linkage functions, such that optimized they can segregate topological structures.

Furthermore, it is assumed that there exists a method to compare two variables (i.e over distances). Practically, this means all data needs to have some numeric based encoding to be compared.

5. Limitations

Such as described by the Section 4.2 in Data Criteria, this imposes the following limitations on data fed into the pipeline:

Low dimensional data, with less than 3 independent dimensions will not be compliant with the data criteria and are not suitable for this approach. Three mutually independent dimensional attributes are required to make simplicial complexes and add structure of the data and so lacking rank would impact the structure. Additionally, data with unclear relationships between measures may be less effective than data with clear relationships between measures because a lot of the power of the R-K Models come from a hierarchical embedding, which if unclear, limits the ability for the models to perform as they should.

As an example, in the Iris dataset [80], all measures are built off the fundamental quantity: length. In spite have 4 columns (sepal width, sepal length, petal width, petal length), all columns are inter-dependent and are not mutually independent and therefore cannot be clustered into separate independent attributes of the central iris event node, other than length, thereby resulting in non-unique Topological signatures and the failure to generate R-K Diagrams.

6. Ontology

In the figure below, we describe a dendrogram with a specific ontology. An ontology in the context of an R-K Model, describes the relationship between two or more measures in the form of a hierarchy. Ontological frameworks have numerous advantages, such that it makes domain assumptions on data explicit and/or to share a common understanding of structural information across metrics. [81]. The ontology can either be learned such as with the Mahria et. al paper titled *A novel approach*

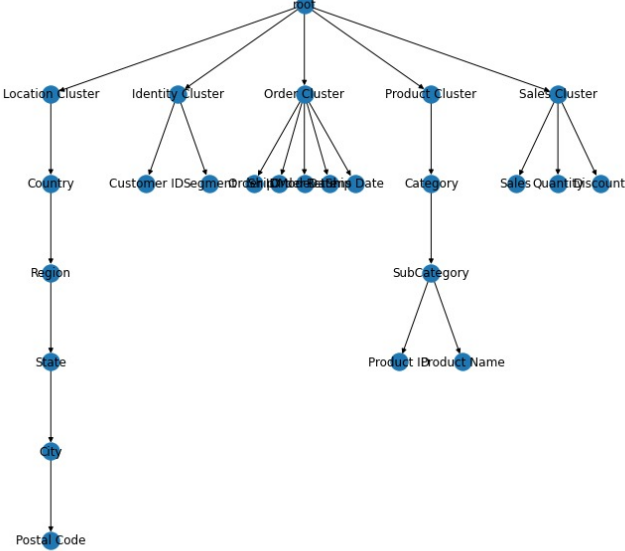


Figure 6.

for learning ontology from relational database: from the construction to the evaluation or formalised by domain experts [81]. There are numerous ontological databases available for describing relationships between known domains. The Web Ontology Language (OWL) is a specific set of web standards and language devised to standardize ontology through *OWL Documents*. [82].

In the figure below, we define a strict ontology in the store sales data. This provides the basis on which all R-K Models are formed. Any R-K Model must have some strict ontological backbone, such as the below, and compliant with data assumptions in 4.2.4 to be valid.

C. R-K Pipeline

The foundational component of any R-K Diagram is an R-K Pipeline. At a base level, the R-K Pipeline can be understood as a Directed Acyclic Graph (DAG) as defined in section 2.3.1, which provides transformational components that result in an composite model we call an R-K Model. Transforms in an R-K Pipeline can be chained against each other, as long as egress from one component complies with the ingress specifications from another component. We can mathematically represent this with the following representation: $\{C_0, C_1, C_2, \dots, C_n\} \in RK_i$ where C_i represents a pipeline component and the egress of C_i is compliant with a set of constraints imposed by C_{i+1} 's ingress.

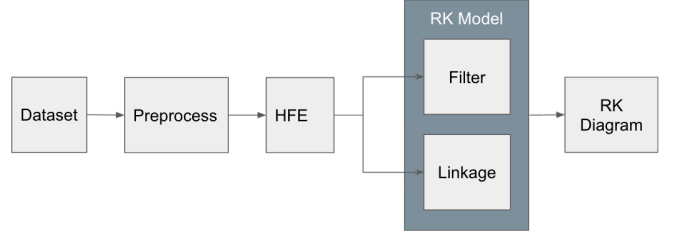


Figure 7. The above represents a simplest R-K Pipeline. In this pipeline, data first gets preprocessed, then moved to a Hierarchical embedding function. From the hierarchy, the standard filters and links provide an R-K model. It is then forked between a compression node and a visualization node. Thus the end result is two R-K Diagrams, one compressed version and one raw version

D. Hierarchical Embedding Function

As discussed in Section 4.2.6, there must exist an explicit ontology related to the measures of the dataset. Let us describe D as the input dataset to the RL Toolkit. Let us describe m_i as a measure within the set of measures M such that $m_i \in M$. To be compliant with this proposed framework, there must exist an ontology O that describes the relationship of the measures w.r.t each-other. For example, w.r.t location data, an ontology could present that a m_{city} is a child of m_{state} which is a child of $m_{country}$. In the datasets that were analysed, we often provided an ontology which merged similar measures into the same “cluster”, for example $mass_1$ and $mass_2$ were ontologically defined as part of the *Mass* cluster in our LIGO analysis. In the Tableau Super Store Sales Dataset, we defined a custom ontology that we used for our representations. Using the R-K toolkit, one can either use pre-defined ontologies or provide custom ontologies for their data.

An Hierarchical Embedding Function (f_H) generates a graph G from a set of measures M such that the resulting graph G , is a DAG which represents a bijective mapping between $m_i \longleftrightarrow G_i$ such that all $V_i \in G$ can be traced back to the original value in the dataset, where V is a vertex. More succinctly, $f_H(M) \rightarrow G$ such that $f_H(G_{v_i}) \rightarrow m_i$ and $f_H^{-1}(G_{v_i}) \rightarrow m_i$. The advantage of this requirement is that any structural graph can be inverted back into original measures used to generate the graph.

Across the pipeline, the graph generated by H_f is referenced as a *Structural Graph* (S). The structural graph provides the baseline ontological structure that forms the basis for all other transformations in the pipeline.

Computationally, to maintain the bijective mapping, we maintain internally a history of steps applied during the transformation such that we can easily provide the inverse function by returning the steps in reverse.

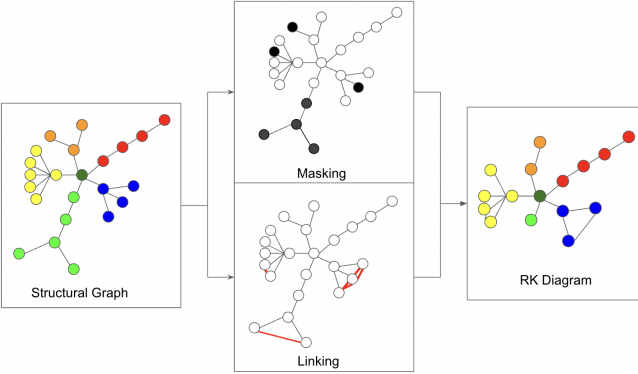


Figure 8. The above image represents the building blocks of an R-K Model. To the left, a structural graph, which is defined in 4.7.1. In the middle, filters and linkage functions are applied resulting in the final R-K Model. The R-K Diagram is simply a rendering of the model

E. R-K Model

The R-K Model is the basis for any R-K Diagram. It represents the composite object that can be used to render an R-K Diagram. In that sense, an R-K Diagram the rendering of an R-K Model, and the R-K Model underlying data-structure for that render.

All R-K Models contain the following 3 components: Structural Graph, Node Masks, and Derived Links

Each component is described in detail below.

1. Structural Graph

The structural graph (S) is the base graph derived through the Hierarchical Embedding Function, also known as the structural graph. The structural graph provides the baseline ontological structure that forms the basis for all other transformations in the pipeline.

Because node masks are reductive operations, the number of nodes in the structural graph represents the *maximal number of nodes in the R-K Diagram* such that $|nodes| \in S \geq |nodes| \in R - KDiagram$. The structural graph however does not represent that maximal number of nodes. The number of possible edges in the R-K Diagram is bounded by the number of combinations of nodes in the structural graph.

The R-K Filters (described below), can bound the possible combinations of edges to less than the number in the original combinatorial graph.

In the case below, we demonstrate two forms of structural graphs. The first is the initial structural graphs that were derived off the Store Sales data outlined in the next section. The second structural graph is built off of similar data, however some nodes were expanded out. Both are viable candidates for structural graphs.

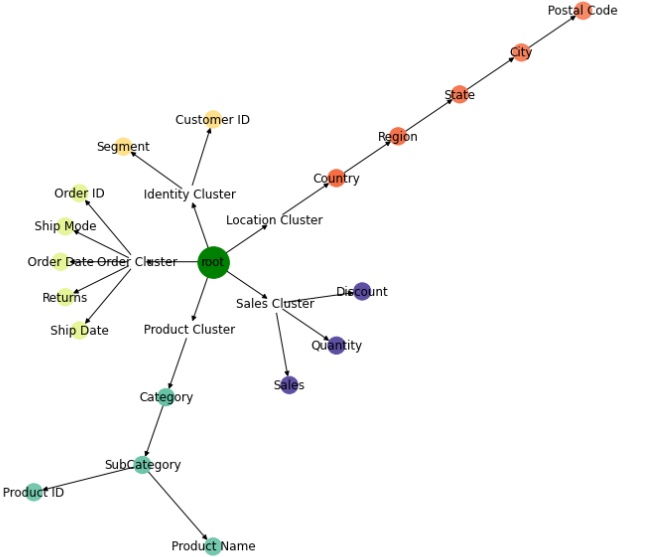


Figure 9. The base structural graph of the Store Sales Data

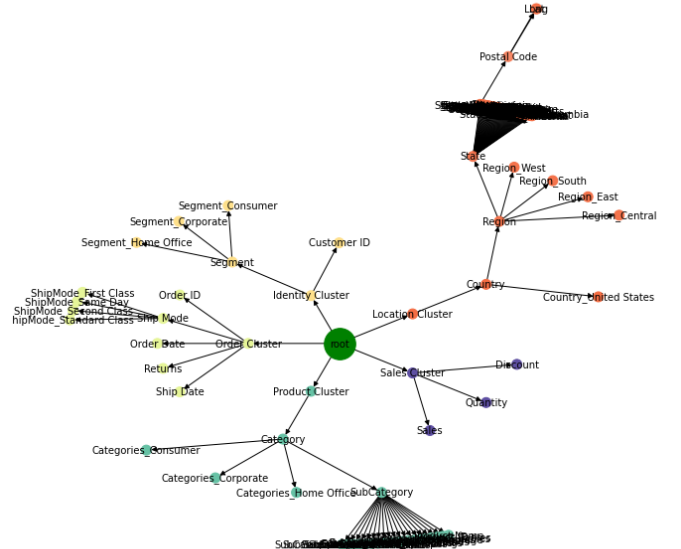


Figure 10. An expanded structural graph

2. Node Masks and Functions

A node mask represents a masking structure that when applied to a structural graph S , reduces the number of nodes into a subgraph S' . The node masks are binary operators, which when set to *true*, filter a node and its direct children.

To derive the node masks, we produce a set of fil-

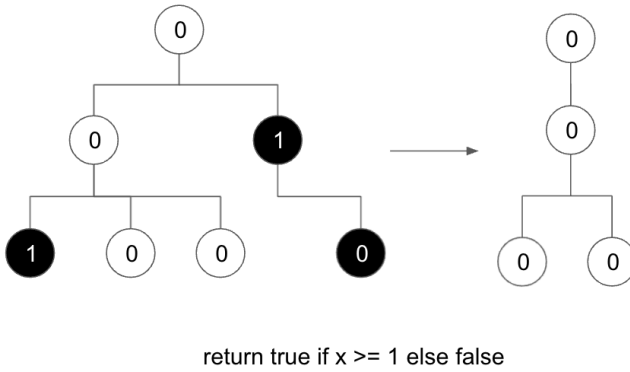


Figure 11. An example node masks with a filter of $z = 1$. All nodes and children of the nodes are removed that have a value $z = 1$ and applied at the root level. Different filters can be applied to different subgraphs.

ters $F_n(G)$, which takes in a graph and returns a mask. We define Filter Functions w.r.t. Simplicial Complexes formed by a combination of nodes and edges, such that filtration of a simplicial complex K is a nested family of subcomplexes $(Kr)_{r \in T}$, where $T \subseteq R$, such that for any $r, r' \in T$ if $r \leq r'$ then $Kr \subseteq Kr'$, and $K = Ur \in TKr$. The subset T may be either finite or infinite. More generally, a filtration of a topological space M is a nested family of subspaces $(Mr)_{r \in T}$, where $T \subseteq R$, such that for any $r, r' \in T$, if $r \leq r'$ then $Mr \subseteq Mr'$ and, $M = Ur \in TMr$. For example, if $f : M \rightarrow R$ is a function, then the family $Mr = f^{-1}((-\infty, r]), r \in R$.

In the pipeline, one can combine multiple filter functions together. The union of the filters provide the final node mask, such that $F_n(G) \cup N_m$, where N_m is the node mask.

3. Linkers

In order to define linkages we must begin with the following mathematical consideration. Let $G = (V, E)$ be an undirected graph without multiple edges or loops. Let $n = |V|$ and $e = |E|$. The linkage of G is defined to be the maximum min-degree of any of the subgraphs of G (the min-degree of a subgraph is the least degree of any of its vertices; the degree of a vertex is taken relative to the subgraph). The width of G is defined to be the minimum, over all linear orderings of the vertices of G , of the maximum, with respect to any vertex v , of the number of vertices connected with v and preceding it in the linear ordering. It has also been mathematically proven in Topology that the width of a graph is equal to its linkage.

Furthermore, according to the French Mathematician Erdős, it has been proven that every graph G has a subgraph with min-degree at least equal to the density $[e/n]$ of G . Therefore, the density is a lower bound for the link-

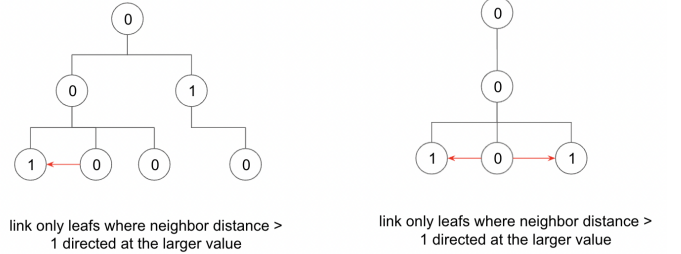


Figure 12. Example of a linker function. The same linker function are applied to two different graphs, providing directed edges across leafs.

age (equivalently, width) of graphs with given numbers of edges and vertices. Given a positive integer j , if in the definition of width we consider not the number of vertices preceding and connected with v but rather the least number of vertices preceding and connected with any cluster of at most j consecutive vertices extending to the right up to v , we get a graph parameter known as j -width.

4. Linkage Math

Let be a layout of a graph $G(V, E)$, i.e., a linear ordering v_1, \dots, v_n of its vertices. The width with respect to v_i of a set S v_i^{-k+1}, \dots, v_i of k consecutive vertices (notationally $\text{widthl}(S)$) is defined to be the number of vertices $\{v_1, \dots, v_{i-k}\}$ in the set adjacent to vertices in S ($1 \leq i \leq k \leq n$). Informally, the width of S with respect to v_i is the number of vertices preceding S and adjacent to elements of S .

Informally, the width of S with respect to v_i is the number of vertices preceding S and adjacent to elements of S . Now, let j be an integer such that $1 \leq j \leq n$. The j -width of a vertex v with respect to v_i is the least width of any set of at most $\min(i, j)$ consecutive vertices extending to the right up to v_i , i.e.,

$$j - \text{widthl}(v_i) = \min\{\text{widthl}(v_i - k + 1, \dots, v_i) : k = 1, \dots, \min(i, j)\}$$

The j -width of G with respect to v_i is defined to be the maximum of j -widthl(v_i) over all vertices v_i of G .

The j -min-degree of a subgraph H of G is the minimum ext-degreeH(S) over all sets S of vertices of H with $1 \leq |S| \leq j$. Obviously, the 1-min-degree of a subgraph is the least degree of its vertices. The j -linkage of G is the maximum j -min-degree of any subgraph of G . Obviously, the 1-linkage of G is the maximum min-degree of any of its subgraphs. The 1-linkage of G is simply called the linkage of G . Furthermore, it has been proven mathematically that for any graph $G(V, E)$, the j -width of G is equal to its j -linkage.

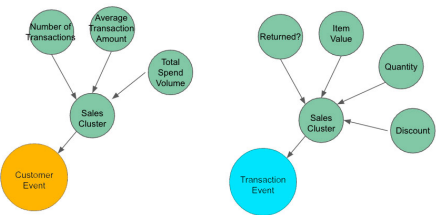


Figure 13. The diagrams above show the effect of the lens on the structural graph. To the left, a lens is chosen from a specific “Customer” event. To the right, a lens is chosen from a “transactions” perspective. The values and metrics associated with each lens are related to the respective lens.

5. Choice of Lens

The choice of lens is critical for the basis of ontology and the R-K Model. Is it the lens at which an “event” is determined from, such that “Lens” defines the root node such that all branching nodes and the hierarchy are birthed from the choice of lens. As an example, in the store sales data, there may exist many lenses, such as a Customer lens, or a Transaction lens. Each lens would provide unique events associated with such events, with different structural graphs as the foundation for each R-K Diagram.

6. R-K Diagram

An R-K Diagram is the render of an R-K Model. Given an R-K Model, an R-K Diagram renders the R-K Model in 2 or 3d space. As an R-K Model is multi-dimensional representation of data, an R-K diagram can display many dimensions in 2D, without data loss that a typical projection model would have.

We tend to use a radial layout for our demonstrations, but any graph layout can be used, with a preference toward deterministic layouts. We prefer deterministic layouts, because it allows easier qualitative comparisons of R-K Diagrams and their differences. Figure 14 demonstrates the deterministic layouts of R-K Diagrams.

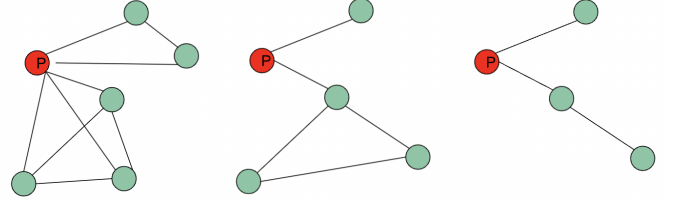


Figure 14. In the R-K Diagrams above, we use a deterministic layout which makes it easier to spot the differences between R-K Diagrams based on visual features

7. Betti Number Analysis for Macroscopic Topological Classification

In this paper, we have only explored topological similarity and divergence measures that are calculated with respect to a combined study of nodes, directed edges, properties of DAGs and corresponding Topological distance measures between any 2 R-K diagrams. However, the R-K pipeline and R-K models are built in a way to allow for the smooth establishment of homotopy equivalence between any 2 well defined spaces unlike point cloud data where such equivalence is not established by default. Hence, this allows for effective ways to compute the number of independent j -dimensional surfaces for higher dimensional embeddings on R-K diagrams in Phase-Space.

This would in turn also allow for smooth ways to drive and obtain the j -th Betti Numbers which would lead to a formalised method to count the number of loops present in unique event-based topological signatures. Thus new metrics can be established to compute and classify the global macroscopic properties of R-K diagrams, thereby leading to the quantification of additional parameters for machine learning templates which bring about further enhancements to the R-K pipeline for the classification and segregation of different R-K diagrams with more distinct divergence measures.

F. Measuring R-K Distance

Critical to the tuning and understanding of R-K Diagrams is the ability to quantitatively measure distance (and in the dual, similarity) across R-K Diagrams. There is a plethora of existing research that has been done on understanding topological and graph distances in Phase Space. For example, in Hilaga et. al, they analyzed a Reeb graph, and using TDA, computed the geodesic normalized distance, where the geodesic distance of a surface from the formula $\mu(v) = \int_{p \in S} g(v, p) dS$ where $g(v, p)$ returns geodesic distance of points u and v on a mesh. [83]. This approach was not well suited for our analysis, because we do not create a mesh in an R-K Diagram, however demonstrates one of many potential ways to compare topological structures against each other.

Another approach by Máté et. al use multiple approaches in *A topological similarity measure for proteins*, in which they use a geometric approach using the Jaccard distance and Hausdorff distance based on the bar-codes used in persistent homology. [84]. Various other appropriate metrics exist that we will not cover in this section but refer to in the citations. [85] [86]

In our implementation, we used a weighted distance function $d(G_1, G_2) \times w$ by applying composite distance function based on geometric and value distance, where the geometric distance was implemented over a Jaccard distance based upon nodes and edges, and the value distance was computed using the Mahalanobis distance similar to Salleh et. al[87]. The final distance equation can be supplied through the following:

$$D(G_i, G_j) = f(T, V) \times w \quad (2)$$

where $f(T, V)$ is a composite function based on topological distance T and value distance V weighted by vector w .

Our approach was inspired by Máté et. al's geometric measures and after concieving of such a method, later found Salleh et. al's using Mahalanobis distance with Jaccard's distance in the paper that validated a simliar approach in *Combining Mahalanobis and Jaccard Distance to Overcome Similarity Measurement Constriction on Geometrical Shapes* [87], in which they combined Mahalanobis and Jaccard distance in a weighted average to provide similarity measures across metrics.

1. Topological Distance

As mentioned in Measuring R-K Distance section, we used an extension and modification of the Jaccard distance to provide the geometric distance across R-K Diagrams. The Jaccard distance is one of many possible distance functions that can be applied toward graph distances. It is simple but effective in many machine learning algorithms and is a widely applied algorithm across many domains. [88]. The formula can be described as:

$$J(A, B) = \frac{|A \cap B|}{|A \cup B|} \quad (3)$$

where A and B are a tuple that represents an edge $V_i \rightarrow V_j$ that V_i is the source node and V_j is the sink.

To be appropriate for the R-K Diagrams, it is critical to evaluate the Jaccard distances against the *directed edges*, such that the distance measure is sensitive to topological differences due to direction. If a Jaccard distance is applied only at the vertex level, key information about the directed edges and the linked vertexes would be lost. This would be ineffective in the R-K Diagram approach hence we utilized Edges for Jaccard measurements, such that critical features in the distance measurement are preserved.

2. Value Distance

The value distance is intended to amplify the effects of the distance measure when topology isn't sufficient to demonstrate differences. For example, in the case of store sales, a purchase could be very similar topologically, but very different in terms of magnitude as the actual sales value differ radically across R-K Diagrams. By comparing the magnitude of the nodes as well as the topology, it provides a clear distinction when topological differences are not sufficient.

There are various methods to compute the value distance that can be effective. Salleh et. al use the Mahalanobis distance as a method to measure the "Value Distance" of a graph. We applied the Mahalanobis distance to provide the distance mesaure. Mahalanobis can be computed by the formula: [87]

$$d_{MH}(G_1, G_2) = \sqrt{(\bar{x} - \bar{y})^T \Sigma^{-1} (\bar{x} - \bar{y})} \quad (4)$$

where: \bar{x} and \bar{y} are the means of the data, $(\bar{x} - \bar{y})^T$ is the transposed of the differences of the mean and Σ^{-1} is the inverse covariance matrix.

We compute the Mahalanobis distance across the entire dataset, and then normalize the values to between 0 and 1 such that we are bound between [0, 1] pre-weighting.

3. Combining the values into a composite distance score

We finally combine the Value Distance and the Topological Distance into a composite distance score by the function:

$$D(G_i, G_j) = f(T, V) \times w \quad (5)$$

where T and V are bound by the range [0, 1] and $\sum w = 1$. This provides us a final distance score in the range [0, 1]. This can be expressed by the following:

$$D(G_i, G_j) = \frac{\sum_{i=1}^n x_i w_i}{\sum_{i=1}^n w_i} \quad (6)$$

[87]

Where

$$\sum_{i=0}^n w_i = 1 \quad (7)$$

4. Similarity

As our results are normalized between 0 and 1, we can compute the similarity as the dual of the distance, such that $Sim(G_i, G_j) = 1 - D(G_i, G_j) = 1 - f(T, V) \times w$.

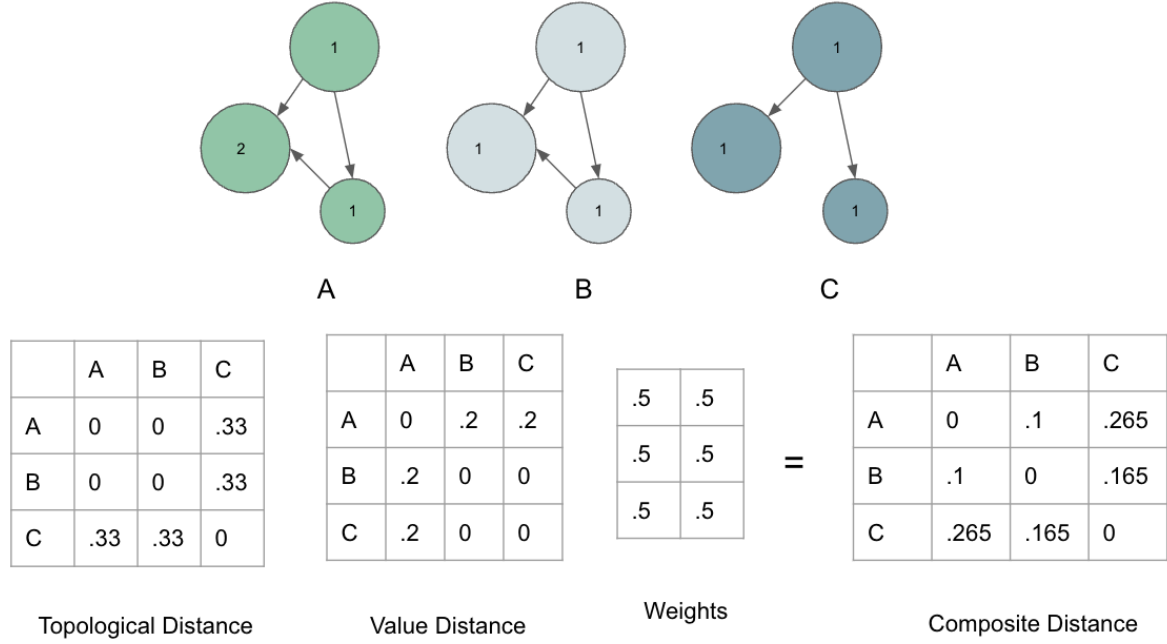


Figure 15. In the top row, all three diagrams have the same topologies but very different values. The value function, encodes this as an important piece of information when comparing the distance of the diagrams between each-other. On the bottom, the bottom left is more topologically similar to the middle such that the cost topologically to the center is 0 where the cost of the bottom right would be greater than 0 because there is a missing edge.

G. Future work on distances

We acknowledge that there is still much research that can be done to improve our distance models and provide more robust measures for R-K Diagram comparisons. The proposal in the above sections outline a starting point for future research.

1. Homotopy & Persistent Homology of R-K Diagrams

The Hierarchical Embedding Function (f_H) of R-K diagrams always ensures that it generates a graph G from a set of measures M such that the resulting graph G , is a DAG which represents a bijective mapping between $m_i \longleftrightarrow G_i$ such that all $V_i \in G$ can be traced back to the original value in the dataset. This is also consistent with respect to ontological relationships between dependent and independent variables which form the basic simplex clusters of our fundamental structural graphs - G . The advantage of this requirement is that any structural graph can be inverted back into original measures used to generate the graph. Now, since the structural graph provides the baseline ontological structure that forms the basis for all other transformations in the R-K pipeline.

Hence, it ensures that all R-K models consistently

render R-K diagrams that are Homotopic with respect to their topological properties and would allow for the smooth computation of persistence diagrams between topologically similar R-K diagrams such as the topological signatures of BH-BH mergers or NS-NS merger signals from LIGO data. These signatures would preserve the same global topological properties of invariance and persistence under continuous deformations of shape, due to the well defined nature of simplicial complexes consisting of interconnected DAGs which eventually give rise to the fundamental structural graphs of all R-K diagrams. Thus it could be quantified both mathematically and computationally and explored as a part of future research on the study of Homotopy & Persistent Homology of different R-K Diagrams.

2. Isometric Compressions, Inverse Function, and Decompression

With R-K Diagrams, we employ isometrically compressible techniques which maintain state change history to provide compression and decompression functions. The compression techniques must be lossless. We can define a compression function $C(G)$, that given a graph returns a compressed version of the graph G' where the number of nodes and edges is equal to or less than G .

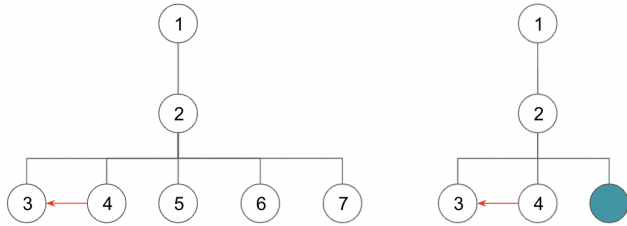


Figure 16. We employed a simple compression model. In this example, nodes 5,6, and 7 are compressed into a single node.

We restrict compressible techniques to require an inverse function, such that $G! + \nabla G = G$. This is critical for the ability to transition between levels of compression.

Because an R-K Diagram can represent a projection that can display many dimensions in 2D space, compression of the R-K Diagram also isometrically projects the diagram into a lower dimensional space, however the visualization can still be visualized at the same space.

Graph compression models have been well evaluated in academia. For example, Gelbert et. al, [89] explore various compression techniques focused on semantic compression, based on: degree, a parameter Beta (which weighs neighbourhood of a cluster), paths, an algorithm called KeepOne and KeepAll, and redundant vertex elimination. [89]

In the first version of the R-K Toolkit, we have shown a limited implementation of graph compression via a 1 degree leaf compressible technique, which compresses all 1 degree leafs into a single leaf branching from the parent node. The steps are maintained internally so that the G can be reconstructed from $G!$. We intend to extend the compressible techniques to others, including those implemented in the Gilbert et al. paper, but did not in the interest of executing the first completed version of the pipeline.

H. R-K Pipeline: Extensibility & Flexibility

The R-K Toolkit and concepts explored in the implementation are a general framework and way of thinking about the data, not a specific implementation. However, each component is intended to be implemented in a way that can be optimized for a particular domain and use case.

V. CASE STUDY: SUPER-STORE SALES DATA ANALYSIS

In order to first demonstrate a generalised application of the *R-K pipeline*, *R-K toolkit* and *R-K WorkBench*, we chose to apply our computational framework on a popular non-physical commercial dataset, that serves as a

benchmark for standardization of various analytical tools and softwares in the domains of Data-Science & Big-Data Analytics. Therefore we shall show the implementation & applications of our generalised R-K Pipeline to a standard super-store sales dataset released by Tableau.[79] This dataset was chosen for **3 primary reasons**:

1. Since the initial analysis was done on LIGO data, we decided to choose an unrelated and orthogonal dataset to prove that the core concepts of the R-K workflow can traverse across domains. The R-K Diagrams are meant to be generalizable across many domains and we wanted to prove it was possible.
2. Store sales require less domain knowledge for demonstration purposes. This makes it an easier dataset to teach the core concepts.
3. It is a widely applied in research and is extremely accessible. A snapshot of the dataset along with the relevant columns for our pipeline is shown in figure 17 for reference and can be matched to the one released by Tableau.[79]

The corresponding code along with our analytical framework and its applications on this dataset can be found on Github. Our results show that we can generate distinct topological signatures for each transaction event, and that the encoding provides descriptive properties that standard distance evaluation methods would not capture.

A. Data Description

The data for store sales consisted of the following information: [8]

- Location Data for where the transaction occurred, in the form of country, region, state, city, and postal code.
- Identity information such as customer id and segment id.
- Information on the order such as the shipment type, returns, shipment date, and shipment mode.
- Product information for the line item, specifically the category, sub category, product id, and product name
- The information of the sale of the line item: sales, quantity, and discount

The data is synthetic data. All data was merged together into a single data-frame within python. The head of the contents can be found below, post merge. The dataset has 9994 entries. A basic description of the numeric entries is available at figure 18. The non-numeric

1	Customer Name	Customer ID	Segment	Order ID	Returns	Order Date	Ship Mode	Ship Date	Sales	Quantity	Discount	Profit	Category	Sub-Category	Product ID	Product Name	Country	Region	State	City	Postal Code
2	Claire Gute	CG-12520	Consumer	CA-2015-102169-No	2015-08-11	Second Class	2015-08-11	261.96	2	0	419.136	Furniture	Bookcases	FUR-FU-10001	Brick & Mortar	United States	South	Kentucky	Henderson	42420	
3	Cliff	CG-12520	Consumer	CA-2015-102169-No	2015-08-11	Second Class	2015-08-11	731.84	3	0	219.822	Furniture	Chairs	FUR-FU-10001	Hot Desk Fab.	United States	South	Kentucky	Henderson	42420	
4	Darin Van Huff	DV-13045	Corporate	CA-2015-108869-No	2015-08-12	Standard Class	2015-08-16	14.62	2	0	6.9714	Office Supplies	Labels	OFF-LA-100003	Self-Adhesive A4	United States	South	California	Los Angeles	90006	
5	Sean O'Donnell	SO-20335	Consumer	US-2015-109991-No	2015-10-11	Standard Class	2015-10-18	957.5775	5	0.45	-383.031	Furniture	Tables	FUR-TA-100003	Berford CR450X	United States	South	Florida	Fort Lauderdale	33311	
6	Sean O'Donnell	SO-20335	Consumer	US-2015-109991-No	2015-10-18	Standard Class	2015-10-18	22.368	2	0.2	2.5164	Office Supplies	Storage	OFF-ST-100007	Eldon Fold 'N' Go	United States	South	Florida	Fort Lauderdale	33311	
7	Brosina Hoffman	BH-11710	Consumer	CA-2014-115812-No	2014-05-09	Standard Class	2014-06-14	48.86	7	0	14.1694	Furniture	Furnishings	FUR-FU-10001	Eldon Expresso	United States	West	California	Los Angeles	90032	
8	Brosina Hoffman	BH-11710	Consumer	CA-2014-115812-No	2014-06-09	Standard Class	2014-06-14	7.28	4	0	1.9656	Office Supplies	Art	OFF-AR-100028	Newell 322	United States	West	California	Los Angeles	90032	

Figure 17. A Snapshot of the Tableau Super-Store Sales Dataset with the relevant columns which have been modelled via the R-K Pipeline

data is preprocessed and encoded into numeric data in the preprocessing step as described in subsection V D.

	Sales	Quantity	Discount	Profit	Postal Code
count	9994.000000	9994.000000	9994.000000	9994.000000	9994.000000
mean	229.858001	3.789574	0.156203	28.656896	55190.379428
std	623.245101	2.225110	0.206452	234.260108	32063.693350
min	0.444000	1.000000	0.000000	-6599.978000	1040.000000
25%	17.280000	2.000000	0.000000	1.728750	23223.000000
50%	54.490000	3.000000	0.200000	8.666500	56430.500000
75%	209.940000	5.000000	0.200000	29.364000	90008.000000
max	22638.480000	14.000000	0.800000	8399.976000	99301.000000

Figure 18. Summary of the Store Sales Data

B. Objective of Analysis

The objective of the analysis was to localize and generate R-K Diagrams that provide unique and descriptive topological signature for the data in the form of an R-K Diagram. Through the R-K Pipeline, these structure would preserve a unique topological representations that allows attributive comparisons across events. We expect that the encoding provided through the R-K Pipeline would capture information that normal techniques will fail to capture, and allow for better cross-event comparisons based upon both value and topological distances.

After deriving the unique topological structures, through machine learning, the goal of this analysis is to finally embed the structures in \mathbb{R}^2 space such that topological differences maximize the inter-R-K Diagram distance and topological similarities minimize the inter-R-K Diagram distance in Phase Space as elaborated subsection II D.

C. Lens Implementation

Since R-K-Diagrams represent event based topological signatures, therefore the choice of lens is critical to how the R-K-Diagrams are formed. In this dataset, **each transaction** was represented as an event. We chose “transactions” as an event lens because of the clear use case which represents a discrete temporal purchase event in a sales store. This is demonstrated in figure 19 for reference and clarity. It is also important to note that we could have chosen alternative lenses such as a customer,

however coercing a customer data source into an event that can be used in the R-K models, involve extracting features from all transaction events of a customer into an “Customer Observation Event”. Such a use case, while possible, is non-temporal and requires aggregation before applying the lens.

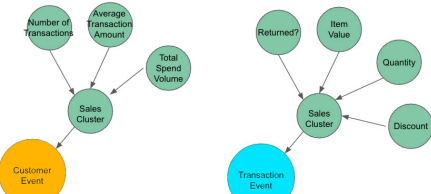


Figure 19. The lens choice used for this analysis. We chose to review the data from a transaction level, but various other “lenses” can be applied where appropriate as demonstrated in the diagram above.

D. Preprocessing

One hot encoding was applied to categorical data. Dates were converted to numbers. Identifiers unique to the event, or with very large cardinality, such as the Customer Id, Product Id, Segment Id, and Product Name, were dropped. Location data was converted into latitudinal and longitudinal positions using Google Map’s API’s and applying a zip code lookup. Failure to search the latitude and/or longitude of a particular zip resulted in removal from the dataset.

The resulting dataset after transformations became 9918 rows and 90 columns. The data was then normalized over a MinMaxScaler so that training the models were more effective.

E. Deriving the Hierarchical Function

We generated an ontology based on our domain understanding of store sales data. The graph was documented as a JSON file and provides the *Structure Graph* of the R-K-Diagrams. The ontology was coerced into a trans-

formation node that take in a Pandas datafram and returns a graph object, with attributes encoded according to the event that was sent to the transform.

The hierarchy was derived by utilizing the domain specific ontological graph. An initial ontology was generated based upon correlation parameters in the data-set along with the application of financial domain knowledge on Super Store Sales data. The ontology graphs used or generated for this purpose can be found in the following link: https://github.com/animikhroy/rk_toolkit_pipeline_diagrams/tree/main/02_notebooks/rk_general_applications/data

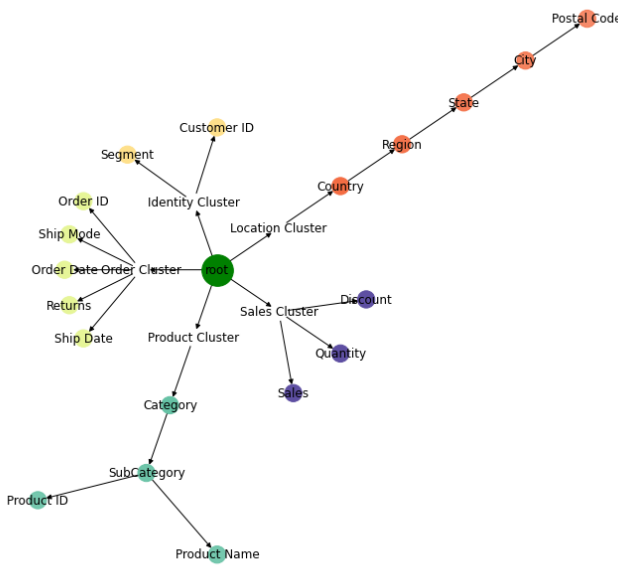


Figure 20. The base hierarchy provided for the store sales data

The structural graph is then generated using the base hierarchy provided for the store sales data. After generating this structural graph, it can be visualized using the R-K Toolkit as shown in the figure 20.

As you can see in figure 21, we have expanded out the original hierarchy with the help of categorical data made available by Tableau. This can be compressed in later steps back to the original form if required using isometric compression techniques available in the R-K Toolkit.

F. Pipeline Construction with Filter and Linker Designs

We used a basic filter (The RangeFilter) and linker called (SimpleChildLinker) design as explained below.

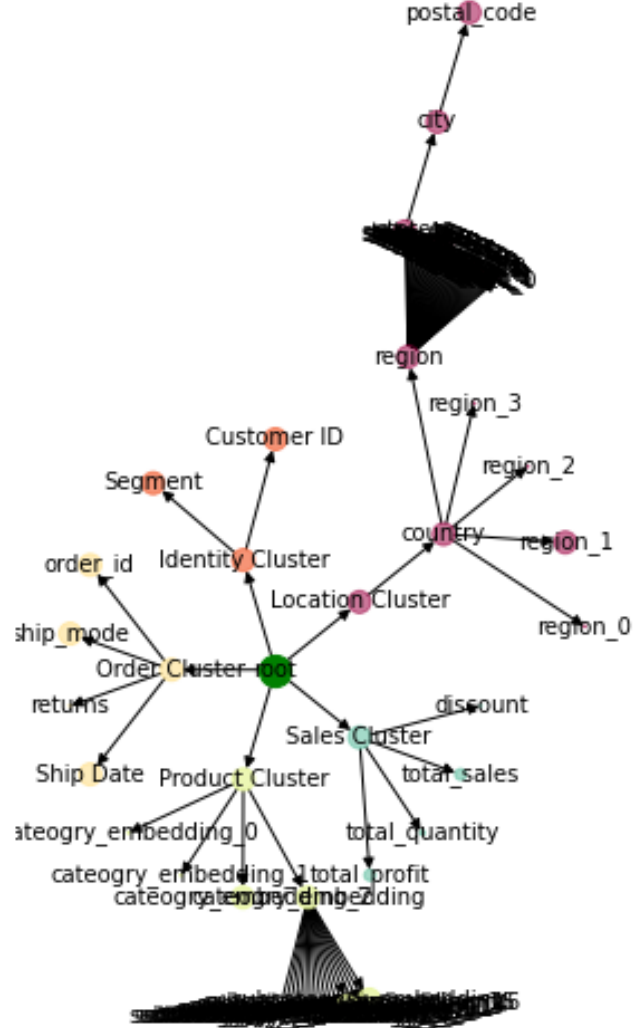


Figure 21. At the top, you have the core structural graph. Below, are 10 corresponding events without transformation, using the structural graph. We can see the distance pre-filters and linkages are fmetric_j where the distance measure is bound between 0 and 1 to evaluate similarity in the R-K pipeline. The distances are purely derived using the value/magnitudinal distance function provided in the R-K toolkit, and the filters and linkage functions that provide topological deviations have not yet been applied at this stage of analysis.

1. RangeFilter

A range filter is one of the simplest filters that is provided in version 1 of the R-K Toolkit. We assign the filters to each level of the hierarchy that contains numeric data.

G. Visualizing an Untrained Network

$$\begin{cases} \text{true} & \text{if } v \notin \{m, M\} \\ \text{false} & \text{else} \end{cases}$$

where:

- v is the value of the node
- m is the minimum boundary condition for the filter
- M is the maximum boundary condition for the filter

2. LeafLinker

We also used the simple leaf linker, which is provided in the R-K Toolkit. The simple leaf linker compares only the leafs of a tree, and provides an edge E in the case the euclidean distance is less than the specified threshold:

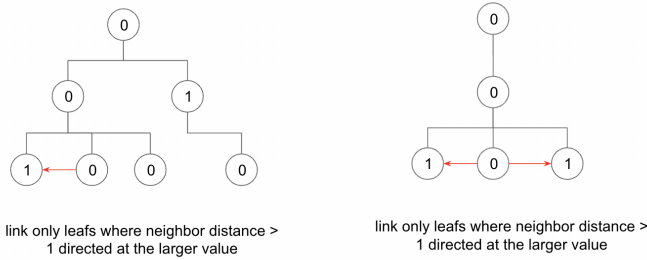


Figure 22. Leaf Linker compares the distances between values with $\epsilon_j \theta$, and links the leafs of the final clusters based upon the threshold.

Mathematically, this linkage is represented below:

$$\begin{cases} E & \text{if } \epsilon_j \leq \theta \\ \text{None} & \text{else} \end{cases}$$

a. where

- n_i and n_j are two leaf nodes
- $\epsilon = \sqrt{\sum_{i=0}^{|C|} \frac{N!}{2(N-2)!}}$
- θ is a defined tolerance for linkage

The LeafLinker's O notation would be $O(n^2)$, however the number of total computations more concretely is $\sum_{i=0}^{|C|} \frac{N!}{2(N-2)!}$ where $|C|$ is the number of clusters and $|N|$ is the number of leafs within the cluster.

The following image below demonstrates the first 10 rows of the store sales data with untrained thresholds. This time the base-structural graph has been updated with appropriate filter and linker functions as described in the previous sections to be able to generate a base R-K Model.

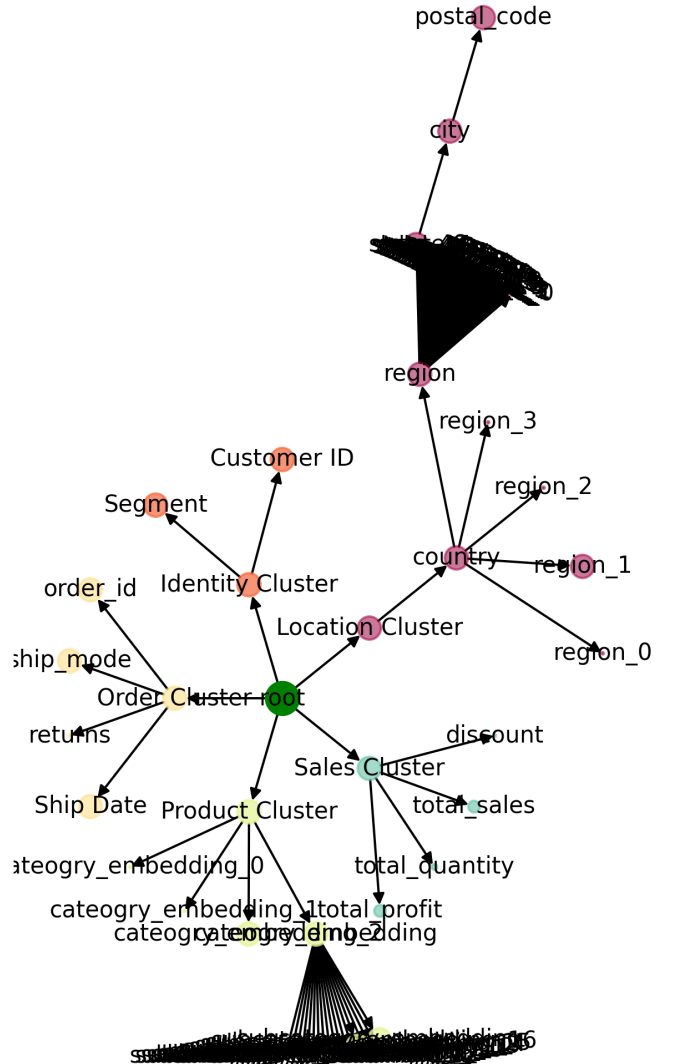


Figure 23. The base R-K Model of the store sales data with appropriate filer and linker functions applied to the pipeline.

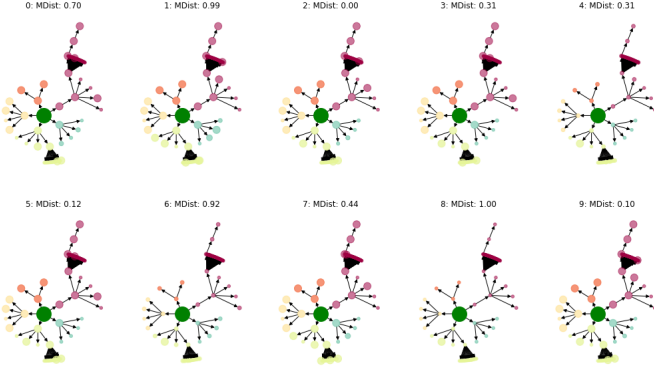


Figure 24. The first 10 events on an untuned network. M Dist is the normalized (MinMaxScaled) Magnitudianal/Value distance of the data in data space as an extension of the Mahalanobis Distance formulation. Prior to training, the total average distance across graphs is 0.88. Topologically, there are no differences because no filters and/or linkages have been applied yet. The Topological Similarity measure in the above R-K Diagrams are all equal to 1. All deltas are derived from the distances of the values.

After filters and linkages have been applied, the untuned loss goes down from **0.88** to **0.78** with a preliminary Simple Child Linker and Range Filter applied to each node with the bounds [0,1].

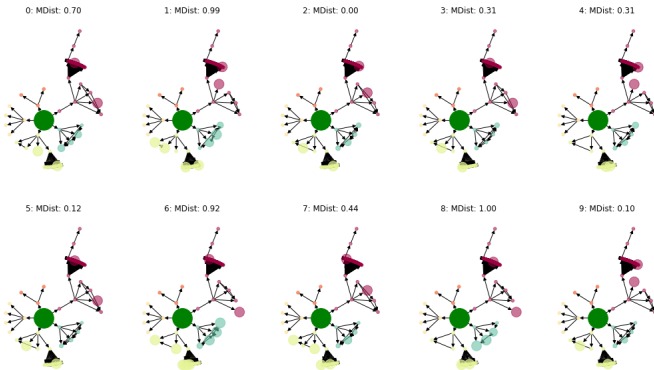


Figure 25. The first 10 events on an untuned network after filters and linkages applied. The initial guess was a RangeFilter of [0,1] applied to all nodes and a SimpleChildFilter with 0.5 as the initial starting point

With filters and linkages, we get an improvement of **.1** from a pure value distances by introducing topological divergence through filters and linkers.

From a qualitative review, we can look at event 6 and event 4, which according to Mahalanobis distance are quite different (.9 and .3) however topologically are quite similar. Conversely, 3 and 4 are very similar in Mahalanobis distance but very different topologically. This divergence would not normally be distinguishable using a traditional distance metric.

We can look at the individual transaction with more detail to get further understanding:

- Event 6 was a large purchase of 697.074 dollars made in Houston. It was a highly discounted transaction and a multi-category purchase with 11 items.
- Event 4 was a medium purchase of 21.376 dollars made in Glendale. It had a 40% discount, was 5 items in a single category. 6 was very different to 4 in terms of Mahalanobis distance but very similar topologically. These are similar topologically because of the high discount rate, and the multi-category transaction type.
- Event 3 was a smaller purchase of 3.928 dollars made in New York. A 20% discount was applied and it was a single category purchase. Thus, Event 3 was very similar to event 4 in terms of Mahalanobis distance but very different topologically. This was very different topologically to Event 4, because unlike event 4; event 3 was a single item purchase.

In conclusion, using our loss function defined in Measuring R-K Distance, we find that the average distance between R-K Models is **0.22**, and inversely, our similarity is **0.78** after applying filters and linkers. Before filters and linkers, topological distances across the models are 0. After filters and linkages, topological distances are 0.2 unweighted. Emergent properties from the data begin to form at this stage, however, to improve the results, we applied optimization and tuning of hyper-parameters via Machine Learning algorithms such that the appropriate weights to apply to the filters and maximize divergence across R-K Diagrams are learned automatically by applying combinatorial machine learning to the data via an implementation of Facebook’s Nevergrad.[90]

H. Training The Pipeline

In order to maximize divergence across R-K Diagrams, we trained our models using Facebook’s Nevergrad [90] optimizers. Thus, as demonstrated in the below sections, by providing an objective function and iterating over the various R-K models in a stochastic batch, we were able to reduce total loss of the set from **0.78** to **0.7**.

This gets us closer to providing a unique topological signatures across R-K Diagrams post training. This post-trained R-K Pipeline, could in theory be utilized across live stream data, to provide unique topological structures to incoming data from a similar dataset. This analysis is merely the beginning of optimization techniques that are possible with the R-K toolkit. Our goal for the following section is to show the potential of R-K Diagrams and Machine Learning, with the expectations that the methodology and implementation will improve with future research.

The loss history can be seen below and the description of how this loss function was obtained can be seen in the next sections.

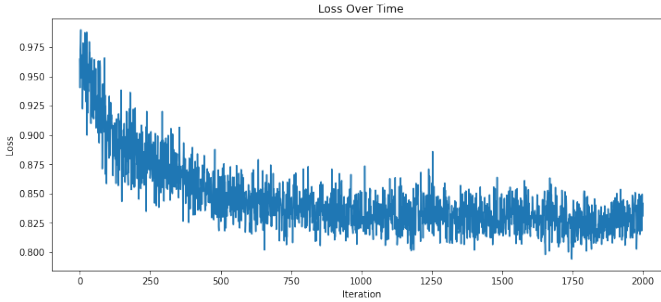


Figure 26. Loss function over 1000 iterations

1. Objective Function

We define an objective function as the following:

$$\frac{\sum_{i=0}^n \sum_{j=0}^n d(g_i, g_j)}{\frac{n!}{2(n-2)!}} \quad (8)$$

The goal of the objective function, as defined above, is to maximize divergence across R-K Diagrams by minimizing the similarity across diagrams. This is determined through a distance function defined in the Measuring R-K Distance subsection, which takes into account topological and magnitudal similarities across R-K Diagrams using a weighted distance function. We chose an even distribution of $[0.5, 0.5]$ for w as a prior, as there is no reason to bias the weights apriori.

Over iteration of θ , we will attempt to minimize the overall loss. Assuming an infinite number of iterations, we would hope that we maximize divergence across R-K Diagrams such that no R-K Diagram is exactly the same except for the same data, which would deterministically produce the same R-K Diagram.

The objective function provided above has large scope for future improvements and research, as ultimately the goal embedding the data into an R-K Diagram would be to maximize topological differences across differences in the shape of the data, and minimize differences of R-K Diagrams across similarity in attributes.

2. Optimizer

Because topological distance functions do not exhibit continuous gradients we employed a gradient free optimization using Nevergrad. [90]. NGOpts is an optimizer built by Facebook and the default suggested optimizer by Facebook. We ran with 5 max workers (parallelization) and a budget (number of allowed evalautions) of 1000.

3. Post Training Results (Pre-Compression)

The final results post training resulted in a loss of **0.825**. The diagrams post training are shown below:

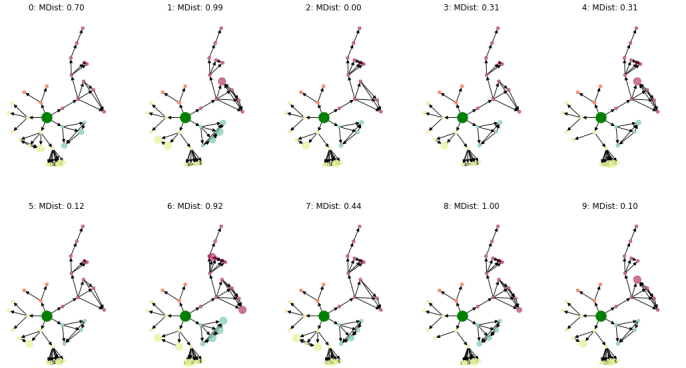


Figure 27. Tuned R-K Diagrams (Pre-Compression)

As you can see in the above, by maximizing distances across R-K Diagrams, we can see distinct topological signatures across events. This allows us to perform a variety of different methods of analysis later on, such as classification (given an R-K diagram, assign a label), estimation (given an R-K Diagram, estimate some value based), or other ML related techniques. There are many possibilities, if one considers the R-K Model as an input layer to a model.

In the case above, we can embed the R-K Diagrams in a 2D space and cluster them based upon attributes of the R-K Diagram.

4. Isometric Compression

Unlike standard dimensionality reduction techniques, compression techniques applied to the R-K Diagrams do not lose resolution in the data and can also maintain a consistent number of dimensions (2 or 3) of diagrams regardless of the number of model dimensions. This makes it far easier to evaluate models in higher dimensional space qualitatively without data loss and is one of the primary advantages to the pipeline.

We used the steps outlined in Isometric Compressions, Inverse Function, and Decompression for graph compression. We used a limited compression technique via a 1 degree leaf compression technique, which compressed all 1 degree or “unlinked” leafs into a single compressed leaf branching from the same parent. The steps are maintained internally so that the original structural graph can be reconstructed from compressed version, thereby providing the inverse transformation. With future research, we may employ various other compressible techniques (outlined in 4.5.9) to the store sales data to achieve better results.

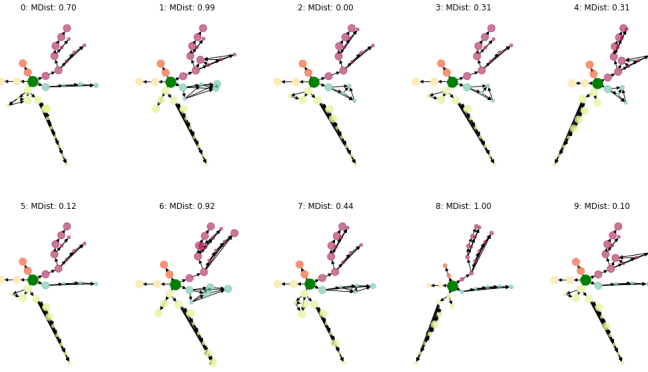


Figure 28. *Isometrically Compressed R-K Diagrams*

5. ML over R-K Diagrams for Variant Use Cases

By generating distinct R-K Diagrams, it is possible to employ many standard Machine Learning algorithms for numerous use cases such as classification, clustering, segmentation, and identification. For example, we could use cluster the R-K Diagrams into segments. Such segments could then be used to optimize store operations or sales across the data. One such classification example has been demonstrated below using a tSNE based localization and clustering technique. This technique provides a 2D embedding of the isometrically compressed R-K diagrams using the information derived from R-K distance and similarity measures via a comparison of Magnitudinal/Value Distance and Topological Distance between the various purchase events represented by their corresponding R-K Diagrams. A sample demonstration of the above can be seen in figure 29 for reference.

Other use cases such as classification also become possible. The classification use case is used in LIGO (described below), which used R-K Diagrams to describe Binary Merger Event Classifications. Since a pipeline is event level, stream data can be fed into the pipeline to generate new R-K diagram, with a single event generating a unique topological signature. As more data comes in, these models can be refined to provide greater sensitivity to topological differences.

6. Conclusion and Future Work

In conclusion, the store sales dataset has demonstrated a novel approach using event driven Topological Graph Theory Analysis on a canonical and standard, non-scientific dataset. It proves our first case of generalizability outside the initial models made for the LIGO analysis.

Future work can be done to improve the R-K pipeline and algorithms such that more distance and accurate signatures are derived from the store sales data. Further more, applying the signatures to various use cases such

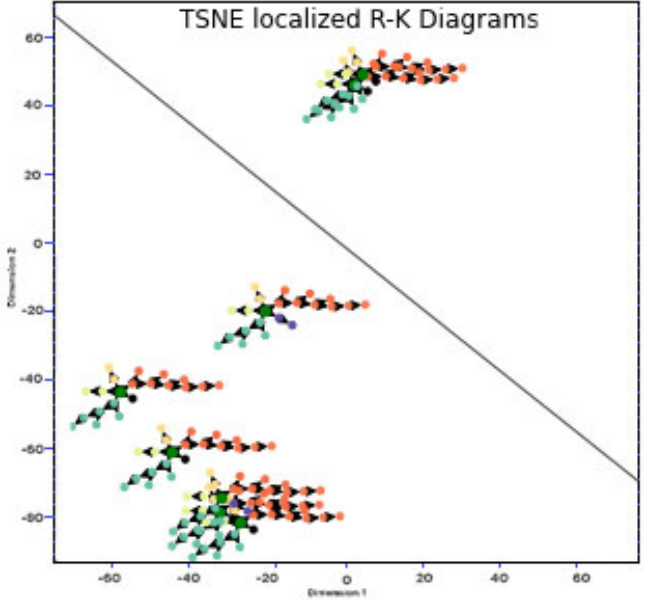


Figure 29. *tSNE localized R-K Diagrams with ML Based clustering via measures of R-K distance between various events with tSNE Dimension 1 and tSNE Dimension 2 plotted on the x & y axis respectively.*

as classification or identification would be a valuable exercise and is in scope for future papers.

VI. CASE STUDY: LIGO DATA ANALYSIS

The previous case study demonstrated an example of "Event-driven" topological signature identification on Tableau Super-Store Sales Data [79] with the help of unique filter-specific R-K Diagrams generated using the R-K pipeline. In this second case study, we aim to extend the identification of unique topological signatures along with a combined "***identification-classification-segmentation***" use-case to address an important scientific problem in the field of Gravitational-Wave Astronomy. This field has been exploding with latest breakthroughs in scientific research and is of special interest in recent years.[91][92] Hence, we shall now demonstrate a more specialized and scientific application of the R-K pipeline on a Physical/Astronomical Dataset (as elaborated in section 4.2.1 with certain domain specific modifications intended for Gravitational-Wave Analysis[35] [36] on LIGO data, which would aid in the identification and classification of Compact Binary Merger Events or ***Compact Binary Coalescences (CBCs)*** [93] [94] such as Black Hole Binaries (BH-BH), Neutron Star Binaries (NS-NS), Neutron Star-Black Hole Binaries (NS-BH) & Black Hole-Candidate Primordial Black Hole Binaries (BH-PBH). We have thus applied the R-K pipeline to data-strains and datasets released by the LIGO Open Science Centre [6] [7] for the the successful demonstra-

tion of our computational framework. The corresponding code along with our modified R-K Pipeline for LIGO and its applications on this dataset can be found on Github: rk-gw-mma & Github: 03-rk-visualiser . This dataset was specifically chosen over other scientific data for the following reasons:

1. To extend the scope of our pipeline and demonstrate a classification use-case on a field of scientific research that would be both relevant and useful in modern day Astronomy
2. To choose a cutting edge area of modern scientific research which involved very large volumes of data with high-dimensional features and properties spanning across multiple data-strains and datasets to prove that the core components of the R-K Work-flow can traverse and analyse such scientific case-studies with distinct advantages over traditional approaches
3. To showcase the flexibility of the R-K pipeline with modifications necessary for specialised scientific study
4. To demonstrate the ease, flexibility & scalability of the R-K pipeline to extend its scope of applications on Multi-messenger Astronomy
5. It is open-source and widely accessible to the scientific community for analysis and applications

A. Methodology

The methodology of this implementation has been focused to address the following domain specific challenges specifically with respect to the classification of Compact Binary Event Merger signals pertaining to ***Black Hole Binaries (BH-BH)***, ***Neutron Star Binaries (NS-NS)***, ***Neutron Star-Black Hole Binaries (NS-BH)*** and ***Black Hole-Primordial Black-Hole Binaries (BH-PBH)***, ***Candidate Dark Matter***:

1. Requirement of multiple separate ML and neural-net pipelines focused on different types of identification & classification problems especially pertaining to Multi-messenger data analysis
2. Dealing with computational complexity and switching from one mathematical model or analytical framework to another for different problems dealing with Multi-messenger data of CBCs.
3. Difficult to compress signature strain data and eliminate noise
4. Difficult to new apply traditional techniques of machine learning and neural-networks over a wide variety of parameters and constraints or implement any theoretical or observational constraints to the same analytical model

5. Standard Neural Nets & ML Models cannot be used for classification due to lack of training data, templates and learning models
6. Immense manual effort needed over months of research and verification for Compact Binary Event Merger signal identification with no computational framework for the automated classification of Binary-Mergers

In order to obtain a holistic methodology for addressing the above challenges and constraints with respect to an efficient computational pipeline to ingest enormous amount of raw-data, segregate confident merger signals and then classify them into a particular category of compact objects (i.e. Black Holes, Neutron Stars, Primordial Black Holes etc.); it is important for us to segregate and specify different data sources for the purpose of our analytical framework. Therefore, the data under consideration has been divided into 3 categories along with its corresponding analytical procedures:

1. Primary Analysis which is carried out on Raw-Strain Data
2. Secondary Analysis which is carried out on the parameter estimates pertaining to the various intrinsic physical properties of compact binary coalescences.
3. Tertiary Data which is carried out on predictions obtained via mathematical modelling and scientific analysis of Secondary Data (left out of scope for the purpose of this publication but introduced as a concept for future applications with the R-K Pipeline.

B. Data Description

As mentioned in the previous section, the LIGO data was divided into 2 parts for primary and secondary analysis.

1. Primary Data Analysis

We can define Primary Analysis on LIGO data as follows: The Primary dataset consisted of strain data with the following information

- the interferometer photodiode output of each detector produces gravitational-wave strain data as a time series sampled at 16384 Hz for LIGO data.
- For the Advanced LIGO detectors, the calibration is valid above 10 Hz and below 5 kHz.
- The detectors also record hundreds of thousands of auxiliary channels, time series recorded in addition to the strain signal, that monitor the behaviour of the detectors and their environment.

- Strain data is down-sampled to 4kHz from the original 16 kHz to reduce the size of LOSC files while (arguably) losing no science content, since the higher frequencies are dominated by optical noise.
- Thus, a 4,096-second file contains 16,777,216 GW-strain samples from a single detector, represented as floating-point "doubles" (eight bytes each).
- Invalid data due to detector malfunction, calibration error, or data acquisition problems are tagged so that they can be removed from analyses.

Any descriptions pertaining to the above dataset will be referred to as "**Primary Data**" in this paper.

2. Secondary Data Analysis

We can define Secondary Analysis on LIGO data as follows: The Secondary analysis was carried out on tabular data on the intrinsic physical parameters of compact binary mergers using Bayesian Methods of Parameter Estimation. [95] [96] [97] [98] [99] consisting of the following information:

- The most important information w.r.t. secondary analysis are the merger event labels on the Gravitational Wave Transient Catalogue as they would serve as the parent node in correspondence with their GPS merger times. [7] [36] e.g. Event Names : GW150914 & GW170817 corresponding to GPS times of 1126259462.4 & 1187008882.4 respectively.
- The tabular data consisted of Mass (1) (M_1), Mass 2 (M_2), Network SNR, Distance (Mpc), χ_{eff} , In-spiral, Final Spin, Total Mass (M_\odot), Chirp Mass (M_\odot), Detector Frame Chirp Mass (M_\odot), Final Mass (M_\odot), Redshift (Z), False Alarm Rate and (yr-1) Pastro measures.
- However, due to the current sensitivity issues and LIGO VIRGO constraints [100] our analysis of compact binary classifications was primarily done between black holes, Neutron stars and primordial black holes based on mass, spin, q-value ratios and red-shift measures with electromagnetic counterparts being added from Multi-messenger sources for further distinction of Neutron Stars w.r.t. Kilonova events has been demonstrated with a sample result in this paper while keeping the main focus on LIGO data in the initial version of this computational framework.
- Hence based on the ontological clustering of dependent and independent clusters the R-K models pertaining to secondary analysis of LIGO Data consisted of 4 independent clusters of Mass, Spin, Q-value ratios (derived from (M_1) & (M_2)) and Redshift.

- The following 4 events: GW170729, GW170817, GW190521 & GW190814 in the chronological order of their GPS times, were chosen with some unique characteristics of mass, spin and q-values to demonstrate our methodology before executing the pipeline on the entire transient catalogue.

Any descriptions pertaining to the above dataset will be referred to as "**Secondary Data**" in this paper.

3. Tertiary Data Analysis

We can define Tertiary Analysis on LIGO data as the data that is obtained from carrying out mathematical transformations on the secondary data thereby giving rise to parameter specific refined measures such as q values, calculation of the evolution of the inward spiral and other measures obtained from theoretical analysis by applying mathematical equations to further evaluate and refine those parameters obtained using secondary analysis.

C. Objective of Analysis

To obtain unique event specific R-K diagrams and to showcase classification of Binary Event Mergers with high Signal to Noise Ratio (SNR) into a particular category of compact objects such as Black Holes, Neutron Stars or Primordial Black Hole Dark Matter.

Modifications to the R-K pipeline have been done to signify confident binary merger signals and to use them as templates in combination with specific parameters and threshold filters to segregate such signals from false positives and detector noise in future. Furthermore, we have also endeavoured to provide a feasible computational pipeline that would enable the identification and classification of such binary mergers into specific category of compact objects based on secondary data analysis i.e. data obtained after on the various intrinsic physical parameters of such compact objects under consideration. Such secondary analysis is not carried out on Primary (Raw-Strain Data) but on secondary data Bayesian inference to calculate the posterior probability distribution over the parameters (sky location, distance, and/or intrinsic properties of the source) given the observed gravitational-wave signal.

D. Lens Implementation

As established earlier the choice of lens is critical for the basis of ontology and the R-K Model. Hence a binary coalescence or a compact binary merger event was chosen as the primary lens in this case study. Thus all parent nodes of R-K diagrams on LIGO data would be represented by the binary-merger event label e.g. GW150914

(a typical BH-BH merger famously recorded in September 2015). Moreover, all central Event nodes pertaining to the "merger-event-lens" will also correspond to their respective GPS merger times in phase-space for the classification and analysis of R-K diagrams that are generated from R-K models build upon the choice of this lens. Furthermore, each attribute representing a characteristic physical parameter associated to a parent node or merger event would have a structural ontology with independent physical variable clusters such as all mass measures (M) and all spin parameters (S) clustered together with their dependent attributes such chirp mass, effective spin etc. as explained in section IV B 1 the unique attributes associated with such events would thereby serve as the foundation for each R-K Diagram in this LIGO data analysis case study.

E. Preprocessing

As the current pipeline uses secondary measures, the preprocessing steps involved in the pipeline was naive. We ingested the secondary data into the pipeline and processed. In future versions of the LIGO R-K Pipeline, the process is intended to be much more elaborate, and eventually involving Bayesian Parameter Estimation over Primary Data as a means of feature extraction.

F. Modifications to the R-K Pipeline

We implemented a standard R-K Pipeline, with 2 stages for optimization. The first stage, involves generating unique topological signatures via a similar method to the store sales data. Training is done to maximize divergence using the same optimization objective function described in the Store Sale's Objective Function.

After optimization, we encoded the R-K Diagram into a vector and trained an SVM over the vectorized diagrams to produce a binary classifier over the data where X represents each vectorized R-K Diagram and Y are labels of Compact Binary Merger events. Thus the pipeline required two levels of optimization to build-up towards our objective of Multi-modal CBC classifications and unique R-K Diagrams for different types of Compact Binaries starting with the raw strain data and going through each successive step. This has been elaborated in figure 30 with the example of a candidate Primordial Black Hole which would be of special interest as a unique application of this novel computational framework.

1. Embedding Optimization

2. Classification Optimization

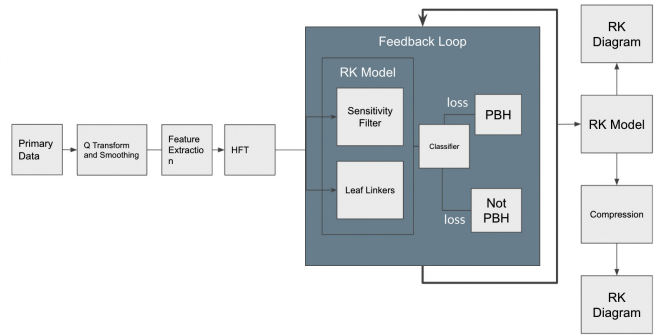


Figure 30. *R-K Pipeline Modifications for LIGO Data Analysis*

These two optimizations, applied sequentially after each-other provide two artifacts:

1. An R-K Pipeline which generates an R-K Diagram from a single event node
2. An SVM Classification Boundary to which the R-K Diagrams can be applied against.

We achieved R-K Diagram vectorization in a similar way to how a "Bag of Words" vectorization would be applied, where the "corpus" is all possible edges for a particular structural graph.

1. Modification Objectives

These modifications to the R-K pipeline were primarily motivated due to the address the following objectives:

1. To serve as a comparative classification framework for generating R-K Diagram based templates to classify and categorize compact-binary mergers with an efficient automated pipeline.
2. To associate unique R-K Diagram classifications having distinct graph and topological properties with their corresponding amplitude spectral densities (ASD) to allow for unique merger signal classification and segregation based on confidence scores of their corresponding R-K Diagrams in future.
3. To enable a complete and holistic plug-and play computational framework linked directly to primary data obtained from the detectors at source followed by effective filtering, noise reduction, Bayesian Parameter Estimation, deriving intrinsic physical parameters to build corresponding R-K models and applying filters and compressors to render the final R-K diagrams.
4. These R-K diagrams could then serve as feedback templates generating more machine learning templates to optimize loss and refine binary merger signal classifications with further distinction.

G. Primary Data Analysis

The primary analysis involves obtaining Gravitational Wave (GW) strain data in HDF5 format from the GW Open Science Center <https://gwosc.org/data/>. This is achieved through the R-K Pipeline data-scraping module. The strain data is then plotted, and the transient gravitational wave signal is extracted from the detector noise. The event spectrograms are then plotted after noise filtering and elimination for further analysis using some relevant methods of Topological Data Analysis as explained below. [7] [21] [26]

One of the key techniques that can be applied at this stage is Persistent Homology, a method used in topological data analysis to study the shape of data and identify features at different scales. This technique can be particularly useful in the context of GW data, as it can help to identify patterns and structures in the spectrograms that may correspond to specific types of GW events. [68] [16] [72] [27]

Another relevant technique is an extended implementation with inspiration from Gunner Carlson et. al.'s Mapper [2], a tool for topological simplification and visualization. Mapper can be used to create a simplified representation of the high-dimensional data contained in the spectrograms via methods of projection and radial comparisons (as explained in the subsequent sections), thereby, making it easier to identify and classify different types of GW signals and separate them from types of terrestrial noise signatures such as blips, whistles, koifish and other types of waveforms. [101]

Furthermore, Topological filtering and noise reduction techniques can be highly effective in the analysis of Gravitational Wave (GW) strain data. These techniques can provide an improvement over traditional filtering methods such as Gaussian, Tukey, and Cosine filters, particularly in terms of isolating the true nature of the wave from the detector noise some of which have been demonstrated as a part of the Ligo R-K Pipeline under the scope of Primary Analysis in this paper.

We especially considered exploring and implementing this technique as one of the key advantages of topological filtering is its ability to preserve the essential features of the data while reducing noise. This is particularly important in the context of GW data, where the signals of interest are often buried in significant amounts of noise. [20] [102] [103] [32]

In the realm of Primary Analysis, it is our firm belief that comprehending the noise is pivotal to the detection of gravitational-wave signals and the inference of the properties of the astrophysical sources that generate them. Misinterpretation of the noise can lead to an event's significance being inaccurately estimated, and to systematic biases in the parameter estimation. To safeguard against these undesirable outcomes, detector characterisation and noise modelling are substantial activities within the LIGO-Virgo Collaboration (LVC) [104].

While many textbook treatments of gravitational-wave

data analysis describe the idealised case of independent detectors with stationary, Gaussian noise, actual LVC analyses are careful to account for deviations from this ideal [35] [91]. This is because real-world detector noise is far from ideal and can be influenced by a variety of factors, including seismic activity, thermal noise, quantum noise, and even anthropogenic noise sources.

The Advanced LIGO and Advanced Virgo detector data exhibit a rich structure in both time and frequency. For a given gravitational-wave source, the noise (as described by its spectral density) governs the measured signal-to-noise ratio (SNR). The spectral frequency content of the LIGO-Livingston detector was averaged over a three-minute period shortly before the first detection of gravitational waves from a binary neutron star merger with the event name GW170817 [104].

The steep shape at low frequencies is dominated by noise related to ground motion. This seismic noise can be particularly problematic for gravitational-wave detectors, as it can mask the signals of interest. To mitigate this, gravitational-wave detectors are often built with sophisticated seismic isolation systems.

Above roughly 100 Hz, the Advanced LIGO detectors are currently quantum noise limited, and their noise curves are dominated by shot noise. This quantum noise arises from the fundamental uncertainty principle of quantum mechanics, and it sets a fundamental limit on the sensitivity of the detectors.

High amplitude noise features are also present in the data at certain frequencies, including lines due to the AC power grid (harmonics of 60 Hz in the U.S. and 50 Hz in Europe), mechanical resonances of the mirror suspensions, injected calibration lines, and noise entering through the detector control systems [35] [104] [91]. These noise sources can create challenges for data analysis, but they can also be used to help calibrate the detectors and understand their performance.

Hence our primary objective in this section is to extract the confident merger signals by segregating them from the noise in gravitational-wave detectors which is crucial for any further analysis in terms of generating the correct Parameter Estimations and the corresponding R-K Diagrams as a part of the Secondary Analysis. Hence, this approach not only helps to improve the detection of gravitational-wave signals but also aids in the accurate inference of the properties of the astrophysical sources that generate them. As our understanding of these noise sources improves, so too will our ability to detect and interpret gravitational-wave signals. [97] [99] [98] The corresponding code along with our modified R-K Pipeline for LIGO and its applications on this dataset can be found on Github: rk-gw-mma & Github: 03-rk-visualiser for reference purposes.

1. Strain Data

The R-K pipeline was retrofitted to run additional precursor steps on strain data as explained in the previous section. This is mainly done as a part of the additional component steps added to the R-K pipeline for reasons explained in section 6.6. The figure below demonstrates plotting of the raw data-strains with initial filters as explained. This process was then extended for all 4 selected events for the purpose of initial analysis and validation, namely: GW170729, GW170817, GW190521 & GW190814. The purpose of choosing all 4 events in parallel was done to demonstrate their eventual representations on an expanded topological "Event-scape" that would spread across a plane of GPS times and merger frequencies for all the events plotted together for the sake of future comparison.

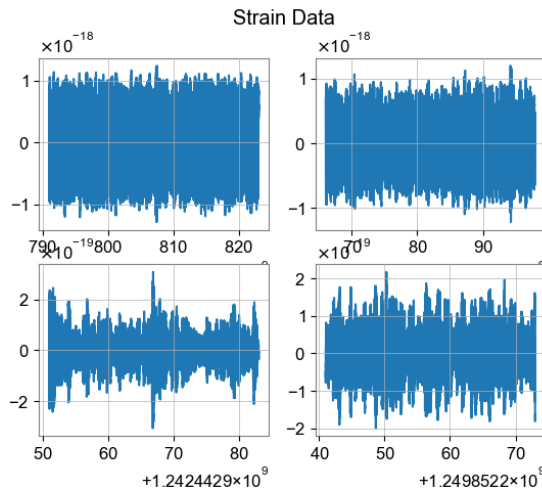


Figure 31. Raw Data Strain from LIGO

A sequence of processing steps was applied in our modified pipeline to the calibrated strains from the LIGO-Hanford detector such as the one showing 4s of data centered on GPS time 1126259462 *September 14, 2015 0950l45 UTC*. This data was obtained from the GW Open Science Center [7]. First a Tukey Window with 0.5s is applied, then the data are whitened using an estimate of the noise spectral density. Finally the data are bandpassed

filtered to enhance features in the passband (35 Hz; 350 Hz), thereby revealing the presence of gravitational-wave signal *GW150914*. This was done as a first trial run using the modified R-K pipeline in accordance with well established research papers. [36] [104] The process described in the research papers were then applied to all 4 selected event stains obtained from the GW Open-Science Center and to showcase the capability of our computational framework in terms of processing primary and secondary data with respect to multiple compact binary merger events in parallel.

2. Spectrograms & Q-Transforms

It was seen that the raw or primary data from the previous stage are dominated by low-frequency noise. Therefore a Tukey window with 0.5 s transition regions was applied to the raw data. Next, the data-stains were all whitened by dividing the Fourier coefficients by an estimate of the amplitude spectral density of the noise, which ensures that the data in each frequency bin has equal significance by down-weighting frequencies where the noise is loud. The data-strains were then inverse Fourier transformed to return to the time domain using the following relation:

$$d(t) \xrightarrow{\text{FFT}} \tilde{d}(f) \xrightarrow{\text{Whiten}} \tilde{d}_w(f) \quad (9)$$

$$\tilde{d}(f) \xrightarrow{\text{Whiten}} \tilde{d}_w(f) = \frac{\tilde{d}(f)}{S_n^{1/2}(f)} \xrightarrow{\text{iFFT}} d_w(t) \quad (10)$$

The above bandpass technique enhances the visibility of features of interest in this band by removing noise outside of the band - seismic and related noise at low frequencies, and quantum sensing noise at high frequencies. However, it is important to note that Note that such narrow band-passing is only used for visualization purposes and is not employed in the LVC analyses.

However, as indicated in LIGO research [36] [91] [96] [104] Wavelets provide a more flexible analysis framework than short-time Fourier transforms. Continuous wavelet transforms are commonly used in LIGO-Virgo data studies to produce spectrograms that provide a visual indication of non-stationary behaviour. Quantitative assessments of non-stationary may also be made by using discrete, orthogonal wavelet transforms. This can be visualised in the best way using normalized q-transforms on the strain data by plotting the noise reduced data strain frequencies against GPS time in a 2-D plane with the normalised energy representing the amplitude spectral densities of each merger-event in the form of the combined plots shown below.

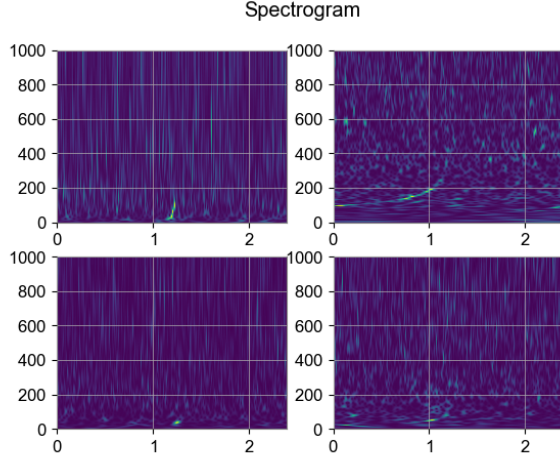


Figure 32. LIGO Spectrograms with Q Transformed ASD

Here the normalised energy of the Q -transform coefficients can be calculated using the following relation:

$$E = \frac{|X(\tau, \phi, Q)|^2}{\langle |X(\tau, \phi, Q)|^2 \rangle} \quad (11)$$

Thus, the Q - transform pipeline can be thought of as an optimal matched filter search for minimum uncertainty waveforms of unknown phase in the whitened data streams.

3. Topological Event Scape

However, we found that the true power of topological analysis could be utilised in the best way possible by merging all events in 3D for shape rendering and signal filtration using noise reduction techniques. This notion is inspired by topological data visualisation techniques which increase the granularity and bring out the details within high dimensional datasets for further distinction and analysis.

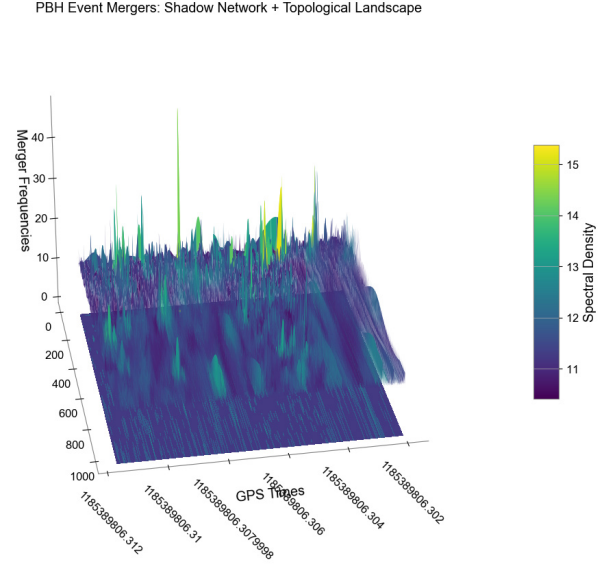


Figure 33. 3D Projected Event-scape with spectral density map of combined events and Phase Projection of Event Signatures according to GPS Time & Frequency

Thus, the above diagram shows a "Topological Event-Scape" of all 4 merger events with GPS times and merger frequencies representing the 2 axes of the 2D plane while the amplitude of the spectral density representing the normalised energy is plotted in the 3D dimension to bring about more enhanced filtering and noise reduction around the Tukey window with appropriate filters. This is also made possible by the fact that all mergers can be combined together and compared with each other using Universal GPS times and because all mergers tend to have their Fourier transformed frequencies within a comparative scale of values.

4. Filtration & Noise Reduction

In this section we outline how we identify and characterize these noise features so that we can either exclude the bad data or assess the impact of remaining components to search for gravitational-wave signals. This concept can be further enhanced to all data-strains in parallel using the R-K pipeline as shown and can be extended to 'n' number of events in theory. However, we have addressed our 4 selected events GW170729, GW170817, GW190521 & GW190814 for the sake of simplicity and clarity.

In this pipeline, noise reduction filters could be applied to all events simultaneously and we used a combination of Gaussian filters and cosine based Tukey filters such as the one defined below:

$$w(x) = \begin{cases} \frac{1}{2} \left\{ 1 + \cos \left(\frac{2\pi}{r} [x - r/2] \right) \right\}, & \& 0 \leq x < \frac{r}{2} \\ 1, & \& \frac{r}{2} \leq x < 1 - \frac{r}{2} \\ \frac{1}{2} \left\{ 1 + \cos \left(\frac{2\pi}{r} [x - 1 + r/2] \right) \right\}, & \& 1 - \frac{r}{2} \leq x \leq 1 \end{cases} \quad (12)$$

PBH Event Mergers: Shadow Network + Topological Landscape

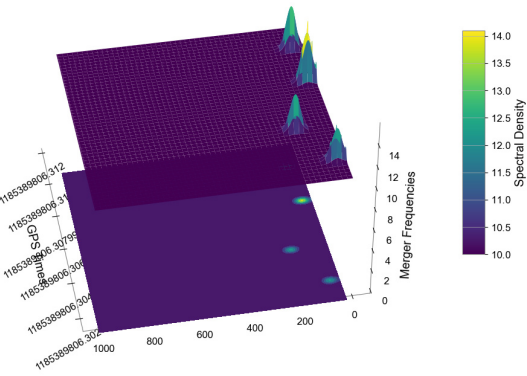


Figure 34. Topological Noise Reduction on Primary data with phase projections

This allowed us to achieve significant noise elimination while preserving the essential frequencies and spectral energy densities of the merger signals about their corresponding GPS times which could also be reverified using established secondary data from LIGO, thereby establishing the validity of this technique as shown in the above diagram.

Furthermore, our computational framework allowed for the visualization and mapping of the peak frequency of the 3D wave spectral densities to their corresponding GPS time stamps using 2D phase projection techniques described in the mathematical formalism of this paper.

5. Phase Projections

The Phase space projections of the peak frequencies of noise-reduced and filtered gravitational wave merger signals not only correspond to their GPS merger times but is very useful to serve as the choice of lens to build R-K models with secondary attributes and parameters clustered about these primary event nodes as we shall see in the following sections of this paper.

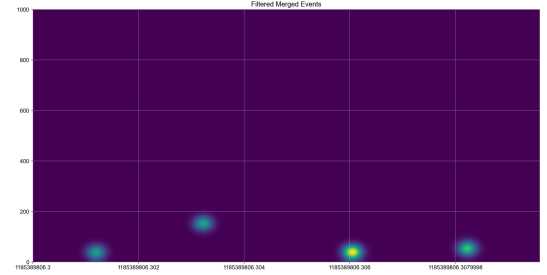
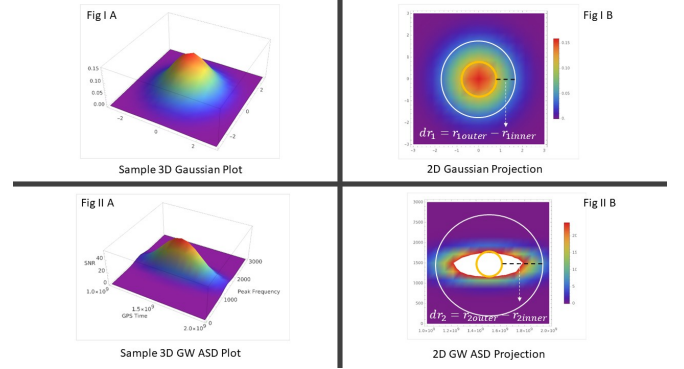


Figure 35. Combined Phase Projections of Noise Reduced Compact Binary Merger Signals

This would in turn allow us to carry out a topological study of the different 3D waves via their corresponding 2D projections, we can start by examining the elliptical 2D projections of the 3D wave functions as seen in case of 36 and simplified further in the figure below to explain our simplified approach towards this topological feature comparison study.

Figure 36. The above diagram demonstrates how $\Delta r = r_{outer} - r_{inner}$ can be determined from 2D projections of 3D GW wave-forms in noise-filtered ASD plots via a simplified study of the topological nature of the wave-forms prior to in-depth modelling with Betti Number Analysis

The 2D projections are essentially heat maps of the 3D functions, where the colour represents the amplitude of the 3D function at a given point in the x-y plane. In our case, the 2D projections are elliptical in nature due to the Gaussian nature of the 3D functions.

To calculate the inner and outer radii of the elliptical 2D projections, we need to find the semi-major and semi-minor axes of the ellipse. However, since we are dealing with a heat map representation of a 3D function, the "radius" in this context refers to the distance from the centre of the ellipse to the point where the amplitude of the 3D function starts to decrease significantly.

Let's denote the 3D function as $f(x, y)$, and its 2D projection (the heat map) as $P(x, y)$. The centre of the ellipse (the peak of the 3D function) is at (h, k) , and the semi-major and semi-minor axes are (a) and (b) , respectively.

The equation of an ellipse in the x-y plane is given by:

$$\frac{(x-h)^2}{a^2} + \frac{(y-k)^2}{b^2} = 1 \quad (13)$$

To find the inner and outer radii, we need to find the values of (a) and (b). This can be done by examining the 2D projection and finding the points where the amplitude of the 3D function (represented by the colour in the heat map) starts to decrease significantly. These points can be considered as the boundaries of the inner and outer radii.

Let's denote the boundary of the inner radius as

$$r_{\text{inner}} \quad (14)$$

and the boundary of the outer radius as

$$r_{\text{outer}} \quad (15)$$

. These can be calculated as follows:

$$r_{\text{inner}} = \min_{(x,y) \in P} \sqrt{(x-h)^2 + (y-k)^2} \quad (16)$$

$$r_{\text{outer}} = \max_{(x,y) \in P} \sqrt{(x-h)^2 + (y-k)^2} \quad (17)$$

where $(x,y) \in P$ means that the point (x,y) is in the 2D projection.

The difference between the outer and inner radii can be calculated as:

$$\Delta r = r_{\text{outer}} - r_{\text{inner}} \quad (18)$$

This gives us a measure of the "spread" of the 3D function in the x-y plane.

So in order to find the inner and outer radii, we can examine the 2D projections and find the points where the amplitude of the 3D function (represented by the colour in the heat map) starts to decrease significantly. These points can be considered as the boundaries of the inner and outer radii.

Once we have the inner and outer radii for each 3D function, we can compare them to study the differences in the "spread" of the 3D functions in the x-y plane. This can give us an idea of how the shape of the 3D function changes with different wave functions.

This method can be used as a simplified starting point for a more detailed topological study of the 3D waves. For a more in-depth analysis, we may need to consider other topological properties of the 3D functions, such as their genus (the number of "holes" in the function), their Euler characteristic, while carrying out corresponding Betti Number Analysis or other topological invariants which are beyond the scope of this initial publication.

H. Secondary Analysis

We shall now extend the pipeline with the exploration of secondary measures obtained using posterior probabilities and Bayesian parameter estimates in established research. [93] [97] [98] [99] It is however, important to note that the current version of the LIGO R-K pipeline does not address the computation of posterior probabilities and Bayesian parameter estimates from Primary Data. This remains to be in the scope of future research which could potentially help automate this entire process thereby generating R-K diagrams directly from detector signal data in near-real time and classifying them into a specific category of compact objects such as Black Holes, Neutron Stars, Primordial Black Hole Candidates etc.

However, for the sake of the first version of the computational framework and R-K pipeline, we have restricted the scope of this paper in carrying out Secondary Analysis on the estimated physical measures corresponding to each merger event as published. [7] [95] [96] The corresponding code along with our modified R-K Pipeline for LIGO and its applications on this dataset can be found on Github: rk-gw-mma-secondary-analysis for reference purposes.

1. Omni-view Plots

Thus using the flexibility and scalability of the R-K pipeline we have plotted an "Omni-view Plot" of all secondary measures plotted against each other with respect to the entire GWTC currently available.

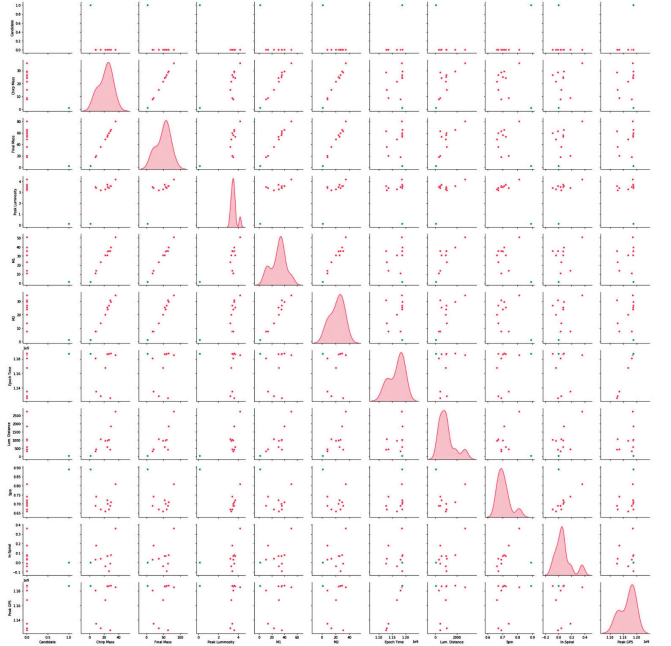


Figure 37. *Omni-view Plot of Secondary-Data-Analysis*

This allows for the graphical comparison of any two parameters thereby helping us identify exceptional properties of various merger events and compare them to the standard ones as done in case of the 4 merger events (GW170729, GW170817, GW190521 & GW190814) selected using this exercise. Now by removing the leading diagonal and all repeated in graphical plots he omni-plot shown in the above diagram, one can easily cluster dependent and independent variable clusters for building R-K models. A more detailed and usable version of this omni-plot is available on <https://youtu.be/iwMsETob58w>.

2. Event Dendograms

The we have built an ontology of from the LIGO data based on dependent and independent variables pertaining to the various intrinsic physical parameters of the compact binary mergers which describes the hierachic relationships between all physical measures to be taken into consideration for building the respective R-K models. The various selected attributes obtained using posterior probabilities and Bayesian parameter estimates are grouped as follows:

- Primary Mass (M_1), Secondary Mass (M_2), Total Mass (M_{\odot}), Chirp Mass (M_{\odot}), Detector Frame Chirp Mass (M_{\odot}) and Final Mass (M_{\odot}) are all grouped together under the mass cluster which is dimensionally independent of all other clusters in the Dendogram.
- Similarly, all spin measures pertaining to χ_{eff} , In-spiral & Final Spin get grouped together in the dimensionally independent spin cluster
- We also consider 2 separate dimensionless ratios representing measures of Red-shift & Q-values (ratio of Primary Mass (M_1) & Secondary Mass (M_2)) in 2 separate independent clusters for comparing characteristic differences between Black Holes, Neutron Stars & candidate Primordial Black Holes.

it is important to note that it is not essential to pre-select a limited set of parameters from the source data (LIGO or otherwise) for the hierarchical feature extraction and building Dendograms using the R-K pipeline. We have chosen a subset of these specific parameters for the sake of simplicity and clarity in the first version of our implementation with reference to the latest developments in the filed of Gravitational Wave Astronomy.

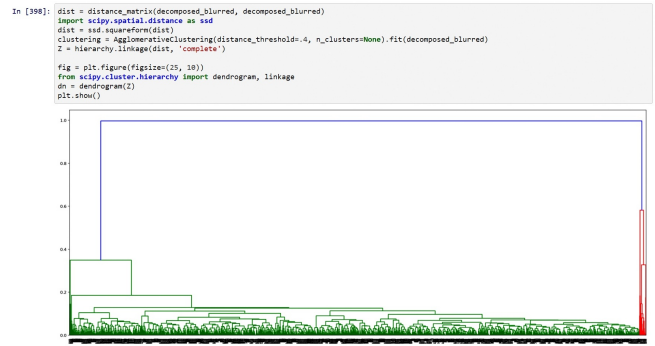


Figure 38. *Dendograms for Event-Based Topological Clustering*

The above diagram shows the primary event node marked in 'red'. This serves as the event node to which the entire mass cluster has been linked via Hierarchical Feature Extraction techniques clustering all the various mass attributes, i.e. Primary Mass (M_1), Secondary Mass (M_2), Total Mass (M_{\odot}), Chirp Mass (M_{\odot}), Detector Frame Chirp Mass (M_{\odot}) and Final Mass (M_{\odot}) grouped together in terms of their interdependencies as shown in the diagram.

3. Clustering of Bayesian Parameters

In this section, we will address the hierarchy defined within each cluster with the example of the spin cluster as shown in the diagrams below. We shall also consider a single event GW 170729 for the purpose of demonstrating each step in this process. The R-K pipeline allows for the flexibility to scale and run clustering on all merger events in parallel resulting in the fundamental structural graph for Gravitational Wave Analysis based on LIGO data.

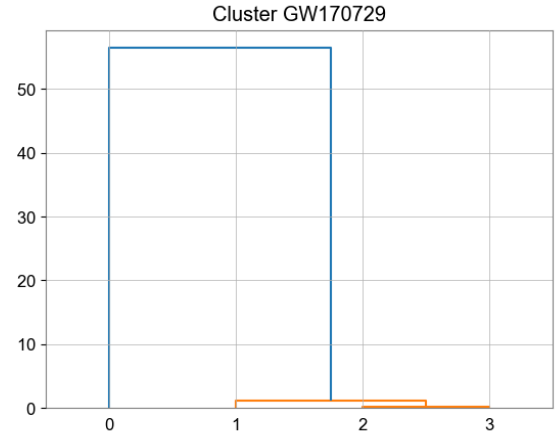


Figure 39. *Single Event Dendrogram GW170729*

The diagram above addresses the very first step of as-

sociated with a single event Dendogram. In this case the parent node or the 'event node' of the binary-merger event GW170729 first gets linked to one cluster at a time. In this case the diagram shows the linking of the spin cluster. All steps in this process take place in the Topological Phase Space and are independent of any choice of coordinates thereby ensuring scalability and flexibility of this framework.

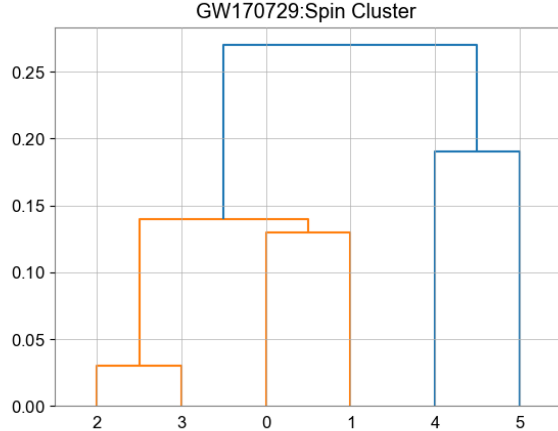


Figure 40. *Spin Clustering of GW170729*

Now, we address the hierarchical grouping and ontological relationships within each cluster. The 3 measures of effective spin, in-spiral and final spin are ontologically linked and clustered together in an optimal way as shown in the figure above.

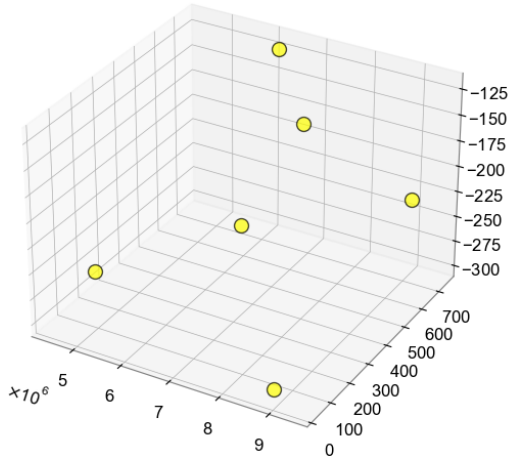


Figure 41. *Spin Nodes of 170729*

The next stage addresses all the nodes of each cluster separately in Phase Space. In this case it takes into account all values of each spin measure within the entire range of estimation error as indicated in the GWTC. for example in case of GW170729 the $\chi_{eff} = 0.37$ with an

error range of +0.21 to -0.25. Hence all min-max error range values are encoded into nodes along with the most probable $\chi_{eff} = 0.37$.

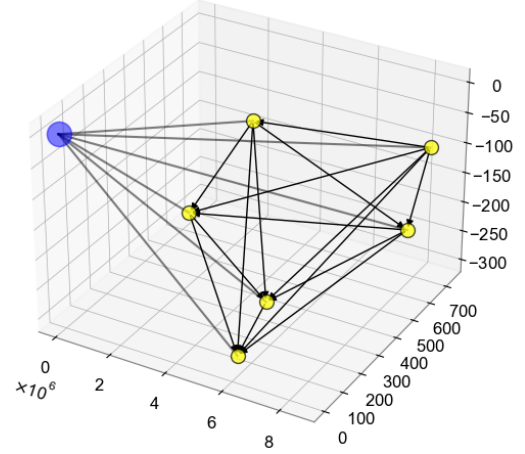


Figure 42. *Spin Simplex of 170729 linking with Central CBC Merger Event node marked in blue*

The final step links all the nodes in the correct manner directed to the highest or lowest value according to the choice of the user. However, in this case we have used the Leaf Linker to connect all the node values with edges within the cluster pointing towards the highest value of each measure. The edges also represent the entire range of possible values with any amount of granularity between the maximum and minimum range of each probable measure. This also gives rise to DAGs and simplicial complexes within each independent cluster of an R-K model. As a final step all nodes in each cluster are then linked to the parent node or the "event node" represented in blue in the above diagram. We have also carried out isometric-compression of such structural graphs based on the euclidean distance using the Leaf Linker algorithm. This single linkage clustering was also done via the Leaf Linker available as a part of the R-K toolkit. Each of the above steps along with the corresponding graph plots can be accessed on Github: rk-visualiser.

4. Unfiltered Structural Graphs

The steps described in the above section were carried out in parallel on each of the selected binary-merger events. This gave rise to 4 independent structural graphs for the binary merger events: GW170729, GW170817, GW190521 & GW190814, as shown in the diagram below.

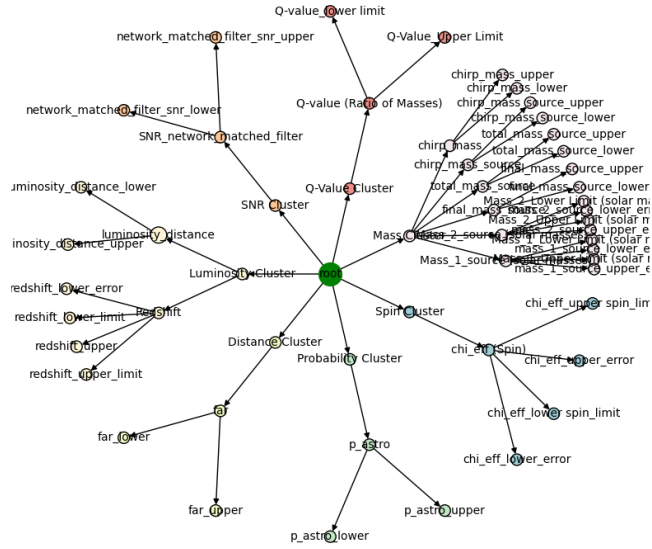


Figure 43. The unfiltered structural graph of all 15 dimensions of Parameter Estimates that provides the base hierarchy of all dependent and independent parameters for LIGO R-K Models and subsequent R-K diagrams of CBCs as generated by the R-K Pipeline

However, as detailed in the previous case-study with store-sales data, these structural graphs rise purely out of all data-points available in the columns of the high-dimensional dataset. Thus node masks and filter functions need to be applied to obtain unique event-driven R-K Diagrams as discussed in section IV E 2 .

5. Data Filters & Sensitivity Thresholds for Filtered R-K Diagrams

The modified R-K pipeline for LIGO comes with a built-in visualizer and a GUI to track each step of the process from loading primary/raw strain data all the way up to plotting R-K diagrams. This is given to users to enable the smooth application of node masks and range filters to all the selected clusters of unfiltered R-K models for all binary merger events. One can use the GUI to run through and validate each step of the process described in this case study. The GUI can be accessed here on [Github](#):03-rk-visualiser and downloaded and run in any native python environment that matches the required software & hardware specifications as mentioned on GitHub.

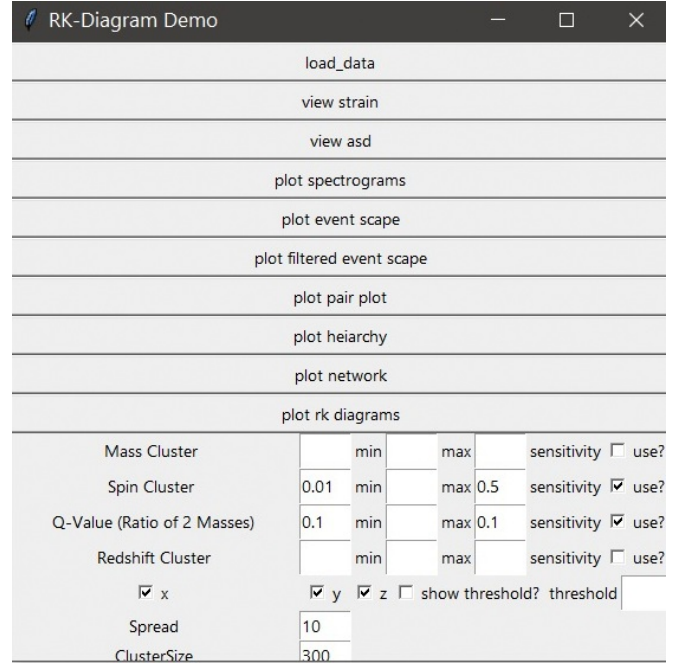


Figure 44. *Sensitivity Thresholds and domain specific filters applied to the R-K Pipeline*

Hence the GUI in the above diagram allows parameter based topological filtering of the base structural graph or the R-K model in a way such that node masks and range filters either suppress or express components of each independent cluster based on any chosen measure and its corresponding filter parameters. In this case our objective was to find R-K diagrams with all spin measures close to 0 and low q -value ratios of around 0.1 in order to segregate potential neutron-star mergers from stellar black holes and primordial black holes. The mass cluster values add further distinction in terms of determining whether the compact binaries are in the mass gap. The choice of these parameters were driven by well established research in this field. [95] [96] [98] [105] [100] [106]

6. Final R-K Diagrams with Isometric Compression

Thus Parameter Based Topological Filtering was carried out on selected clusters such as Mass, Spin, Q-Ratio & Red-shift with the Range Filter algorithms applied within pre-set ranges of $\chi_{eff} = 0.01$ & $q = 0.1$ [105] [106] [96] considering all error bars to obtain the corresponding R-K diagrams of the 4 selected events as described below in the order of their GPS merger times.

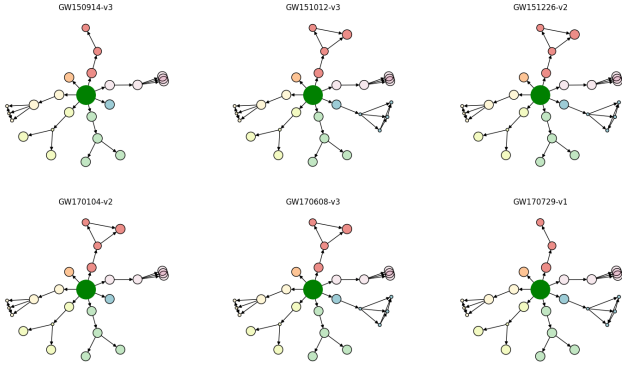


Figure 45. A set of 6 filtered R-K Diagrams generated without corresponding cluster labels in accordance with GWTC-transient catalogue data derived using Parameter estimations and appropriate filters for visual clarity

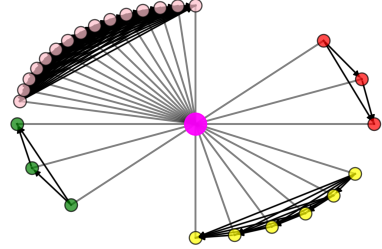


Figure 47. Final R-K Diagram of GW170729

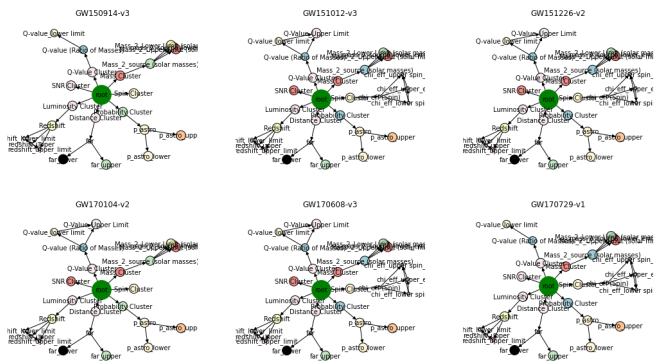


Figure 46. A set of 6 filtered R-K Diagrams generated with corresponding cluster labels in accordance with GWTC-transient catalogue data derived using Parameter estimations and appropriate linkages, filters and sensitivity thresholds as explained in this section.

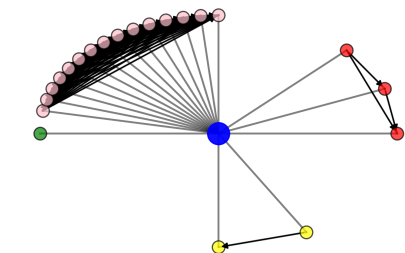


Figure 48. Final R-K Diagram of GW170817

The first R-K Diagram under consideration is that of the event GW170729 as shown above. In this case we find $\chi_{eff} \leq 0.058$ & $q \geq 1.09$. The mass values don't fall in the mass gap range and hence represent all characteristics of a typical stellar black hole.

The second R-K Diagram under consideration is that of the event GW170817 as shown above. In this case we find $\chi_{eff} = 0.01$ & $q \leq 0.89$. The mass values don't fall

in the mass gap range but the q value differs significantly from that of a candidate primordial black hole. This can be further verified by adding an electromagnetic counterpart from multi-messenger data which has been left out of scope for the purpose of this paper but could be easily added to the R-K models by extending the R-K pipeline in future. Thus the detection of an electromagnetic counterpart, with low χ_{eff} close to 0 and q value close to 1 establishes this event as a compact binary NS-NS (Neutron Star) merger.

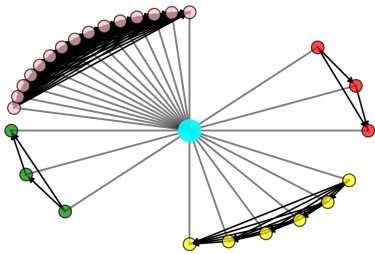


Figure 49. Final R-K Diagram of GW190521

The third R-K Diagram under consideration is that of the event GW190521 as shown above. In this case we find $\chi_{eff} \leq 0.9$ & $q \geq 4$. The mass values don't fall in the mass gap range and hence this binary merger event also represents all characteristics of a typical stellar black hole much like GW170729 and both have topologically similar R-K diagrams.

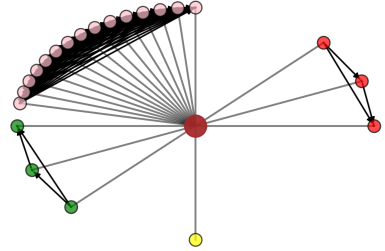


Figure 50. Final R-K Diagram of GW190814

The fourth and final R-K Diagram under consideration is that of the event GW190814 as shown above. This is also the most interesting one under consideration as in this case we find $0.04 \leq \chi_{eff} \leq 0.05$ & $q = 0.1$. The mass values definitely fall in the mass gap with no electromagnetic counterpart. Hence it has a lot of prominent features that are indicative of a candidate Primordial Black Hole (Dark Matter). However, further increase in detector sensitivity combined with added parameters such as more accurate detection of high Redshifts which would be a distinguishing characteristic of candidate Primordial Black Holes. However, LIGO and VIRGO are currently not sensitive enough to detect such high red-shifts and therefore we require more sensitive probes like the Einstein Telescope for further parameter based distinction in future. But as discussed earlier, the R-K pipeline is designed in a highly scalable manner to include Multi-messenger data-streams in future to provide further distinction between R-K diagrams of different compact binaries.

7. Untuned R-K Diagram Event-Scape

Thus all R-K diagrams of any given set of compact binary merges can be represented in a transformed Event-scape in 3D space with the x-axis representing the GPS time, y-axis representing the peak frequency values and the z axis representing the amount of SNR or signal to noise ratio as shown in the diagram below. The higher the SNR value the more confident we can be with respect to the detection and classification of distinct compact binaries.

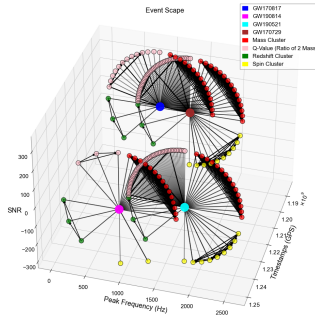


Figure 51. All 4 Event Based R-K Diagrams in 3D

The above diagram shows multiple merger events plotted in the event-scape for which the topological distance or divergence and similarity measures were computed using templates from matched filters with respect to the 4 selected events. In order to test the accuracy and effectiveness of classification we set template labels on the 4 classified events. In order to show a proof of concept we assigned absolute labels to all 4 merger events such that GW170729 and GW190521 were assigned the label of BH-BH merger, GW170817 was labelled as a NS-NS merger and GW190814 was labelled as a PBH-PBH merger.

I. Intra-class Distance and Similarity Measures of CBCs

This resulted in an initial average intra-class topological distance separation of **0.17** between BH-BH mergers upon applying the parameter specific Range Filters and Node Masks discussed in the previous sections. This would imply an intra-class similarity of **0.83** between BH-BH mergers. An average intra-class topological distance separation of **0.18** between NS-NS & NS-BH mergers upon applying the parameter specific Range Filters and Node Masks discussed in the previous sections. This would imply an intra-class similarity of **0.82** between NS-NS & NS-BH mergers. It was also interesting to note an inter-class topological distance separation of **0.32** between BH-BH and confident NS-NS mergers which would imply a lower order inter-class similarity of **0.68** and verifies the effectiveness of R-K diagrams and the R-K pipeline to a significant extent. Comparative studies based on similarity measures of the candidate PBH was left for the next section as no clear or conclusive results were obtained using the untuned models.

1. Tuned Results with Combinatorial Machine Learning Optimization

In order to maximize divergence across R-K Diagrams, we trained our models using Facebook's combinatorial Nevergrad [90] optimizer. Thus, as demonstrated in the

below sections, by providing an objective function and iterating over the various R-K models in a stochastic batch, we were able to reduce total loss of the set across different labelled classes over 1000 iterations.

Tuning and intra-class loss optimization for Black Hole Candidates.

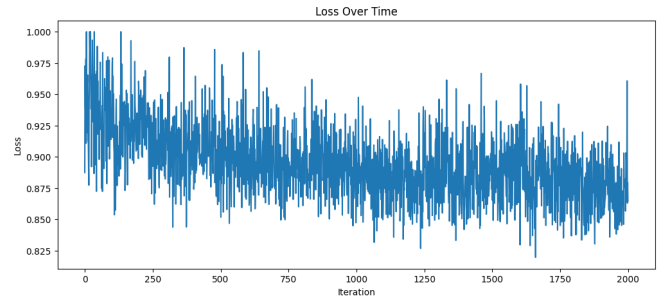


Figure 52. Loss Optimization graph to optimize distance and intra-class similarity measures among all BH-BH Candidates

Tuning and intra-class loss optimization for Neutron Star candidates including NS-BH mergers.

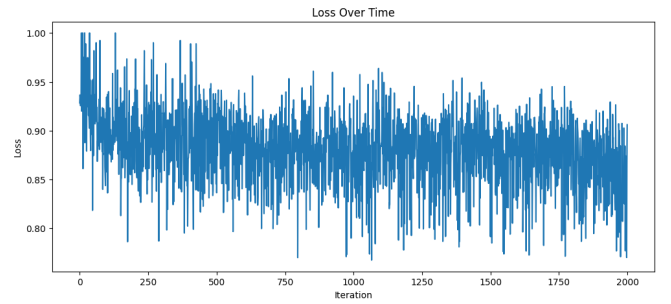


Figure 53. Loss Optimization graph to optimize distance and intra-class similarity measures among all NS-NS and NS-BH Candidates

After optimization, we encoded the R-K Diagrams into a vector and trained an SVM over the vectorized diagrams to produce a multi-modal classifier over the data where X represents each vectorized R-K Diagram and Y are labels of various CBC events. Thus the pipeline required two levels of optimization. The SVM generated a plane of separation between R-K diagrams as shown in the form of a grid in the diagram below.

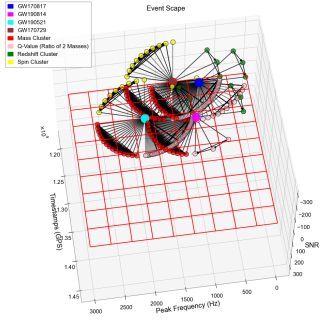


Figure 54. All 4 Event Based R-K Diagrams in 3D with SVM threshold grid

This has allowed us to achieve a more precise intra-class topological separation between **BH-BH** mergers, which were observed with an average similarity measure within the range of [0.91, 0.95], and **NS-NS** mergers within a range of [0.85, 0.89]. The candidate **PBH / NS-BH** exhibited an intra-class similarity of 0.82, due to the limited quantity of support and training data available to enhance accuracy scores across this class. Furthermore, a more detailed study of the unique topological signatures and R-K diagrams of Primordial Black Holes is definitely promising but beyond the scope of this paper and should be left for future research due to the lack of conclusive data and sufficient observational parameters at present.

However, this clearly underscores the unique potential of the R-K models based on Topology and Graph Theory. These models are capable of producing R-K diagrams with distinct topologies across different classes and calculating R-K distance and similarity scores with a reasonable degree of accuracy, all without the need for a large number of support vectors or extensive training data.

J. Median R-K Diagram Topologies of different CBC classes and Inter-Class Distance Measures

1. Median Topology of R-K Diagrams with all Parameter Estimates



Figure 55. Median Topology of R-K Diagrams with all 15 Parameter Estimates

Median Topology of R-K Diagrams with all 15 Parameter Estimates and simulated EM counter-parts shown in the purple graph cluster. As we can see, Each class

of CBC belonging to a distinct category such as : BH-BH (high-mass), BH-BH (low-mass), NS-NS, NS-BH & Candidate PBH mergers exhibit a distinct median topology in the R-K diagrams, which can be analysed based on their topological properties, such as the number of nodes, edges, and clusters, as well as their spatial distribution and connectivity and then we can obtain a final similarity score by applying the R-K Distance Function.

For instance, high-mass BH-BH mergers might exhibit a higher magnitudinal value of each node in its mass cluster while representing a distinctly different simplex in its q-ratio cluster in the corresponding R-K diagrams, which also reflect the high mass ratios and spin magnitudes associated with these events.

On the other hand, low-mass BH-BH mergers might exhibit a more dispersed distribution of nodes and edges which are lower in magnitude compared to high-mass BH-BH mergers in the median R-K diagram, combined with the difference in mass ratios and spin magnitudes that these events can encompass. The distinct spatial distribution and connectivity of nodes in this diagram provide a different topological 'fingerprint' that can be used to distinguish low-mass BH-BH mergers from their high-mass counterparts.

Similarly, NS-NS mergers and Candidate PBHs also exhibit their own distinct 'topological features' in their corresponding R-K diagrams, reflecting the specific properties and characteristics of these events. For example, NS-NS mergers might exhibit a cluster of nodes and edges corresponding to the EM counterpart parameter, while Candidate PBHs would exhibit no nodes and edges in this cluster.

Thus analysing these topological 'fingerprints', the R-K Pipeline can identify and classify different types of CBC signatures based on their distinct topological properties. This provides a powerful tool for the analysis and classification of CBC events, and can potentially offer new insights into the nature and properties of these astrophysical phenomena.

2. Median Topology of Isometrically Compressed R-K Diagrams with 4 selected parameter clusters for comparative analysis and demonstration

These R-K Diagrams only contain filtered clusters pertaining to Mass, Spin, Q-Ratio and Redshift of each CBC Merger event without any corresponding EM counterparts as shown in the diagrams below for a more simplified comparison of what was explained in the previous section. This focuses only on the most important identifying characteristics without EM counterparts across each class of CBC under consideration in this paper.

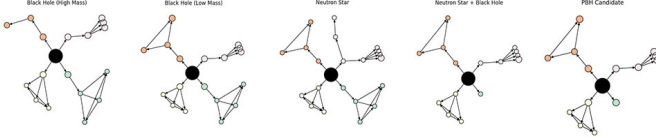


Figure 56. Median Topology of Isometrically Compressed R-K Diagrams with 4 selected parameter clusters for comparative analysis

3. Inter-class distance and similarity scores across different CBC R-K Diagram Topologies

	Class 1	Class 2	Topological Distance	Value Distance	Average Distance	Average Similarity
0	Black Hole (High Mass)	Black Hole (Low Mass)	0.052632	1.432186e-12	0.026316	0.973684
1	Black Hole (High Mass)	Neutron Star	0.181818	3.149037e-12	0.090909	0.909091
2	Black Hole (High Mass)	Neutron Star + Black Hole	0.300000	2.543632e-12	0.150000	0.850000
3	Black Hole (High Mass)	PBH Candidate	0.263158	2.025491e-12	0.131579	0.868421
4	Black Hole (Low Mass)	Neutron Star	0.136364	3.500533e-13	0.068182	0.931818
5	Black Hole (Low Mass)	Neutron Star + Black Hole	0.250000	1.689759e-13	0.125000	0.875000
6	Black Hole (Low Mass)	PBH Candidate	0.210526	5.484502e-14	0.105263	0.894737
7	Neutron Star	Neutron Star + Black Hole	0.272727	3.297362e-14	0.136364	0.863636
8	Neutron Star	PBH Candidate	0.318182	1.281197e-13	0.159091	0.840909
9	Neutron Star + Black Hole	PBH Candidate	0.062500	3.175236e-14	0.031250	0.968750

Figure 57. Inter-class distance and similarity scores across different CBC R-K Diagram Topologies

The above table provides a comprehensive comparison of different classes of Compact Binary Coalescence (CBC) events, which are astronomical events involving the merger of two compact objects such as black holes or neutron stars. The table is based on the analysis of gravitational wave signals using R-K Diagrams and the R-K Distance Function, which are tools used in topological data analysis to study the shape and structure of data. The R-K Diagrams provide a visual representation of the data, while the R-K Distance Function provides a measure of the topological distance or dissimilarity between different classes of CBC events.

The columns in the table represent the following:

1. Class 1 (CBC Event) & Class 2 (CBC Event):

These columns list the two classes of CBC events being compared. The classes include high-mass and low-mass black hole mergers (BH-BH), neutron star mergers (NS-NS), mergers involving a neutron star and a black hole (NS-BH), and candidate primordial black holes (PBH).

2. Topological Distance:

This column provides a measure of the topological distance between the two classes of CBC events. This is a measure of how different the topological structures of the events are, with lower values indicating more similarity.

3. Value Distance:

This column provides a measure of the value distance between the two classes of CBC events. This is a measure of how different the

values (such as mass, spin, etc.) of the events are, with lower values indicating more similarity.

4. *Composite Distance*: This column provides a measure of the composite distance between the two classes of CBC events. This is a combined measure that takes into account both the topological and value distances. Importantly, the composite distance is the inverse of similarity, meaning that lower values indicate higher similarity.
5. *Average Similarity Score*: This column provides a measure of the average similarity between the two classes of CBC events. This is a measure of how similar the events are on average, with higher values indicating more similarity.

This is a preliminary result with median topologies of each class of R-K diagrams without training the R-K pipeline on the non-gradient combinatorial optimiser function which will be addressed in case of our final multi-modal classification demonstration with t-SNE.

4. Comparison of NS-BH & PBH Candidate R-K Diagrams

Comparison of CBC topologies NS-BH, and candidate PBH-BH with additional parameters such as EM counterparts with simulated multi-messenger data show a distinct difference in topologies of the two candidates as expected in accordance with theoretical predictions. Thus they could provide an effective means for the R-K Multi-messenger Pipeline to identify and classify these signatures with reasonable accuracy and confidence in future, albeit with more support and training data.

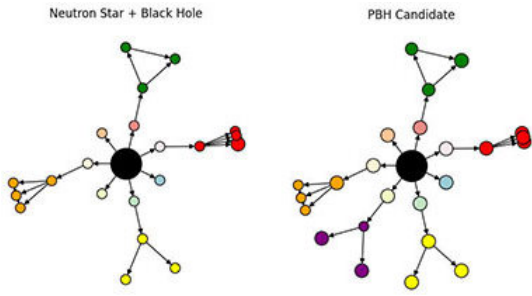


Figure 58. Comparison of CBC topologies NS-BH, and candidate PBH-BH with additional parameters such as EM counterparts from multi-messenger data.

5. NS-BH & Candidate PBH R-K Diagram Comparisons

Comparison of compressed CBC topologies NS-BH, and candidate PBH-BH without additional parameters such as EM counterparts with simulated multi-messenger data. It is clearly demonstrated that the NS-BH and PBH-candidate events display the same topology but

would vary at the level of the magnitudinal value of nodes and edges which creates separation for them upon applying the R-K Distance Function. However, their overall topologies are similar without the simulated EM counterparts which further validate the effectiveness of the R-K Pipeline in matching domain-specific theoretical predictions.

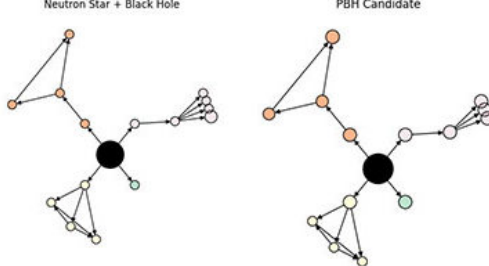


Figure 59. Comparison of Compressed CBC topologies NS-BH, and candidate PBH-BH without additional parameters such as EM counterparts from multi-messenger data.

K. Multi-modal classification of CBC R-K Diagrams with R-K Distance & t-SNE Optimization

We localised the R-K Diagrams using the T-distributed Stochastic Neighbor Embedding (T-SNE). T-SNE is a tool to visualize high-dimensional data by trying to minimize Kullback-Leibler Divergence between low dimensional embeddings and the higher dimensional data. [107]. It is an importnat dimensionality reduction technique widely used in machine learning.[108] Some of its benefits which are relevant to our computational framework are elaborated below:

1. Improved data exploration: t-SNE reduces the dimensions of complex datasets while preserving their structure, making it easier to visualize and interpret the data.
2. Enhanced clustering: t-SNE is useful for grouping similar data points together in exploratory data analysis, which allows for pattern detection and relationship discovery.
3. Efficient classification: t-SNE is a valuable tool in classification tasks, as it can separate data points into distinct classes based on their underlying characteristics. [109] [110]

Overall, t-SNE is a valuable addition to our machine learning R-K Toolkit, thereby allowing for better understanding and classification of complex datasets and applications such as Clustering, Segmentation and Multi-modal Classifications.[111] Hence, using the original data from the previous step, we localized to a two dimensional surface embedding each root of the R-K Diagram. This is done by using summary information of the R-K model

via metric and topological evaluation methods in our R-K Distance Function.

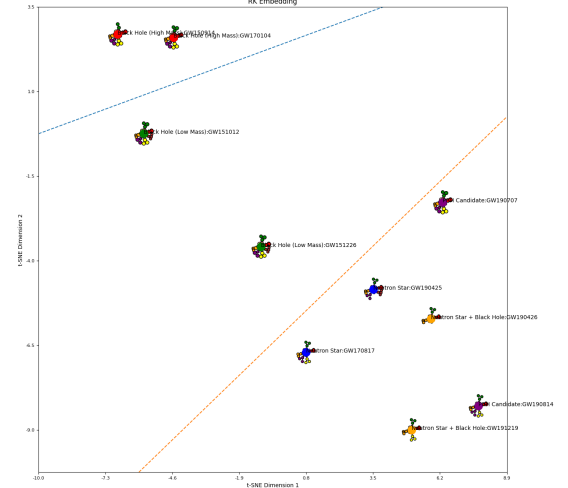


Figure 60. A t-SNE localised embedding of R-K Diagrams showing multi-modal classification of Compact Binary Mergers across different classes

Figure 59 shows a t-SNE localised embedding of a few randomly plotted R-K diagrams of each CBC category from the 92 merger events with distinct multi-modal classification across different classes as one of the final outputs of the LIGO-R-K Pipeline. The t-SNE visualization helps to show the distinct multi-modal classification of the different classes of merger events.

In the context of this paper, we have not only used t-SNE for the purpose of achieving multi-modal classifications of CBC merger events via the R-K Distance Function but also as an effective dimensionality reduction technique to simplify both the visualization and computation required for the representation of R-K diagrams across different CBC classes. In Figure 59 the t-SNE visualization helps to show the distinct multi-modal classification of different classes of black hole merger events based on their intrinsic properties of mass, spin, q-values etc. with the help of the resultant R-K diagrams.

The machine learning model in the R-K pipeline uses t-SNE and R-K Distance to maximise inter-class separation between High-Mass Black Holes, Low-Mass Black Holes and NS-NS, NS-BH/Candidate-PBH mergers and separate them distinctly using SVM (Support Vector Machine) slopes.[112] This resulted in **final Inter-class similarity measures** between high-mass black holes (BH-BH) , neutron stars (NS-NS), (NS-BH)& candidate PBH were found to be between **0.78 & 0.83** with distinctly different R-K Diagrams that were separated by the SVM classification slopes as demonstrated in Figure 59. Most importantly it is able to do so on a very limited data-set via the generation of the median topologies of R-K Diagrams belonging to each CBC category in an effective manner which could improve significantly with more injection studies with more diverse support and train-

ing data. However, as demonstrated earlier the median topologies of NS-BH and Candidate PBH mergers are indistinguishable without adding the EM-counterparts from multi-messenger data and hence no inter-class separation was demonstrated in the figure as the R-K Diagrams were only modelled purely on LIGO Open Science Data.[7]. Furthermore, inter-class separation was not shown between NS-NS and NS-BH/Candidate PBH events as the pipeline was trained on the R-K Diagram of a single NS-NS merger pertaining to GW 170817. Hence, we can conclude that more support-data is required to achieve distinct inter-class separation between NS-NS and NS-BH/Candidate PBH events, which can be addressed in a separate follow-up study using simulated GW injections.

1. Mapping R-K Event-Scape to Primary Data Signatures

The fine-tuned results of the R-K Event-Scape provides distinct categorical R-K diagrams representing a specific class of compact binary mergers as shown in the previous section. However, it is important to note that these fine-tuned R-K diagrams can then be remapped to the Q-transformed spectral densities from Primary Analysis.

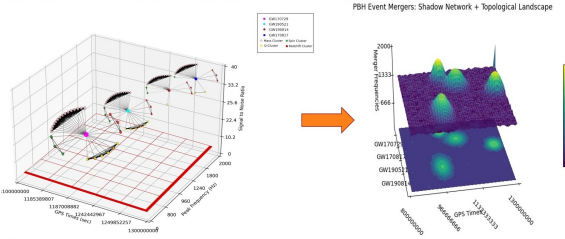


Figure 61. Mapping R-K Event-Scape to Primary Data

A study could then be conducted using the automated R-K pipeline to find any meaningful correlations between the topological characteristics of the merger signals obtained from the detectors at source and their corresponding labelled counterparts obtained in the form of R-K Diagrams from the R-K pipeline. Since the final R-K Diagrams have been vectorized for the purpose of classification using SVMs, therefore they could serve as templates for the segregation and classification of future gravitational wave merger signals obtained from compact binary mergers after the established steps of noise-filtering are carried out on the same. This would allow for near-real time segregation and classification of confident binary mergers which would keep improving over time with the addition of more SVM parameters from Multi-messenger data-streams and future advancements in LIGO.

L. Current Limitations & Immediate Applications

M. Scope of Work in Future

In this section we have showcased an example of a schematic representation of how the R-K pipeline could complement and augment the capabilities of the current LIGO Analysis Pipeline which has been published by Abbott et.al. [96] as shown in the diagram below.

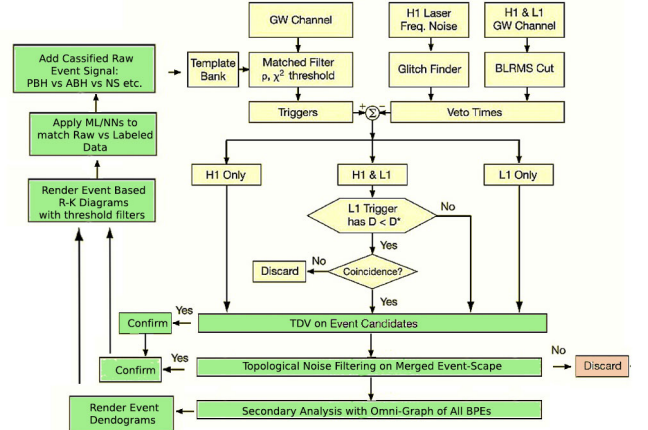


Figure 62. Modifying and augmenting a current version of the LIGO Analysis Pipeline with Topology, Graph Theory & Machine Learning based components of the R-K pipeline in future to operate near-real-time at the detector source

In the diagram above, the components marked in yellow represent the existing components of the LIGO Analysis pipeline as established by Abbott et.al.[96]. However, the green components of the diagram represent components of the R-K pipeline that could further augment and enhance its existing capabilities in terms of gravitational wave signal identification and the automated segregation and classification of compact-binary mergers. This can be achieved through effective computational frameworks involving Topology and Graph Theory where conventional machine learning techniques and neural networks have limited scope of application as proposed in this paper. Furthermore, R-K Diagrams can not only be used to explore interesting ways of providing compact binary merger classifications, but they can also enrich the template banks for future identification, segregation and classification of gravitational wave merger signals detected at source.

An example of such a template bank has been conceptualised in the diagram below. In this case, any tertiary analysis parameters obtained from future research papers could be easily added to this TDA pipeline to better classify compact binary merges. Even though each binary merger could render R-K diagrams that vary in geometry, they would have strong categorical correlation with respect to topological similarity measures demonstrated in this paper.

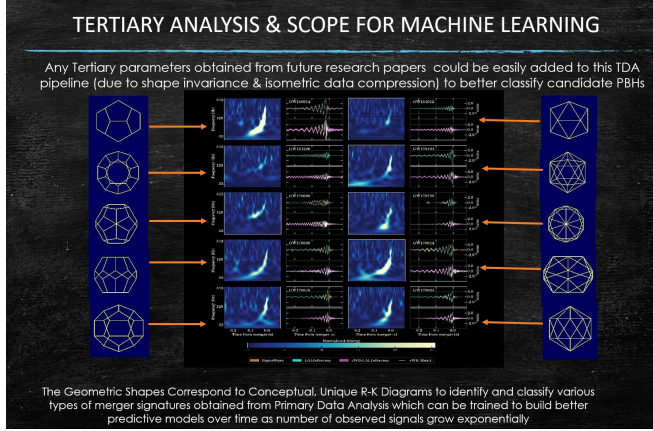


Figure 63. *Binary Merger Event Classifications based on Tertiary Analysis and ML Predictions based on training of Similarity & Divergence Measures between Topological Signatures of Merger Events*

In the above diagram, the geometric shapes correspond to conceptual, unique R-K Diagrams to identify and classify various types of merger signatures obtained from Primary Data Analysis which can be trained to build better predictive models over time as number of observed signals grow exponentially along with the addition of new parameters to R-K models using Multi-messenger data-streams.

N. Results & Discussions

Thus, the LIGO case study has clearly demonstrated the validity of this novel approach to Topological Graph Theory using R-K diagrams by providing a modular, flexible and scalable computational framework for the purpose of gravitational wave detector signal identification and compact binary merger classifications. It addresses some of the existing challenges with respect to the analysis of low-mass-low-spin compact binary mergers pertaining to Neutron Stars and candidate Primordial Black Holes by addressing the topological similarity and divergence across classes with effective ways of addressing computational complexity. It also provides an automated classification framework where conventional methods using machine learning and neural networks fall short due to lack of training data and limitations in terms of optimizing loss on multiple high dimensional data parameters all at once. One of the most unique advantages of this novel approach using R-K diagrams lies in the ability to extract ontology-driven meaningful data-summaries from high dimensional, complex datasets containing significant amount of noise. It is also able to reduce analytical complexities significantly by providing a coordinate independent framework in phase-space, where discreet similarity or divergence measures can be obtained by varying changes on multiple data parameters all at once. Thereby, it reduces complex classification problems

to their corresponding topological similarity/divergence measures and determines the overall classification via computing the R-K Distance Functions between any 2 R-K diagrams in topological phase-space. This approach can also be used to enrich template banks for future predictive modelling on raw/primary gravitational wave signals obtained from detectors at source and be used to separate them from terrestrial noise signatures via topological classification of different wave signal parameters. It could then be scaled to include all multi-messenger data-streams to provide meaningful data summaries using R-K models and filtered, compressible R-K diagrams. Thus, novel techniques such as this could be eventually used to gain unique perspectives on all of Dark Matter using Multi-Messenger data sources in the near future.

O. Immediate & Future Scope of Work

The implementation and applications involving the first version of the R-K Pipeline demonstrate its potential to scale and mature in the fields of Gravitational Wave and Multi-messenger Astronomy with some promising immediate and future applications.

We primarily aim to follow up this paper with a robust and well rounded set of injection studies involving simulated Gravitational Wave Signals, as this initial version only focuses on the limited data available at the LIGO Open Science Center [7]. These injection studies would involve the injection of simulated gravitational wave signals into real data to test the performance of R-K Pipeline and its corresponding ML classification models. Such simulated gravitational wave signals can be generated using numerical relativity simulations, which solve the Einstein field equations to simulate the behavior of black holes and other astrophysical objects. These simulations can be used to generate realistic gravitational wave signals that can be injected into real data to test the performance of data analysis pipelines.

There are many scientific references that discuss the use of injection studies in the context of gravitational wave analysis pipelines to test the corresponding computational framework and software libraries. One example is the paper "Parameter estimation for compact binaries with ground-based gravitational-wave observations using the LALInference software library" by Collin Capano et al.,[113] [114] which describes the use of injection studies to test the performance of the LALInference software library for parameter estimation of compact binary mergers. Another example is the paper "Testing gravitational-wave searches with numerical relativity waveforms: Results from the first Numerical INjection Analysis (NINJA) project" by B. M. S. et al.[115], which describes the use of injection studies to test the performance of gravitational wave searches using numerical relativity wave-forms, which severs as a possible methodology to follow.

Our follow-up study would also involve more advanced,

rapid-parameter-estimation techniques as our initial R-K Pipeline, utilises GWpy [116] and PyCBC [117] software packages for its parameter estimation module. This is the only component of the LIGO R-K Pipeline that does not execute in real-time in this current version. So we estimate that the speed and accuracy of the entire computational pipeline can be enhanced to near-real-time, at the detector source, with more advanced Hyper-fast gravitational wave posterior parameter estimations using variational inference techniques such as **VITAMIN** (<https://github.com/hagabbar/Vitamin>). This has been recently developed by the LIGO research groups at the University of Glasgow and the California Institute of Technology. [118]

We also recognise that this paper was primarily focused on laying the foundation of the R-K Toolkit, the R-K Pipeline and R-K Diagrams for the purpose of establishing this novel approach with relevant applications to showcase its capabilities. However, we also acknowledge that rigorous injection studies with simulated gravitational wave signals and a more robust classification/segmentation case-study on CBC signals vs terrestrial noise need to be addressed in a separate follow-up paper. This paper will also contain the ROC & AUC parameters pertaining to the deep-learning based identification and classification of numerous simulated data samples, as the real CBC signal datasets at the LIGO Open Science Center [7] are very limited for such Machine Learning studies within the scope of this publication.

The demonstrated results of the R-K Toolkit, the R-K Pipeline and R-K Diagrams in the LIGO case study, also open up a wide range of future opportunities for their integration with various software frameworks and platforms in the field of gravitational wave detection and Multi-messenger Astronomy. One such potential avenue of interest is to further integrate the R-K Pipeline with the **Wavefier** (<https://commpla.com/works/wavefier/>) software prototype developed by the European Gravitational Observatory for a *real-time Gravitational Wave Transient Classifier* which can be further extended to a *real-time Multi-Messenger Signal Classifier* using the **R-K Toolkit & Pipeline** as demonstrated in the diagram below. [119]

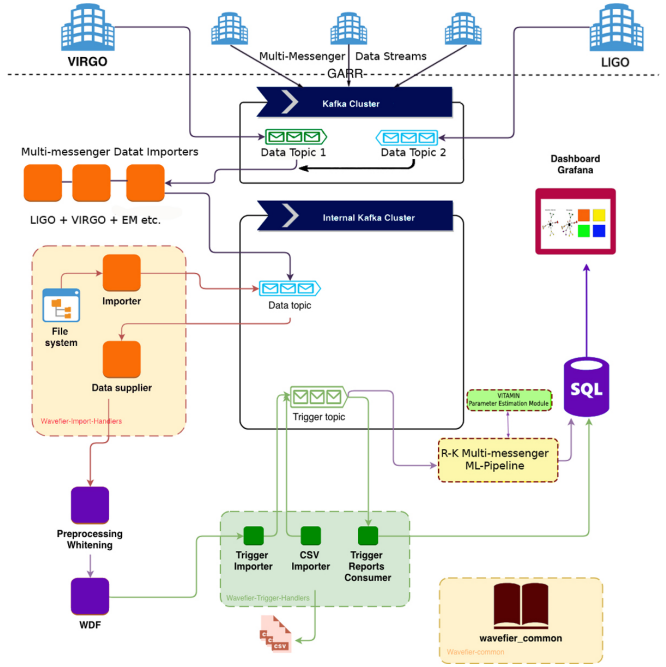


Figure 64. The above diagram demonstrates a conceptual example of how the R-K Pipeline could be scaled-up for the purpose of Multi-messenger Data Analysis by integrating it with the Wavefier prototype developed by the European Gravitational Observatory. The diagram also includes necessary modifications to the software architecture along with an integration with the VITAMIN hyper-fast parameter estimation module.

Figure 63 proposes a revised and updated draft of the EGO **Wavefier** prototype architecture (as proposed here: <https://commpla.com/works/wavefier/>) by integrating it with the R-K Pipeline for machine learning based identification, classification and segmentation of disparate Multi-messenger data-streams in real-time. Furthermore, all these separate multi-messenger datasetsstreams could be modelled together using a single R-K Pipeline via appropriate customizations to the R-K Toolkit and R-K Model for multi-modal analysis, similar to the LIGO Case Study explored in this paper. Figure 63 also demonstrates an integration of the VITAMIN hyper-fast parameter estimation module with the R-K Pipeline to generate deep-learning based parameter estimates pertaining to the filtered wave-signals in real-time. This certainly provides some promising scope of work for the R-K Pipeline and R-K Toolkit in the near future.

Future work also needs to be done to improve the scalability and efficiency of the R-K Pipeline in handling larger data sets, especially as new gravitational wave detectors come online and Multi-messenger sources produce ever-increasing amounts of data. Another possibility is to explore the use of R-K Models and Diagrams in other areas of astronomy, such as the detection and characterization of fast radio bursts, gamma-ray bursts, and other transient astrophysical events that emit across the electromagnetic spectrum including the identification and clas-

sification of Transiting Exoplanets.

VII. SUMMARY AND CONCLUSIONS

We introduced a novel approach toward **Topological Graph Theory Analysis**, by combining TDA and Graph Theory, using a foundational ontology. We encoded vectorized associations between data points for smooth transitions between Graph and Topological Data on two disparate datasets: (1) A generalised implementation on a standard store sales dataset[79] (2) A specialised scientific implementation on LIGO Open Science Gravitational Wave data. This resulted in filter specific, Homotopic, event-driven unique topological signatures which we have named "**R-K Diagrams**". With respect to the Tableau store-sales data, we find that unique topological structures were derived between distinct purchase events with a loss (measured in similarity between a set of R-K Diagrams) in the range of [0.78, 0.88]. In the case of the classification case study with LIGO Open Science data, we recorded a high accuracy of classification with respect to known merger signals and a average similarity measure of BH-BH Mergers falling between the range of [0.9, 0.96] and NS-NS Mergers between a range [0.59, 0.65]. The candidate PBH measured an inter-class similarity of 0.71 with w.r.t. to NS-NS mergers and 0.62 w.r.t. BH-BH mergers with distinctly different R-K Diagrams. This certainly presents an interesting case for further classification studies in future with more sensitive and varied data-streams. Therefore, we believe the findings of our work will lay the foundation for many future scientific and engineering applications of stable, high-dimensional data analysis with the combined effectiveness of **Topological Graph Theory** transformations.

The results obtained verify the basis of this novel approach in the following ways: (1) Distinct topological structures were created from the data and we have done so both on a store sales data and LIGO data. (2) These topological structures have emergent properties that when evaluated and compared to, have the capacity to provide meaningful insights into the data that standard data analysis techniques would not identify. For example, topological differences were exposed in the analysis that could not be exposed over metric based analysis such as euclidean distance, covariance-based 'Mahalanobis Distance', and other standard metric based distance measures. (3) This computational pipeline demonstrates a framework with the necessary attributes and components required to consistently switch between Graph and Topological Data Analytics. (4) This novel approach allows for the simultaneous study of global inter-class differences in topological representations of events and attributes as well as the local intra-class differences between such topological structures at the level of DAGs or simplexes. (5) Most importantly this methodology allows for coordinate indepen-

dent multivariate loss optimization using combinatorial techniques of machine learning which are scalable up-to 'n' parameters/attributes for any given choice of lens. This provides an alternative approach to address some of the limitations of conventional machine learning and the current applications of neural networks (including transfer learning) which require abundant training data and can optimize loss for only one target variable at a time. (6) Finally, the resulting structures provide an extensible representation, which can be applied to different methods of analysis in science and technology at large, with problems that require ML based classification, identification, segmentation and other similar techniques.

We also acknowledge that this novel approach is still very young and can mature significantly over time. We identify the following key areas for improvement:

1. Better filters and linkage functions.
2. Better encoding and standardization formats for hierarchical feature transformation.
3. Improved methods for optimization and training of R-K Pipelines.
4. Better distance functions against R-K Diagrams.
5. Improved parameter estimation with Hyper-fast gravitational wave posterior parameter estimation using variational inference techniques such as VITAMIN. [118]
6. Better encoding methods for graph pipelines.
7. Improved software and toolkit maturity.

Additionally, the R-K approach could be extended to other scientific and business domains where high-dimensional data analysis is necessary, such as in genomics, climate science, neuroscience, financial analytics, customer recommendation engines, zero-knowledge proofs and identity data maps in web3/web5. As the R-K approach continues to mature, it is likely to become an increasingly important tool for classifying, visualizing, and interpreting complex data sets across a range of scientific and business verticals. We believe that this computational framework and its varied applications will mature and expand rapidly. Combining the advantages of topology and graph theory analysis with an underlying ontology can provide a novel and powerful method of analysing data, in which hidden properties and underlying patterns undiscovered by other data analysis techniques can emerge with unique event-driven **R-K Diagrams**.

A. Acknowledgements

We would like to sincerely thank Prof. Chris Byrnes (Prof. of Astronomy, University of Sussex) & Prof.

Soumitra Sengupta (Amal Kumar Raychaudhuri Chair Professor of Physics, Indian Association for the Cultivation of Science) for believing in this vision and guiding us throughout the process to ensure its fulfilment with their valuable inputs, inspiration and support. Prof. Kathy Romer (Prof. of Astrophysics & DoSE, School of MPS, University of Sussex) for her unending support throughout the process of competing this original work. Dr. Ravi Cheruvu (Visiting Scientist, Carnegie Mellon University) for his critical suggestions and comments especially pertaining to a non-gradient based approach for optimising loss to achieve maximally divergent **R-K Diagrams** with the corresponding ML components in the **R-K Pipeline**. Dr. Sudhakar Varanasi (IIT-Kharagpur, IISc-Bangalore) for his overall guidance and valuable suggestions regarding the generalized applications of this novel approach across various industrial

verticals. Prof. Stephen Fairhurst (Head of Gravity Exploration Institute, University of Cardiff), Prof. Harry Ian (Senior Lecturer in the Institute for Cosmology and Gravitation, University of Portsmouth) & Prof. John Veitch (Senior Lecturer of Physics & Astronomy, University of Glasgow) for important discussions and suggestions pertaining to LIGO Data Analysis during the initial formulation of this novel approach in Gravitational Wave Analysis. Prof. Siong Heng (Senior Professor, LIGO Group, University of Glasgow), Dr. Daniel Williams, Dr. Joseph Bailey (LIGO Group, University of Glasgow) and Prof. Elena Cuoco (Head of Data Science, European Gravitational Observatory & the Co-Chair of Machine Learning, LIGO-Virgo Collaboration) for their valuable feedback and discussions regarding the future prospects of the computational framework and pipeline demonstrated in this paper.

-
- [1] M. J. Greenberg and J. R. Harper, *Algebraic topology: a first course* (CRC Press, 2018).
 - [2] G. Singh, F. Mémoli, G. E. Carlsson, *et al.*, PBG@ Eurographics **2** (2007).
 - [3] C. Epstein, G. Carlsson, and H. Edelsbrunner, Inverse Problems **27**, 120201 (2011).
 - [4] O. Courtney, *Statistical Mechanics of Simplicial Complexes*, Ph.D. thesis, Queen Mary University of London (2019).
 - [5] L. M. Seversky, S. Davis, and M. Berger, in *Proceedings of the IEEE conference on computer vision and pattern recognition workshops* (2016) pp. 59–67.
 - [6] M. Vallisneri, J. Kanner, R. Williams, A. Weinstein, and B. Stephens, in *Journal of Physics: Conference Series*, Vol. 610 (IOP Publishing, 2015) p. 012021.
 - [7] T. L. O. S. Collaboration, Ligo data release catalogue, Available at <https://www.gw-openscience.org/eventapi/html/> (2015-2021).
 - [8] (2021).
 - [9] J. L. Gross and T. W. Tucker, *Topological graph theory* (Courier Corporation, 2001).
 - [10] C. P. Bonnington and C. H. Little, *The foundations of topological graph theory* (Springer Science & Business Media, 2012).
 - [11] D. B. West *et al.*, *Introduction to graph theory*, Vol. 2 (Prentice hall Upper Saddle River, 2001).
 - [12] D. Archdeacon, A survey. Congressus Numerantium **115**, 18 (1996).
 - [13] P. C. Kainen, in *Graphs and combinatorics* (Springer, 1974) pp. 76–108.
 - [14] B. Bollobás, *Modern graph theory*, Vol. 184 (Springer Science & Business Media, 2013).
 - [15] J. A. Hartigan, *Clustering algorithms* (John Wiley & Sons, Inc., 1975).
 - [16] G. Carlsson and F. Mémoli, arXiv preprint arXiv:0808.2241 (2008).
 - [17] M. Fiore and M. D. Campos, in *Computation, Logic, Games, and Quantum Foundations. The Many Facets of Samson Abramsky* (Springer, 2013) pp. 37–51.
 - [18] P. Healy and N. S. Nikolov, in *International Symposium on Graph Drawing* (Springer, 2001) pp. 16–30.
 - [19] J. A. Bondy, U. S. R. Murty, *et al.*, *Graph theory with applications*, Vol. 290 (Macmillan London, 1976).
 - [20] J. Tierny, (2017).
 - [21] Topological data analysis (tda).
 - [22] S. Manoff, Classical and Quantum Gravity **18**, 1111 (2001).
 - [23] T. I. S. of Units, List of physical quantities, Available at https://en.wikipedia.org/wiki/List_of_physical_quantities (1960-2021).
 - [24] M. W. Mahoney, L.-H. Lim, and G. E. Carlsson, SIAM News **42** (2009).
 - [25] P. G. Goerss and J. F. Jardine, *Simplicial homotopy theory* (Springer Science & Business Media, 2009).
 - [26] G. Carlsson, Bulletin of the American Mathematical Society **46**, 255 (2009).
 - [27] V. De Silva and R. Ghrist, Algebraic & Geometric Topology **7**, 339 (2007).
 - [28] M. Offroy and L. Duponchel, Analytica chimica acta **910**, 1 (2016).
 - [29] L. Wasserman, Annual Review of Statistics and Its Application **5**, 501 (2018).
 - [30] D. D. Nolte, Physics today **63**, 33 (2010).
 - [31] A. Björner, Journal of Combinatorial Theory, Series A **102**, 88 (2003).
 - [32] A. Forrest, J. Hunton, and J. Kellendonk, *Topological invariants for projection method patterns* (American Mathematical Soc., 2002).
 - [33] J. Lee, *Introduction to topological manifolds*, Vol. 202 (Springer Science & Business Media, 2010).
 - [34] C. Spandl, Mathematical Logic Quarterly **53**, 493 (2007).
 - [35] P. Jaradowski and A. Królak, Living Reviews in Relativity **15**, 1 (2012).
 - [36] B. F. Schutz, *Gravitational wave data analysis*, Vol. 253 (Springer Science & Business Media, 2012).
 - [37] A. Zomorodian and G. Carlsson, Discrete & Computational Geometry **33**, 249 (2005).
 - [38] F. Chazal, High-dimensional topological data analysis (2016).
 - [39] A. C. Gilbert and K. Levchenko, in *Proceedings of the LinkKDD workshop at the 10th ACM Conference on*

- KDD*, Vol. 124 (2004).
- [40] E. Kruja, J. Marks, A. Blair, and R. Waters, in *International Symposium on Graph Drawing* (Springer, 2001) pp. 272–286.
- [41] V. Nastase, R. Mihalcea, and D. R. Radev, *Natural Language Engineering* **21**, 665 (2015).
- [42] M. Yıldırım, F. Y. Okay, and S. Özdemir, *Expert Systems with Applications* **176**, 114840 (2021).
- [43] S. Bhattacharya and J. Poray, in *2016 International Conference on Computer, Electrical & Communication Engineering (ICCECE)* (IEEE, 2016) pp. 1–8.
- [44] T. B. Encyclopedia, History of graph theory, Available at <https://www.britannica.com/topic/graph-theory> (2021).
- [45] I. M. James, *History of topology* (Elsevier, 1999).
- [46] C. Hermida, M. Makkai, and J. Power, in *Proceedings. Thirteenth Annual IEEE Symposium on Logic in Computer Science (Cat. No. 98CB36226)* (IEEE, 1998) pp. 199–206.
- [47] H. Fleischner, *Eulerian graphs and related topics* (Elsevier, 1990).
- [48] M. Mihail and P. Winkler, *Algorithmica* **16**, 402 (1996).
- [49] C. E. Aull and R. Lowen, *Handbook of the history of general topology*, Vol. 3 (Springer Science & Business Media, 2013).
- [50] L. Debnath, *International Journal of Mathematical Education in Science and Technology* **41**, 769 (2010).
- [51] V. De Silva and G. E. Carlsson, in *PBG* (2004) pp. 157–166.
- [52] A. Phinyomark, E. Ibanez-Marcelo, and G. Petri, *IEEE Transactions on Big Data* **3**, 415 (2017).
- [53] F. Chazal and B. Michel, arXiv preprint arXiv:1710.04019 (2017).
- [54] S. Eilenberg, *Annals of Mathematics* , 407 (1944).
- [55] S. Mac Lane, *Categories for the working mathematician*, Vol. 5 (Springer Science & Business Media, 2013).
- [56] J. P. May, *Simplicial objects in algebraic topology*, Vol. 11 (University of Chicago Press, 1992).
- [57] graph theory — problems & applications — britannica, <https://www.britannica.com/topic/graph-theory>, (Accessed on 11/14/2021).
- [58] J.-G. Dumas, F. Heckenbach, D. Saunders, and V. Welker, in *Algebra, Geometry and Software Systems* (Springer, 2003) pp. 177–206.
- [59] P. A. Suci, Topology:homotopy, <https://web.northeastern.edu/suci/U565/U565sp10-homotopy.pdf>, (Accessed on 11/14/2021).
- [60] A. Alatorre, F. Becerra, and J. Casillas, *American Journal of Advanced Research* **2**, 1 (2018).
- [61] M. B. Botnan, lecture_notes.pdf, https://www.few.vu.nl/~botnan/lecture_notes.pdf (2020), (Accessed on 11/14/2021).
- [62] P. Niyogi, S. Smale, and S. Weinberger, *Discrete & Computational Geometry* **39**, 419 (2008).
- [63] A. Zomorodian and G. Carlsson, *Computational Geometry* **41**, 126 (2008).
- [64] R. Ghrist, *Math. Data* **25**, 273 (2018).
- [65] Wolfram, Betti number – from wolfram mathworld, <https://mathworld.wolfram.com/BettiNumber.html>, (Accessed on 11/14/2021).
- [66] E. B. Curtis, *Advances in Mathematics* **6**, 107 (1971).
- [67] V. Salnikov, D. Cassese, and R. Lambiotte, *European Journal of Physics* **40**, 014001 (2018).
- [68] T. Nakamura, Y. Hiraoka, A. Hirata, E. G. Escolar, and Y. Nishiura, *Nanotechnology* **26**, 304001 (2015).
- [69] G. Carlsson and A. Zomorodian, *Discrete & Computational Geometry* **42**, 71 (2009).
- [70] F. Chazal and A. Lieutier, *Computational Geometry* **40**, 156 (2008).
- [71] Rezno, Notes.pdf, <https://www.math.colostate.edu/~renzo/teaching/Topology10/Notes.pdf>, (Accessed on 11/14/2021).
- [72] M. Kramár, A. Goullet, L. Kondic, and K. Mischaikow, *Physical Review E* **87**, 042207 (2013).
- [73] A. Kesselman, Rk toolkit: Rk toolkit for building rk-diagrams and rk-models (2021).
- [74] scikit-learn: machine learning in python — scikit-learn 1.0.1 documentation (2021).
- [75] 6.1. pipelines and composite estimators (2021).
- [76] andorsk, andorsk/rk-workbench: R-k workbench builds a toolkit for ds workflow development using rk-diagrams (2021).
- [77] ml tooling, ml-tooling/ml-workspace: All-in-one web-based ide specialized for machine learning and data science. (2021).
- [78] G. I. Barenblatt, *Dimensional analysis* (CRC Press, 1987).
- [79] Tableau, (2012).
- [80] (2021).
- [81] B. Ben Mahria, I. Chaker, and A. Zahi, *Journal of Big Data* **8**, 10.1186/s40537-021-00412-2 (2021).
- [82] (2012).
- [83] M. Hilaga, Y. Shinagawa, T. Kohmura, and T. Kunii, *Topology Matching for Fully Automatic Similarity Estimation of 3D Shapes*.
- [84] G. Máté, A. Hofmann, N. Wenzel, and D. W. Heermann, *Biochimica et Biophysica Acta (BBA) - Biomembranes* **1838**, 1180–1190 (2014).
- [85] G. K. Mazandu and N. J. Mulder, *Advances in Bioinformatics* **2012**, 1–17 (2012).
- [86] M. Reuter, *International Journal of Computer Vision* **89**, 287–308 (2009).
- [87] .
- [88] T. Roughgarden and G. Valiant, *CS168: The Modern Algorithmic Toolbox Lecture 3: Similarity Metrics and kd-Trees* (2021).
- [89] A. Gilbert and K. Levchenko, *Compressing Network Graphs*.
- [90] Nevergrad - a gradient-free optimization platform — nevergrad documentation (2020).
- [91] M. Bailes, B. Berger, P. Brady, M. Branchesi, K. Danzmann, M. Evans, K. Holley-Bockelmann, B. Iyer, T. Kajita, S. Katsanevas, *et al.*, *Nature Reviews Physics* **3**, 344 (2021).
- [92] The gravitational-wave “revolution” is underway - scientific american, <https://www.scientificamerican.com/article/the-gravitational-wave-revolution-is-underway/>, (Accessed on 11/27/2021).
- [93] L. S. Collaboration, V. Collaboration, *et al.*, *GRB Coordinates Network* **25187**, 1 (2019).
- [94] L. S. Collaboration, V. Collaboration, *et al.*, *GRB Coordinates Network* **25324**, 1 (2019).
- [95] A. Hall, A. D. Gow, and C. T. Byrnes, *Physical Review D* **102**, 123524 (2020).
- [96] B. Abbott, R. Abbott, R. Adhikari, A. Ageev, B. Allen, R. Amin, S. Anderson, W. Anderson, M. Araya, H. Ar-

- mandula, *et al.*, Physical Review D **69**, 122001 (2004).
- [97] M. Van Der Sluys, I. Mandel, V. Raymond, V. Kalogera, C. Röver, and N. Christensen, Classical and Quantum Gravity **26**, 204010 (2009).
- [98] P. G. Krastev, K. Gill, V. A. Villar, and E. Berger, Physics Letters B **815**, 136161 (2021).
- [99] S. Bhagwat, V. De Luca, G. Franciolini, P. Pani, and A. Riotti, Journal of Cosmology and Astroparticle Physics **2021** (01), 037.
- [100] G. Bertone, A. M. Coogan, D. Gaggero, B. J. Kavanagh, and C. Weniger, Physical Review D **100**, 123013 (2019).
- [101] Gravity spy — zooniverse, <https://www.zooniverse.org/projects/zooniverse/gravity-spy>, (Accessed on 07/02/2023).
- [102] G. Carlsson, Nature Reviews Physics **2**, 697 (2020).
- [103] P. Niyogi, S. Smale, and S. Weinberger, SIAM Journal on Computing **40**, 646 (2011).
- [104] B. P. Abbott, R. Abbott, T. D. Abbott, S. Abraham, F. Acernese, K. Ackley, C. Adams, V. B. Adya, C. Affeldt, M. Agathos, *et al.*, Classical and Quantum Gravity **37**, 055002 (2020).
- [105] D. Finstad and D. A. Brown, The Astrophysical Journal Letters **905**, L9 (2020).
- [106] V. De Luca, V. Desjacques, G. Franciolini, A. Malhotra, and A. Riotti, Journal of Cosmology and Astroparticle Physics **2019** (05), 018.
- [107] Scikit, Scikit-tsne (2014).
- [108] L. Van der Maaten and G. Hinton, Journal of machine learning research **9** (2008).
- [109] M. Wattenberg, F. Viégas, and I. Johnson, How to use t-sne effectively. distill (2016) (2016).
- [110] G. C. Linderman and S. Steinerberger, SIAM Journal on Mathematics of Data Science **1**, 313 (2019).
- [111] S. Arora, W. Hu, and P. K. Kothari, in *Conference on learning theory* (PMLR, 2018) pp. 1455–1462.
- [112] C. Cortes and V. Vapnik, Machine learning **20**, 273 (1995).
- [113] A. B. Nielsen, C. D. Capano, O. Birnholtz, and J. Westerweck, Physical Review D **99**, 104012 (2019).
- [114] S. Kulkarni and C. D. Capano, Physical Review D **103**, 104002 (2021).
- [115] B. Aylott, J. G. Baker, W. D. Boggs, M. Boyle, P. R. Brady, D. A. Brown, B. Brügmann, L. T. Buchman, A. Buonanno, L. Cadonati, *et al.*, Classical and Quantum Gravity **26**, 165008 (2009).
- [116] D. M. Macleod, J. S. Areeda, S. B. Coughlin, T. J. Massinger, and A. L. Urban, SoftwareX **13**, 100657 (2021).
- [117] C. M. Biwer, C. D. Capano, S. De, M. Cabero, D. A. Brown, A. H. Nitz, and V. Raymond, Publications of the Astronomical Society of the Pacific **131**, 024503 (2019).
- [118] H. Gabbard, C. Messenger, I. S. Heng, F. Tonolini, and R. Murray-Smith, arXiv preprint arXiv:1909.06296 (2019).
- [119] E. Cuoco, B. Patricelli, A. Iess, and F. Morawski, Nature Computational Science **2**, 479 (2022).
- [120] A. Grigor'yan, Y. Muranov, V. Vershinin, and S.-T. Yau, in *Forum Mathematicum*, Vol. 30 (De Gruyter, 2018) pp. 1319–1337.
- [121] G. Kour and R. Saabne, in *Frontiers in Handwriting Recognition (ICFHR), 2014 14th International Conference on* (IEEE, 2014) pp. 417–422.
- [122] G. Kour and R. Saabne, in *Soft Computing and Pattern Recognition (SoCPar), 2014 6th International Conference of* (IEEE, 2014) pp. 312–318.
- [123] G. Hadash, E. Kermany, B. Carmeli, O. Lavi, G. Kour, and A. Jacovi, arXiv preprint arXiv:1804.09028 (2018).
- [124] Topological data analysis (tda).
- [125] T. J. VanderWeele and J. M. Robins, Epidemiology **18**, 561–568 (2007).
- [126] F. Strazzieri and R. J. Sánchez-García, CoRR, abs/1806.06142 (2018).
- [127] B. Eriksson and R. Nowak, .
- [128] A. Björner, Handbook of combinatorics **2**, 1819 (1995).
- [129] D. Cohen-Steiner, H. Edelsbrunner, and J. Harer, Discrete & computational geometry **37**, 103 (2007).
- [130] H. Edelsbrunner, D. Letscher, and A. Zomorodian, in *Proceedings 41st annual symposium on foundations of computer science* (IEEE, 2000) pp. 454–463.
- [131] J. A. Hartigan, *Clustering algorithms* (John Wiley & Sons, Inc., 1975).
- [132] A. Hatcher, *Algebraic topology* (2005).
- [133] E. Miller and B. Sturmfels, *Combinatorial commutative algebra*, Vol. 227 (Springer Science & Business Media, 2004).
- [134] M. Penrose *et al.*, *Random geometric graphs*, Vol. 5 (Oxford university press, 2003).
- [135] J. B. Tenenbaum, V. De Silva, and J. C. Langford, science **290**, 2319 (2000).
- [136] H. Edelsbrunner, D. Letscher, and A. Zomorodian, in *Proceedings 41st annual symposium on foundations of computer science* (IEEE, 2000) pp. 454–463.
- [137] K. Grove, in *Proceedings of Symposia in Pure Mathematics*, Vol. 54 (1993) pp. 357–385.
- [138] Z. Cang and G.-W. Wei, PLoS computational biology **13**, e1005690 (2017).
- [139] H. Adams, T. Emerson, M. Kirby, R. Neville, C. Peterson, P. Shipman, S. Chepushtanova, E. Hanson, F. Motta, and L. Ziegelmeier, Journal of Machine Learning Research **18** (2017).
- [140] G. Favelier, C. Gueunet, A. Gyulassy, J. Kitware, J. Levine, J. Lukasczyk, D. Sakurai, M. Soler, J. Tierny, W. Usher, *et al.*, arXiv preprint arXiv:1806.08126 (2018).
- [141] A. Patania, F. Vaccarino, and G. Petri, EPJ Data Science **6**, 1 (2017).
- [142] R. A. Kesselman A., Ontological representation of store sales data (2021).
- [143] S. Manoff, arXiv preprint gr-qc/0006024 (2000).
- [144] S. Bird, I. Cholis, J. B. Muñoz, Y. Ali-Haimoud, M. Kamionkowski, E. D. Kovetz, A. Raccaelli, and A. G. Riess, Physical review letters **116**, 201301 (2016).
- [145] B. P. Abbott, R. Abbott, T. Abbott, M. Abernathy, F. Acernese, K. Ackley, C. Adams, T. Adams, P. Adesso, R. Adhikari, *et al.*, Physical review letters **116**, 061102 (2016).